



RICHTER GEDEON



Budapest University of Technology and Economics
Inorganic and Analytical Chemistry Department

In silico methodologies aiding fragment-based drug discovery

Thesis

PhD student

Márton Vass

Gedeon Richter Plc.

Supervisor

Dr. György Miklós Keserű

Research Centre for Natural Sciences,
Hungarian Academy of Sciences

2014

Acknowledgements

I would like to express my gratitude to everyone who directly or indirectly contributed to the realization of this thesis. The list would be rather long and even I couldn't compile the complete list. However, there are a few who deserve my dedicated acknowledgements.

First and foremost I would like to thank my supervisor György Keserű, who with his energetic spirit led me on the way of science since the last years of university. His flow of ideas and analyzing mind kindled my own aspiration to knowledge and his incentive led me on at difficult periods. Similar gratitude goes to Ákos Tarcsay, my colleague at Gedeon Richter who actually taught me the methods and especially the tricks of the field. It was and is a pleasure to work together and pursue our scientific path together. I am grateful to him for the patience, the scientific and personal discussions we had and his friendly attitude at every moment. I would also like to thank Gedeon Richter Plc. and specifically András Visegrády, my superior at Gedeon Richter, who made it possible for me to conduct the research and find that extra time that culminated in the writing of this thesis.

Of course I couldn't have written this thesis without the love, help and support of my family, my mother Éva, my father József and my sister Réka and other members of my extended family. I am truly grateful for every moment I spend with them and the spirit I received from home. For every question they ask and every minute they listen. I hope my sister will also enjoy the wonders of science. Similar gratitude goes to Bence Török, which I cannot express in words, and his whole family who like me and care about me so much.

Finally I would like to thank the colleagues who did substantial part in the work discussed in this thesis. I thank Balázs Jójárt, Ferenc Bogár and Gábor Paragi from the University of Szeged, who performed the molecular dynamics simulations and evaluations, Éva Schmidt and Ferenc Horti from Gedeon Richter, who performed pharmacological measurements and Éva Ágainé Csongor from Gedeon Richter for the syntheses.

*Valami nem létezőnek a helye,
ahová sejtetően más nemigen passzol.*

Simon Márton · Polaroidok 513

*The space for something non-existent,
where presumably nothing else really fits.*

Translation by Márton Vass

Table of contents

Chapter 1 – Preface	13
1.1 Fragment-based drug discovery	15
1.2 Computer-aided drug design	20
1.2 G protein-coupled receptors	23
1.4 Aims of this thesis	24
Chapter 2 – Introduction	27
2.1 Generation of fragment libraries	27
2.2 Virtual fragment screening (VFS)	29
2.2.1 Fragment docking and scoring	30
2.2.2 Performance of virtual fragment screening	31
2.2.3 Advanced binding free energy methods used in FBDD	32
2.2.4 VFS in high-throughput X-ray screening	35
2.2.5 VFS against other enzyme targets	36
2.2.6 VFS without a target crystal structure	38
2.2.7 The SAMPL3 challenge for VFS	39
2.2.8 VFS on non-enzyme targets	40
2.2.9 Concluding remarks on VFS	42
2.3 Fragment optimization and <i>de novo</i> drug design	42
2.3.1 Optimization potential of fragments	42
2.3.2 Physical background of fragment optimization	43
2.3.3 De novo drug design	45
2.3.4 Strategies of fragment evolution	46
2.3.5 De novo design algorithms	47
2.3.6 Ligand-based de novo design	50
2.3.7 Fragment-based lead discovery on GPCRs	51
2.3.8 Ligand efficiency metrics in fragment-based design	52
Chapter 3 – Methods	57
3.1 Methods used in primary site screening	57
3.1.1 Homology modeling of the H ₄ and 5HT ₆ receptors	58
3.1.2 Molecular dynamics simulations using NAMD	58
3.1.3 Binding site clustering	60

3.1.4 Protein structure preparation	60
3.1.5 Compilation of the ligand set for the CXCR ₄ receptor	61
3.1.6 Compilation of the in-house fragment library	61
3.1.7 Ligand structure preparation	61
3.1.8 Docking using Glide	62
3.2 Methods used in secondary site modeling	63
3.2.1 Compilation of the protein-ligand complex data set	63
3.2.2 Compilation of the protein-fragment complex data set	64
3.2.3 Homology modeling of the D ₂ receptor	65
3.2.4 Protein structure preparation	65
3.2.5 Compilation of the fragment libraries for linking	66
3.2.6 Ligand structure preparation	66
3.2.7 Docking using Glide	67
3.3 Experimental methods	70
3.3.1 Human recombinant H ₄ binding assay	70
3.3.2 Human recombinant D ₂ and D ₃ binding assays	70
Chapter 4 – Results	73
4.1 Virtual screening against GPCRs	73
4.1.1 The impact of the structure source	74
4.1.2 The impact of the binding site character	78
4.1.3 The impact of the frame selection method	78
4.1.4 The impact of MD ensembles	79
4.1.5 Application domain of the proposed methodology	80
4.2 Virtual fragment screening against GPCRs	82
4.2.1 Analysis of receptor binding sites	82
4.2.2 Single structure and ensemble docking results	83
4.2.3 Pharmacological activities	85
4.2.4 Binding modes	89
4.3 Multiple ligand docking	91
4.3.1 Docking performance for the first ligand	92
4.3.2 Docking performance for further ligands	93
4.3.3 Performance on drug-like ligands and closed sites	94
4.3.4 Case study: application to cooperative CYP binding	96
4.3.5 Case study: application to fragment binding to HSP90	101

4.4 Multiple fragment docking	103
4.4.1 Self-docking results	103
4.4.2 Case studies: HSP90, PTP1B and HTX	105
4.4.3 Cross-docking results	107
4.5 Fragment linking for dopamine D ₃ receptor ligands	108
4.5.1 Primary site docking results	109
4.5.2 Secondary site docking results	110
4.5.3 Biological activities	111
Chapter 5 – Conclusions	115
Thesis points	117
References	119
Appendix A	133
Appendix B	135
Appendix C	136
Appendix D	137
Appendix E	138
Appendix F	142
Appendix G	143
Appendix H	145
Appendix I	146
Appendix J	147
Appendix K	148

List of abbreviations

ADMET	absorption, distribution, metabolism, excretion, toxicity
ASA	accessible surface area
AUC	area under (the ROC) curve
CADD	computer-aided drug discovery
clogP	calculated water-octanol partition coefficient
CNS	central nervous system
CYP	cytochrome P450
ECL	extracellular loop
EF	enrichment factor
FBDD	fragment-based drug discovery
FEP	free energy perturbation
GPCR	G protein-coupled receptor
HA	heavy atom (count)
HBA	hydrogen bond acceptor (count)
HBD	hydrogen bond donor (count)
HM	homology model
HTS	high-throughput screening
HTX	high-throughput X-ray crystallography
ICL	intracellular loop
IFD	Induced Fit Docking
IFP	interaction fingerprint
LE	ligand efficiency
LELP	ligand-efficiency-dependent lipophilicity
LLE	ligand-lipophilicity efficiency
logP	water-octanol partition coefficient
MD	molecular dynamics
NMR	nuclear magnetic resonance (spectroscopy)
NROT	number of rotatable bonds
PDB	Protein Data Bank
PPI	protein-protein interface
PSA	polar surface area
QSAR	quantitative structure-activity relationship
RMSD	root-mean-square deviation (of atomic positions)
ROC	receiver operating characteristic (curve)
SAR	structure-activity relationship
SD	standard deviation
SILE	size-independent ligand efficiency
SP	standard precision
SPR	surface plasmon resonance (spectroscopy)
TM	transmembrane (helix)
VFS	virtual fragment screening
XP	extra precision
XRD	X-ray diffraction

Chapter 1 – Preface

Raising the standards of life is a continuing aim of humanity to which developments of science have contributed tremendously. Human welfare includes the satisfying of biological and social needs, ensuring social security, human relationships, freedom and health. Fighting and preventing diseases and developing solutions for unmet medical needs are the primary goals of pharmaceutical research. Modern vaccines and drugs helped increase life expectancy from 31 to 67 years in the 20th century. These discoveries are the fruits of the work of many great scientists and the scientific community as one. The wonders of biology and the intricate nature of the human body have enchanted many a great mind.

For the pharmaceutical industry productivity is also an important factor. The drug discovery process is lengthy and costly: in 2010 the average time to bring a new drug to the market was estimated at 13.5 years and the average capitalized cost at \$ 1.8 billion [1]. The costs have increased considerably in recent decades due to scientific, economical and regulatory changes, while the productivity of the pharmaceutical industry has remained at a constant level. As only every tenth new molecule entering the clinical phase will eventually reach the market and the attrition in Phase II and Phase III clinical trials is the highest, the most successful way of improving productivity would be to bring new chemical entities with higher transition probability to the clinic. Around 30% of the candidates are terminated due to clinical ineffectiveness [2] as visible from Figure 1, which the industry tries to leverage with better target selection and translational research, early phase proof-of-concept studies, repositioning of safe but ineffective candidates, etc.

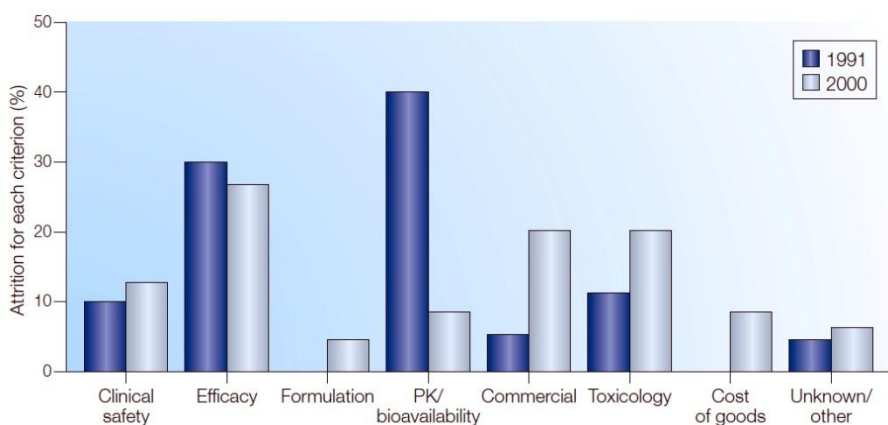


Figure 1. Reasons for drug attrition in 1991 and 2000 [2].

Another 30% of the candidates are terminated due to safety liabilities (20% for toxicity and 10% for clinical safety), for which poor ADMET properties are responsible. ADMET stands for absorption, distribution, metabolism, excretion and toxicity, the determinants of pharmacokinetic and pharmacodynamic properties of drugs. *In vitro* and *in vivo* experiments can help identifying such liabilities in the discovery phase; however, the analysis of recently patented compounds and launched drugs revealed that also physico-chemical parameters have a great impact on ADMET properties of drugs lying in the background of attrition. It was shown that patented compounds have increased molecular mass and lipophilicity (expressed by the calculated water-octanol partition coefficient *cLogP*) [3], which carries on to increased molecular mass of launched drugs as well, while lipophilicity seems to be virtually constant [4]. Increase of both parameters is associated with lower oral absorption as shown in the pioneering work of Lipinski [5], while higher lipophilicity is also associated with adverse effects and *in vivo* toxicology liabilities through the promiscuity of the compounds [4]. This trend has come to be known as ‘molecular obesity’ [6]. From this it can be seen that drug development is a multi-dimensional optimization process in which many parameters must be simultaneously controlled and improved. This multi-parameter optimization model is schematically indicated in Figure 2. It is proposed that progressing candidates with favorable physico-chemical properties could reduce ADMET related attrition in the clinic and thus improve productivity. Fragment-based drug discovery (FBDD) is a recently emerged and quickly spreading technology due to its speed and inherent ability to control the various parameters important for drug discovery. FBDD is now seen as a method capable of reducing attrition and providing drug candidates even for new biological targets that were previously thought to be intractable.

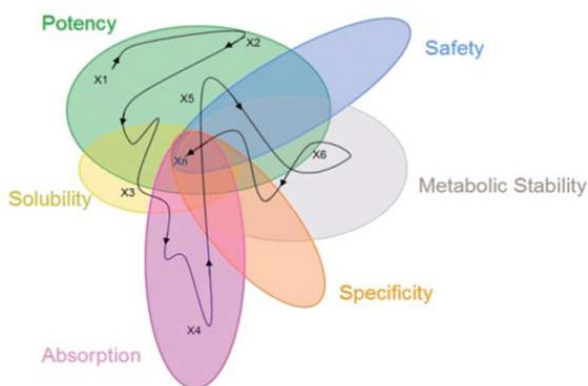


Figure 2. Schematic representation of the multi-parameter optimization pursued in drug development [6].

1.1 Fragment-based drug discovery

Fragment-based drug discovery involves the selection, screening and optimization of molecular fragments. Fragments are polar compounds of low molecular weight (typically 100–250 Da or 6–20 non-hydrogen atoms) and of low complexity that are able to make optimal interactions with the protein target [7]. Due to the reduced complexity as opposed to lead-like or drug-like molecules identified in high-throughput screening (HTS), they usually bind to the biological targets with much lower binding affinity (typically in the μM – mM range) but with better complementarity to the binding site and higher ligand efficiency, which is the contribution of each non-hydrogen atom to the binding affinity. Hits from HTS usually contain suboptimal interaction points and their optimization is difficult since the areas of the molecule needed to be changed are not known. Fragments are better starting points for optimization since they are optimally bound in a specific region of the binding site but they are small in size and need to be built up to larger molecules (Figure 3).

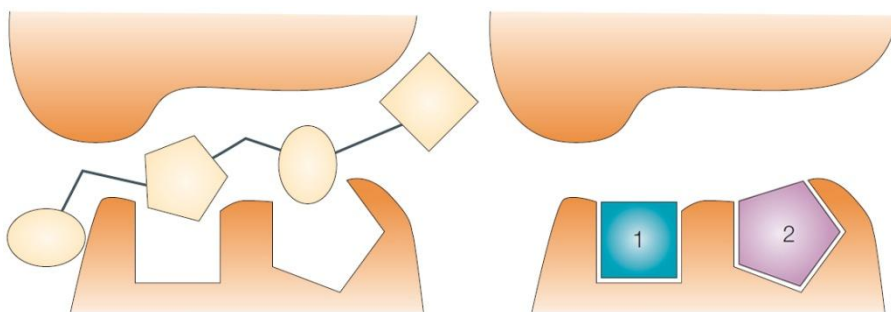


Figure 3. Schematic representation of a low quality HTS hit (left) and high quality fragment hits (right) [redrawn from 7].

The concept of FBDD started in the early '80s with theoretical considerations on the additivity of the binding free energy of parts of a larger molecule and the entropy loss of linking the parts [8]. Andrews proposed analyzing ligand binding in terms of the free energy per functional group [9]. The fragment concept was exploited in *de novo* computational drug design software like CAVEAT, which identified small molecular fragments predicted to bind in the protein binding site and linked them to generate drug-like idea compounds [10]. X-ray solvent mapping was used to characterize protein binding sites [11]. Ringe and Mattos transferred protein crystals to organic solvents such as benzene and dimethyl formamide to identify sites of aromatic or hydrogen bonding interactions and proposed that drug-like molecules can be obtained by linking these

crystallographic solvent molecules. The first report of dedicated fragment-based design dates back to 1996 when Fesik et al. devised the SAR by NMR method to identify proximally bound fragments (with binding affinities 2 μ M and 0.1 mM) in a protein binding site and synthetically linked them to obtain a compound with binding affinity of 19 nM [12]. In 2000 Nienaber et al. reported the first X-ray crystallographic fragment screen and the structure-guided optimization of a 56 μ M fragment hit to an orally available

Table 1. Fragment derived approved drugs and candidates in the clinic in 2013 with originators and mechanism of action [15].

Approved		
Vemurafenib (PLX4032)	Plexxikon	B-Raf(V600E) inhibitor
Phase II/III		
MK-8931	Merck	BACE1 inhibitor
Phase II		
AT13387	Astex	HSP90 inhibitor
AT7519	Astex	CDK1,2,4,5 inhibitor
AT9283	Astex	Aurora, Janus kinase 2 inhibitor
AUY922	Vernalis/Novartis	HSP90 inhibitor
Indeglitazar	Plexxikon	pan-PPAR agonist
Linifanib (ABT 869)	Abbott	VEGF and PDGFR inhibitor
LY2886721	Lilly	BACE1 inhibitor
LY517717	Lilly/Protherics	FXa inhibitor
Navitoclax (ABT 263)	Abbott	Bcl-2/Bcl-xL inhibitor
PLX3397	Plexxikon	FMS, KIT and FLT-3-ITD inhibitor
Phase I		
ABT-518	Abbott	MMP-2 and 9 inhibitor
ABT-737	Abbott	Bcl-2/Bcl-xL inhibitor
AZD3839	AstraZeneca	BACE1 inhibitor
AZD5363	AstraZeneca/Astex	AKT inhibitor
DG-051	deCODE	LTA4H inhibitor
IC-776	Lilly/ICOS	LFA-1 inhibitor
JNJ-42756493	J&J/Astex	FGFr inhibitor
LEE011	Novartis/Astex	CDK4 inhibitor
LP-261	Locus	Tubulin binder
LY2811376	Lilly	BACE1 inhibitor
PLX5568	Plexxikon	kinase inhibitor
SGX-393	SGX	Bcr-Abl inhibitor
SGX-523	SGX	Met inhibitor
SNS-314	Sunesis	Aurora inhibitor

0.37 μM lead compound [13]. These papers raised the attention of big pharmaceutical companies and small biotechs were also founded on the emerging technology. The latter used FBDD for soluble enzyme targets such as kinases that could be easily tackled using X-ray and NMR, while big pharma first only used it as a last resort when no other methods provided suitable starting points. However, FBDD then turned out to be a successful method and was used as a primary hit finding and lead optimization technology. It has already provided the market with an approved drug Vemurafenib [14] and several others in clinical development [15], demonstrating the potential of fragment hits to be quickly developed into leads and drug candidates. The idea-to-approval time of Vemurafenib was reportedly only 6 years. The 25 fragment derived clinical candidates in 2013 are summarized in Table 1.

The underlying theory behind the success of FBDD is an ongoing field of research. Hann proposed complexity theory, a simplified model in which he calculated probabilities of measuring the binding of compounds of varying complexity with a single binding mode in the protein binding site (yellow curve in Figure 4) and found that the optimum is at reduced complexity compared to HTS hits [16]. Kuntz collected binding affinity or functional data of strongly bound ligands and plotted the binding free energy against the number of non-hydrogen atoms [17]. He found that there is a sharp increase of maximal binding free energy until around 10 heavy atoms and this maximal binding free energy per non-hydrogen atom is around 1.5 kcal/mol/atom (line indicated in Figure 4) and only metal ions and special ligands can surpass this limit. It was proposed that larger molecules don't follow this trend because in their binding van der Waals and hydrophobic interactions dominate, which cannot sustain such high interaction energies. Indeed, Keserú and Ferenczy later found that fragment binding is enthalpy driven as opposed to entropy driven binding of larger molecules, which is

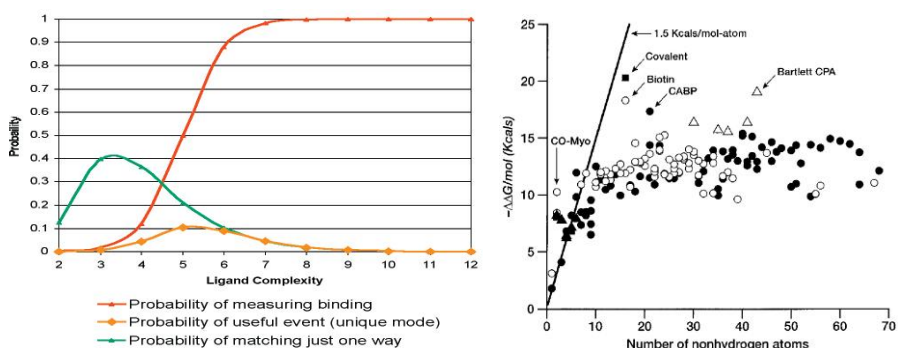


Figure 4. Determinants of the complexity theory of Hann (left) [16] and maximal binding free energy plotted against number of non-hydrogen atoms (right) [17].

sustained by two near optimal geometry hydrogen bonds on average as can be seen from Figure 5 [18]. These hydrogen bonds are usually close by in the molecule therefore this finding is in line with the high contribution to binding free energy of only a small number of heavy atoms. The region in the protein binding site featuring these interaction points is usually referred to as the ‘hot spot’. Following Andrews’s and Kuntz’s footsteps Hopkins proposed the binding free energy per non-hydrogen atom termed ligand efficiency as a useful metric for hit prioritization in HTS and fragment screening [19], which indeed found widespread application in FBDD and intense discussions in the literature. The implications of these concepts on fragment optimization will be described in more detail in the next chapter.

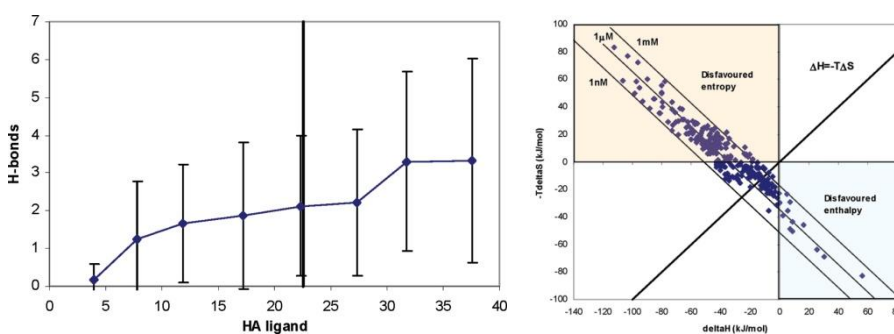


Figure 5. Number of H-bonds in protein-ligand complexes as a function of the number of ligand heavy atoms (left) and enthalpic and entropic components of binding in fragment-protein complexes (right) [18].

Another advantage of fragments is the higher coverage of chemical space than that of lead-like or drug-like molecules. The number of drug-like molecules compliant with Lipinski’s rule of five is estimated at 10^{60} [20], which is a tremendous number compared to the size of compound libraries screened in HTS usually in the 10^5 - 10^6 range and we will never have the chance to screen a significant fraction of this huge chemical space. On the other hand fragment-like molecules have been exhaustively enumerated up to 13 non-hydrogen atoms and there are about 353 million of them [21], which extrapolates to about 10^{12} up to 20 non-hydrogen atoms. This is still a large number but the screening of 10^3 - 10^4 fragments gives a much larger coverage of the chemical space. Added to this is that fragments are more efficient in probing the shape and pharmacophore elements of protein binding sites what justifies the success of screening even small libraries.

For fragment-based drug discovery the very first thing needed is a firm decision to follow through the whole process in the fragment mindset: not pursuing potency but rather ligand efficiency and systematically testing optimization hypotheses with targeted syntheses. After this a high quality

fragment library is needed for screening. Due to generally low affinities fragment hits are typically identified by sensitive biophysical screening methods, such as X-ray crystallography [22], nuclear magnetic resonance (NMR) [23], surface plasmon resonance (SPR) [24], etc. and thorough validation of hits by orthogonal screening methods is needed. The majority of the reported FBDD projects utilized structural information obtained preferably by X-ray crystallography or by specialized NMR experiments and relied on structure-based design in hit-to-lead optimization. The two main strategies of fragment hit elaboration are growing and linking [7], schematically depicted in Figure 6. In the first one a single fragment is decorated with additional functionalities that complement the rest of the binding site, while in the second two (or more) fragments need to be identified that bind to the target simultaneously and in close proximity and a suitable synthetic linker between them. As an example the growing of Vemurafenib, the first approved drug derived from a simple azaindole fragment hit is shown in Figure 7. An example of fragment linking is the discovery of ABT-737, an inhibitor of the Bcl-X_L protein-protein interface [15].

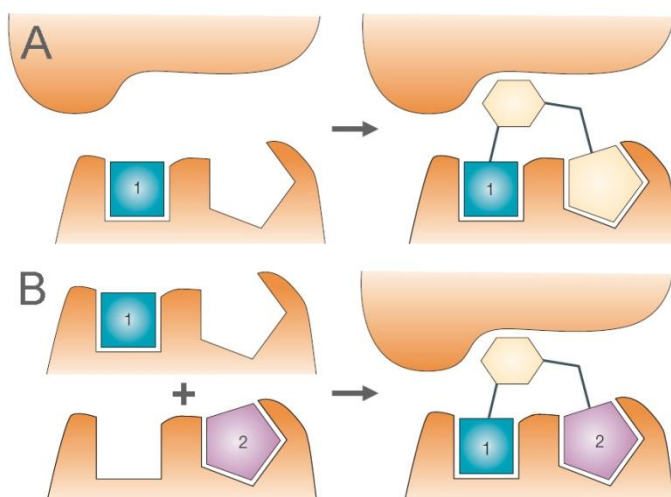


Figure 6. Schematic representation of fragment growing (A) and fragment linking (B) [redrawn from 7].

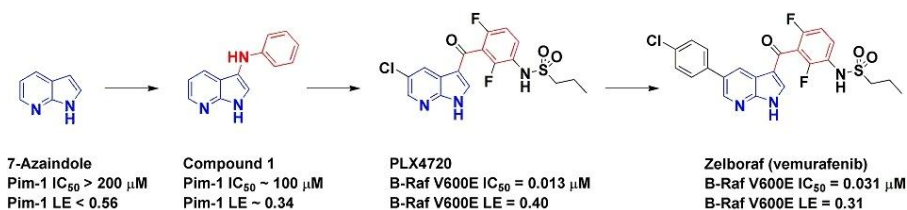


Figure 7. Optimization of Vemurafenib from the azaindole hit by growing [14].

1.2 Computer-aided drug design

The aim of computer-aided drug design (CADD) is to support and guide the drug discovery process by utilizing previous general medicinal chemistry knowledge and knowledge of the biological target in the design and synthesis of new molecular entities. The use of such knowledge helps rationalizing decisions made in design and thus reduces the cost and time of the process. Computational methods are constantly developing and with the increasing computational capacities (according to Moore's law) more complex questions may be asked and more accurate predictions can be made. By incorporating the data available and exploiting the increasing resources methods of CADD have shown remarkable performance in understanding and predicting natural phenomena. The use of specialized software, hardware, graphical processing units (GPUs) and cloud computing allowed previously daunting problems such as protein folding [25] and protein functional activity [26-28] to be tackled.

However, computational methods rely always only on a model of nature and thus have to be handled with care and their limits must be known to the user. There is always a balance between accuracy and speed and as the complexity of the systems considered in medicinal chemistry is immense, one cannot expect currently available computational methods to agree fully with experimental results. Not to mention that chemical and even more so biological experiments also have variance. Therefore a central concept in CADD is enrichment, which expresses the ratio of success (measured in any way but most often as the ratio of active molecules in a selected collection of molecules) with and without the use of a given computational method. There are fast methods used in the early phase of drug discovery when the number of considered molecules may be in the thousands to millions range, which have limited accuracy and provide limited enrichment. This process is called virtual screening since the library is screened only computationally to reduce it to a size manageable by experimental screening [29]. On the other end, there are time consuming methods with much higher accuracy and enrichment that can only be used later in the lead optimization phase when the number of molecules in consideration is only a few [30]. Therefore, all of the computational methods can find their suitable place in the drug

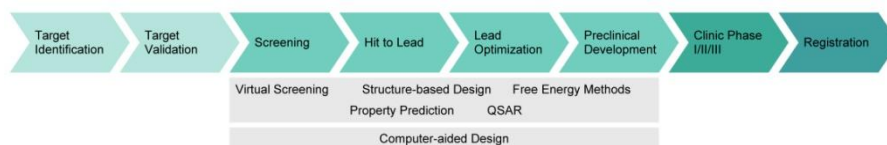


Figure 8. The role of computer-aided drug design in the drug discovery process.

discovery process and they work best in combination with experimental techniques of similar throughput as shown in Figure 8.

The analysis of large amounts of data available from public and company databases led to general guidelines for medicinal chemists such as Lipinski's Rule of 5 for predicting whether a compound could likely be an orally active drug in humans [5]. The rule is based on the molecular mass, the water-octanol partition coefficient (logP) and the number of hydrogen-bond donors and acceptors of the molecule. As mentioned earlier these parameters influence other ADMET parameters as well, and after analyzing in-house data of GSK, ADMET rules of thumb were also proposed by Gleeson [31]. By analyzing data of compounds acting in the central nervous system (CNS) a composite score based on these and further parameters, the polar surface area and the acidity of the molecule, was proposed to predict potential CNS activity [32]. In order to calculate these rules and scores for new compounds, also means of predicting the properties are required. Statistical methods are used to build up models based solely on compound structure that are able to predict e.g. the logP, acidity, solubility and ADMET parameters [33]. Prediction of these parameters is cheaper and faster than measurements and has the advantage of being available before synthesis. Predicted parameters are therefore used to filter compounds for experimental testing and to guide the design process towards compounds with better profiles.

If a reasonable amount of activity data against a biological target is available, similar statistical methods can be used to build up target specific quantitative structure-activity relationship (QSAR) models, which attempt to predict the biological activity of a compound based on its chemical structure [34]. Public databases of biological activity data have expanded largely in the last decade enabling more accurate bioactivity models to be built. ChEMBL is the largest such database collecting data from scientific literature using automatic text mining algorithms [35]. A remarkable recent paper described an automated ligand design algorithm based on bioactivity data from ChEMBL and common synthetic transformations that was able to computationally redesign an approved acetylcholinesterase inhibitor drug into brain-penetrable ligands with specific polypharmacology and selectivity profiles for G-protein-coupled receptors [36]. Models incorporating knowledge of only the ligands acting on a biological target – such as QSAR – are called ligand-based methods, while models incorporating knowledge of the three-dimensional molecular structure of the biological target are called structure-based methods. Other ligand-based methods include the calculation of chemical or 3D shape similarity of the compounds, various advanced variations of QSAR such as field-based QSAR and pharmacophore modeling. The latter tries to identify an abstract description of molecular

features which are necessary for molecular recognition of a ligand by the biological target based on known ligands of the target.

Structure-based computational methods enable the understanding of physical protein-ligand interactions important for biological activity and thus a more rational design process. The majority of the reported fragment optimizations used structural information to devise growing or linking strategies based on the structure of the protein-fragment complex. These methods rely on the shape and charge complementarity of the ligand and the binding site, which is the same principle as Emil Fischer suggested in 1894 as the “lock and key” model for enzyme substrates. The largest source of protein structures is the Protein Data Bank (PDB) database, which stores structures determined by X-ray crystallography, NMR and electron microscopy made available to the public [37]. When the structure of a protein is not known but that of a close homologue is, comparative modeling (or homology modeling) may be performed to predict the unknown structure. This is based on the observation that proteins that have similar amino acid sequences also have similar tertiary structures [38]. Molecular docking is the most frequently used method to predict the binding conformation of a ligand in the binding site of the target and also estimate the binding affinity [39]. Scoring functions are used to evaluate different possible conformations of a single ligand and rank different ligands by predicted affinity. Since docking is a fast method, its accuracy is limited

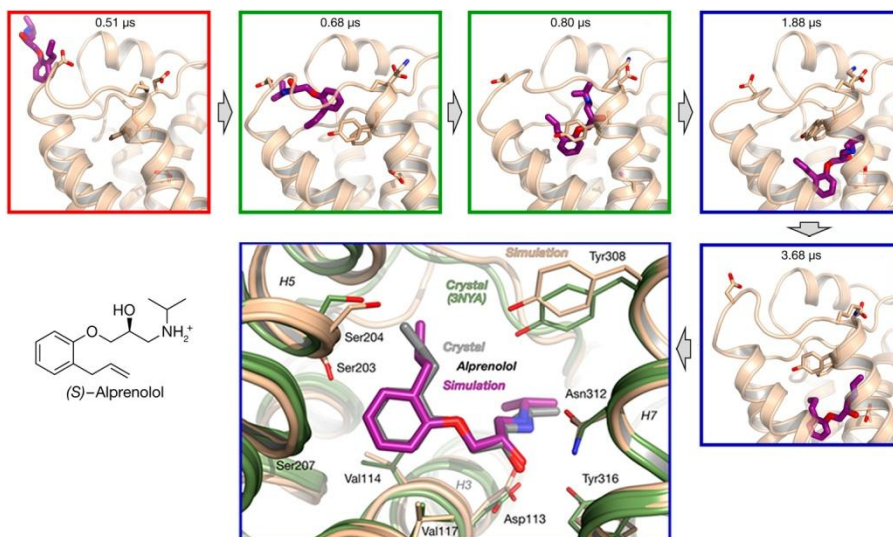


Figure 9. The quality of structural information attainable by high performance computing. In a 5 μ s long unbiased molecular dynamics simulation a binding event of *S*-alprenolol to the β_2 -adrenergic receptor was observed, which perfectly reproduced the experimental binding conformation [redrawn from 28].

but more advanced rescoring methods and the incorporation of protein flexibility can raise accuracy. Knowledge of the binding mode is necessary for understanding structure-activity relationships (SAR) and to propose rational synthetic modifications. Molecular dynamics (MD) simulations may be used to explore dynamic and transient features of protein-ligand interactions and to estimate the entropic contribution to binding free energy [40]. MD simulations have benefited hugely from the increasing computational capacities. It has recently been used for example to understand kinetics of protein folding [25], gating mechanism of voltage-gated ion channels [26], activation of G protein-coupled receptors [27] and mechanism of ligand binding at the atomic level (see Figure 9) [28].

1.3 G protein-coupled receptors

G protein-coupled receptors are a family of membrane embedded proteins also called seven-transmembrane (7TM) proteins based on their alpha-helical fold (see Figure 10). Seven alpha helices are connected by three extracellular and three intracellular loops, and an eighth amphipathic helix can usually also be found in their structures [41]. They recognize a wide variety of interacting partners outside the cell ranging from photons and ions to small molecules, lipids, peptide hormones, and even proteins. Ligand binding brings about conformational rearrangements of the helices and finally activates signal transduction pathways inside the cell. Different GPCRs interact with a number of G proteins inside the cell but recently β -arrestins and other binding partners and signalization pathways have also been heavily investigated.

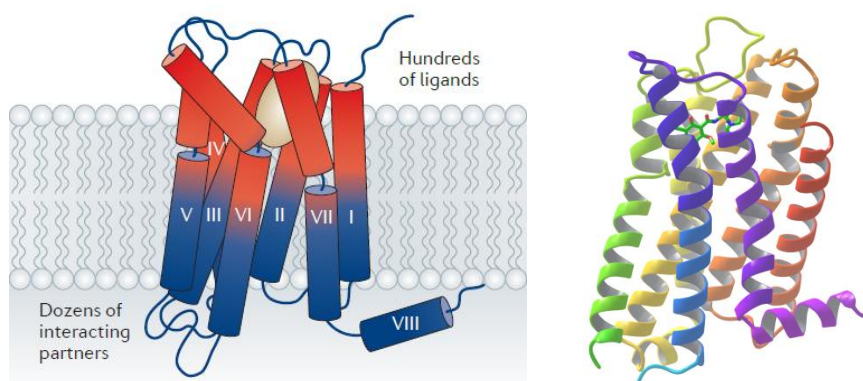


Figure 10. Schematic representation of G protein-coupled receptors with helix numbers indicated (left) [43] and ribbon diagram of a GPCR, namely the D₃ dopamine receptor in complex with eticlopride (right). Helices are color coded from red (helix I) to magenta (helix VIII).

A study in 2006 analyzed biological targets of existing drugs and concluded that one third of marketed drugs act on rhodopsin-like (class A) GPCRs [42] thus constituting the largest drug target family, hence the interest in the structure and dynamics of these receptors is high. However, only recent developments in the stabilization and crystallization of membrane proteins could facilitate experimental determination of their structures. The first crystal structure of bovine rhodopsin was determined in 2000 and starting from 2007 the X-ray structures of 20 other GPCRs relevant for the pharmaceutical industry have been publicly disclosed [43]. This number is still small compared to the total of 779 distinct receptor isoforms, however, these structures had a huge impact on our understanding of GPCR functional activity, made it possible to apply structure-based computational modeling to this important target family and enabled comparative modeling of yet unknown GPCR structures [44].

1.4 Aims of this thesis

During the preparation of this thesis I was a member of the Computer-Aided Drug Design team in the Discovery Chemistry Laboratory at Gedeon Richter Plc. Our team's tasks included the general support of medicinal chemistry by introduction of external and development of in-house predictive tools, project specific virtual screening using either ligand-based or structure-based methods depending on the biological target, evaluation of HTS results and the support of hit-to-lead optimization. Thus we made use of a wide variety of computational methods depending on the needs of the specific projects.

Also Richter took on the fragment-based approach in medicinal chemistry little prior to the beginning of my employment there and later on this became my area of research. Since fragment-based drug discovery needs different methods both experimentally and in computation it was also my responsibility to follow the literature of this field and to explore and develop computational methodologies applicable in the fragment-based discovery process. This of course required the understanding of the specific methods both in classic small molecule-based setups and in fragment-based setups. Therefore my first aim was to summarize the computational methods applied in fragment-based drug discovery with a focus on the advances of recent years in the field of computational FBDD. Chapter 2 discusses these trends with methods used in fragment library design, virtual fragment screening and fragment optimization. A part is dedicated to FBDD on non-enzyme targets and specifically to G protein-coupled receptors, which – conducting CNS research – make up a major target class pursued in Gedeon Richter.

My second aim was to evaluate different protocols for fragment virtual screening on GPCR targets. This work started with method development on small molecule data sets and the results were subsequently used in a fragment screening setup. Since structural information on GPCRs is still restricted to a few targets, the use of experimentally determined structures as well as homology models in virtual small molecule and fragment screening was evaluated. The effect of incorporating protein conformational flexibility into both methodologies was also studied and compared to using a single structure for virtual screening. While method development in the small molecule setup was performed on retrospective data sets, prospective fragment screening was carried out and the obtained fragment hits can be used in a further work as starting points for optimization.

My third aim was to study computational methodologies applicable for finding starting points for fragment linking. Therefore besides primary site (or hot spot) fragment screening I evaluated the performance of a sequential docking protocol for identifying fragments bound in possible secondary sites of proteins. The experimental counterpart of this method is straightforwardly called second-site screening, which gave the idea for using the same methodology virtually. This work also started with method development on a small molecule data set and when results were encouraging, a fragment data set was also compiled and performance of the protocol was tested. During model development another potentially interesting application emerged, namely the prediction of cytochrome P450 enzyme activators. The cytochrome P450 enzyme family is relevant for medicinal chemistry as these are responsible for the metabolism of a large fraction of drugs and many times for drug-drug interactions. Taking second-site fragment screening forward I have used the protocol to identify fragments for linking inside the binding pocket of the D₃ dopamine receptor and also assessed the selectivity of the synthesized compounds against the D₂ dopamine receptor on a structural basis.

Chapter 3 in the present thesis describes the methods used throughout the work separated into methods used in primary and secondary site screening. Chapter 4 discusses the results separated in a similar manner while Chapter 5 draws the conclusions and presents the thesis points of the research in the context of the studied field.

Chapter 2 – Introduction

In this chapter computational methods used in the various stages of fragment-based drug discovery will be discussed with focus on recent developments. Computational medicinal chemistry provides complementary methods for experimental FBDD and works best if results of the two are combined and interpreted in light of each other. In the screening phase computational methods can aid the construction of high quality compound libraries suitable for the specific screening approach. Virtual screening can reduce in-house libraries to a size manageable by experimental screening and suggest commercial compounds for purchase. Computational tools can be used in hit prioritization and expansion of the chemical space around selected hits. Structure-guided optimization is effective in an iterative cycle with X-ray crystallography or NMR and ligand-based methods can be used throughout optimization in the absence of structural information.

2.1 Generation of fragment libraries

In a study in 2003 Congreve et al. from Astex analyzed fragment hits that were identified by X-ray crystallography against a range of targets and found that hits had on average molecular weight <300 Da, number of hydrogen bond donors ≤ 3 , number of hydrogen bond acceptors ≤ 3 and $\log P \leq 3$ [45]. Being all criteria multiples of three, in the footsteps of Lipinski's Rule of Five for orally available drugs, they called these the Rule of Three (see Table 2). They added that also number of rotatable bonds ≤ 3 and polar surface area $\leq 60 \text{ \AA}^2$ might also be useful criteria for fragment selection, however, only the aforementioned four rules caught on very quickly in the FBDD community. These rules were first considered by the community as hard limits for fragment selection. Later on the Rule of Three

Table 2. Physico-chemical parameters in Lipinski's Rule of Five for orally active drugs [5] and Congreve's Rule of Three for fragment hits [45].

Parameter	Lipinski Rule of Five	Congreve Rule of Three
molecular weight	< 500 Da	< 300 Da
$\log P$	≤ 5	≤ 3
hydrogen bond donors	≤ 5	≤ 3
hydrogen bond acceptors	≤ 10	≤ 3
additional	one violation allowed	NROT ≤ 3 PSA $\leq 60 \text{ \AA}^2$

suffered much criticism and recently came to be known as the Voldemort rule, or the rule-which-must-not-be-named, despite the original paper only suggesting them as guidelines. The authors themselves published a review on the Rule of Three ten years later and concluded that a number of different useful criteria emerged over time [46]. At present the community uses heavy atom number rather than molecular weight and the limit is often reported as 20 (or even lower) corresponding to an average molecular weight of 260 Da well below the original suggestion. Hydrogen bond donor and acceptor number limits may also be too strict for specific targets [47]. It is also recognized that optimal property ranges for different screening techniques are different [48]. Solubility and purity are also very important factors and requirements can vary among screening protocols. There may also be special requisites of methods such as fluorine content for ^{19}F NMR detection [49]. Three-dimensionality (expressed usually by the fraction of sp^3 atoms) has recently been suggested as an important feature for pharmacophore representation [50] as well as removal of reactive moieties or those causing assay interference by e.g. redox cycling or aggregation [51]. Finally, the often subjective attractiveness for medicinal chemists is sometimes also checked visually before purchasing a fragment library. These led to the observation that nowadays there are as many fragment criteria systems as many groups engaged in FBDD.

There are two main strategies for fragment library design: the forward and the backward approach. In the forward approach existing in-house or commercial compound libraries are filtered using the aforementioned fragment criteria and possibly by target-specific criteria. Computational methods can be used to calculate the physico-chemical parameters contained in the Rule of Three, predict ionization, solubility, three-dimensionality, etc. [52] Currently the number of commercially available Rule of Three compliant fragments is 3-400,000, which must still be reduced for a reasonable screening library size. Chemical diversity can be maximized using clustering algorithms, though it is recognized that in the fragment size domain even small changes in chemical structure can cause a large difference in biological activity, since fragments have large per atom contributions to the affinity. Target or target family specific computational methods may be used to assemble focused libraries such as the kinase and phosphatase sets constructed at Astex using both pharmacophore criteria and structure-based virtual screening [22] or the bromodomain set constructed by GSK using pharmacophore criteria [53]. Computational methods are also essential in fragment cocktailing, that is, when samples containing multiple fragments are screened against a biological target as is frequently done in NMR or X-ray crystallography [22]. In NMR maximal diversity of NMR signals must be achieved among fragments contained in

one cocktail, while for crystallography maximal electron density shape diversity should be ensured in order to unambiguously infer which fragment is the true hit.

In the backward approach databases of drug-like molecules with known bioactivities are decomposed into their constituting fragments in hope of finding privileged fragments with a higher chance of being hits [52, 54]. Source of such molecules can be marketed drugs, natural products or target specific bioactive molecules from the ChEMBL database, patents, etc. RECAP is the most widely used fragmentation method employing retrosynthetic rules for breaking 11 acyclic bond types to generate chemically stable fragments [55]. Substructure enumeration and subsequent filtering can identify a wider selection of fragments than retrosynthetic methods, however, stability and chemical feasibility must be checked for in a separate step. Prioritization of the huge number of fragment substructures is usually performed by frequency analysis in the starting databases. Wang and Hou identified high quality fragment substructures of approved and experimental drugs using this method [56]. Co-occurrence analysis of fragment pairs can also be helpful in identifying privileged structural motifs or unexplored parts of chemical space [57]. Fragments generated by these methods are either purchased from vendor catalogues or unavailable fragments must be synthesized. Ideas for novel fragments can also be drawn from virtual enumeration, such as the GDB-13 database, which exhaustively enumerated molecules up to 13 non-hydrogen atoms [21] or heterocycles predicted to be chemically feasible but which have not yet been synthesized [58]. These sources can be used in virtual screening and synthesis of the top compounds can add valuable compounds to the screening library.

2.2 Virtual fragment screening (VFS)

Sensitive biophysical methods usually require large amounts of purified protein and extended data collection or data analysis times, therefore screening library sizes must generally lie in the range of a few hundred to a few thousand. Compared to the 3-400,000 commercially available fragments or the fragment-like chemical space of approximately 10^{12} compounds this number is still low. Virtual fragment screening (VFS) provides a means either of reducing in-house libraries to a screenable size or selecting focused compound sets from commercial sources or for synthesis that enrich actives against the specific biological target. Though structure-based methods show preponderance in reported VFS case studies, ligand-based methods are also described in the literature in context of VFS. A central question in the field is whether methods developed

previously for drug-like molecules work with a similar or inferior performance for fragments and what new methods can be devised to improve performance specifically for fragment-like compounds.

2.2.1 Fragment docking and scoring

Despite recent advances in docking algorithms, fragment docking still remains a challenging task. As fragments are usually small compared to the whole protein binding site but usually have multiple H-bond acceptors and donors, the selection of the valid pose from the pool of nearly isoenergetic interaction permutations by scoring functions is not easy. Common experience is that the valid poses are most often generated by the docking programs (sufficient sampling), but sometimes poses with alternative interaction patterns are scored higher (inaccurate scoring). It is also a challenge that while scoring functions have been trained on complexes of high-affinity drug-like compounds, fragments are small and have much lower affinities.

In a study on a data set of 190 high-resolution fragment complexes Sándor et al. found that Glide was accurate enough in the prediction of fragment binding modes, however, they found poor correlation between docking scores and experimentally determined binding affinities: the R^2 value was 0.3 for well-docked fragments [59]. In self-docking setups they found a docking success rate (binding mode RMSD < 2 Å) of 80% accompanied by an average RMSD of 1.17 Å (see Figure 11). In cross-docking experiments they observed a 77% success rate and an average RMSD of 1.30 Å when using the single best X-ray structure for each target.

In another study by Verdonk et al. on 106 fragment and 100 drug-like compound complexes using GOLD with different scoring functions for pose selection and scoring, the authors reported a maximum of 70 % success rate (binding mode RMSD < 1.5 Å) and 43% success rate for cross-docking [60]. It was shown that the generally used RMSD cutoff of 2 Å for successful docking of drug-like molecules is too large for fragments and a proposed cutoff of 1.5 Å can discriminate between docking solutions capturing relevant interactions and misdocked cases (see Figure 11). The authors also divided the data set to high- and low-affinity and high- and low-LE subsets and concluded that success rates depend most on the ligand efficiencies of the docked compounds. Thus, when docking high-LE compounds a higher fidelity of the docked binding modes can be expected.

In a prospective docking study on AmpC β -lactamase 4 of 8 experimentally determined fragment binding modes provided RMSDs between 1.2 and 1.4 Å and further two had the same specific interactions as predicted [61]. In a recent communication on 32 ternary fragment

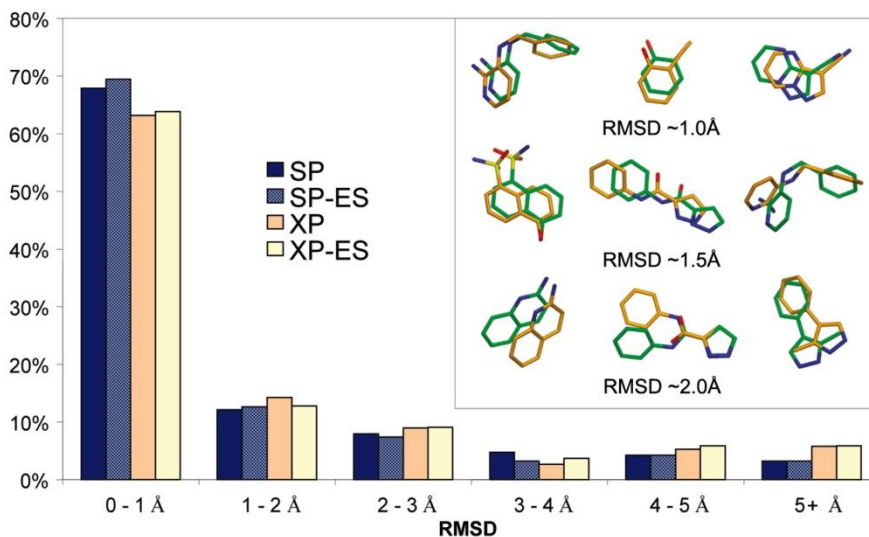


Figure 11. RMSD distribution of the docking poses generated by various docking protocols using Glide [59]. The inset shows examples of docking solutions of fragments with different RMSD values [redrawn from 60].

complexes, 75% of the hot spot binding fragments were docked with an RMSD < 1 Å, while the success rate was lower for second-site fragments, probably because they lack such high-quality interactions with the target as is possible inside the hot spot. Selection of the true binding mode from several docking solutions can be improved by the use of interaction fingerprints [62] or improved scoring functions [63]. These studies have shown that while fragment binding mode prediction is comparable to the performance on drug-like compounds, affinity prediction is in need of new and more accurate methods. Also incorporation of protein flexibility and explicit solvation effects need to be taken into account.

2.2.2 Performance of virtual fragment screening

Only a few papers in the literature can be found that systematically evaluate different computational methodologies used in virtual fragment screening. One of the first investigative studies was published by an AstraZeneca team exploring various docking and scoring protocols for fragment docking by Glide [64]. In this work the authors tested Glide SP and Glide XP scoring with and without the expanded funnel option developed for the enhanced sampling of possible binding modes. The MM-GBSA rescoring scheme was also tested. The performance of fragment docking was evaluated on two targets, prostaglandin D2 synthase (PGDS) and DNA ligase in self-docking, cross-docking and virtual screening paradigms against

experimental activity data. The authors found that self- and cross-docking accuracy was similar to what had generally been reported for lead-like molecules. In virtual screening areas under the receiver-operating characteristic curves (AUC) were modest, between 0.54 and 0.67 (where 0.5 means random sampling and 1.0 perfect separation of actives and inactives). Surprisingly, MM-GBSA re-scoring of docked poses for PGDS did not improve self-docking, cross-docking, or even virtual screening enrichment. For the ligase test case, the use of various hydrogen-bond constraints did not significantly improve the docking performance. For both test cases, GlideSP with default settings was able to produce enrichment of actives over random sampling. The enrichment rates obtained for the ligase test case, especially for tighter binders, were within the ranges reported for virtual screening of drug-like molecules (AUC between 0.66 and 0.72).

The same group also evaluated the effect of MM-PBSA rescoring on the PGDS data set and found that early enrichment can be improved, but the choice of the force field used is important [65]. The authors concluded that if only one protein structure is available, then MM-PBSA-based rescoring schemes can increase the odds of finding more actives in the first 1 % of the ligand database.

Fragment docking and virtual fragment screening validation studies reviewed here suggest that sampling is not the major issue associated with virtual fragments screening. This is indicated by the fact that the expanded sampling option and other fragments specific settings did not improve the performance of docking programs. Contrarily, however, scoring is one of the major challenges, which is responsible for most of the docking failures found when docking fragments. This can be alleviated by the use of more computationally intensive rescoring methods. Though the AstraZeneca team found no effect of MM-GBSA, they found improvement by using MM-PBSA-based rescoring methodologies. There are further rescoring schemes in literature, which are described in the following, shown to provide even higher accuracy in binding affinity prediction.

2.2.3 Advanced binding free energy methods used in FBDD

More accurate scoring of congeneric series of ligands can be achieved by computationally intensive physics-based methods that treat the energetics of protein-ligand binding and solvation rigorously, as shown recently. These methods are usually not applicable in high-throughput setups, only as a rescoring method on selected compounds that have passed previous filters and ranked high in a protocol. Examples include MM-PBSA, MM-GBSA, QM/MM methods, thermodynamic integration (TI), free-

energy perturbation (FEP), linear interaction energy (LIE) methods and grand canonical Monte Carlo (GCMC) simulations.

MM-PBSA and MM-GBSA combine the molecular mechanics interaction energies with polar solvation energies calculated from the exact Poisson-Boltzmann equations or the Generalized Born approximation and apolar solvation energies based on solvent-accessible surface area calculations. These methods use implicit solvation and are thus in the mid-range of accuracy and computational cost. It has been shown that they can increase ranking performance in fragment docking studies [65, 66] and affinity ranking of congeneric series [67, 68], however, in other studies their use didn't improve self-docking, cross-docking or enrichment, suggesting that the performance of the methods may be system dependent [64, 69]. With the proliferation of massive parallelization and GPU-enhanced computing even more costly methods, such as quantum mechanics may be used for rescoring of docking poses. Gleeson et al. showed that while GOLD retrieved X-ray binding modes in only 44% of their data set as top poses, minimizing and rescoring 2-3 diverse docking solutions with B3LYP/6-31G**//UFF increased the success rate to 77% [70].

Molecular dynamics or other conformational sampling-based free-energy calculation methods require higher computational costs; however, with efficient parallelization, specialized hardware or GPU-enhancement, these are also gaining momentum as an *in silico* aid in drug design. These methods evaluate ratios of the partition function in order to estimate binding free-energy differences between bound and unbound states of the same ligand or bound states of different ligands. This way they are capable of estimating entropic contributions to the free-energy, which is not possible using a single low-energy conformation. Conformational sampling may be performed by taking into account multiple poses from docking [71], multiple copy simultaneous searching (MCSS) [72], systematic sampling [73], grand canonical Monte Carlo (GCMC) sampling with or without explicit water molecules [74-76] or explicit solvent molecular dynamics [77]. Molecular dynamics is used in various free-energy difference methods such as linear interaction energy (LIE) [78], thermodynamic integration (TI) [79] and free energy perturbation (FEP) [80-82]. These methods are all reported to be able to provide affinity predictions with mean errors down to 1-2 kcal/mol, which is the current limit of prediction accuracy. Though system dependency is still reported for these methods, GCMC and FEP are especially promising tools in drug discovery.

In GCMC a sequence of simulations at successively decreasing chemical potentials of the ligand is run using random particle translation, rotation, insertion and deletion steps with a Metropolis acceptance criterion. The binding free-energy is a direct outcome (a particular level of chemical

potential) of the simulation and no processing of the trajectory is needed to calculate it. The method is faster than classical MD simulations, very easy to parallelize, can be used in combination with implicit solvent models or explicit water molecules, the number of parameters to be set for the simulation is small and its outcome is independent of an assumed starting binding conformation as in FEP. The performance of course depends on the accuracy of the force field and the solvation model used. While the method is very promising, it has not been incorporated in standard user-friendly drug design packages yet.

In FEP an alchemical transition between two similar ligands is simulated (see Figure 12). The force field parameters of the starting ligand are gradually changed to the parameters of the final ligand and the conformational space is sampled for each stage of the interleaving procedure. The binding free-energy difference is calculated by integrating the energy differences along the simulation path. This method also provides very good affinity predictions, but it is also dependent on the accuracy of the force field, the exhaustiveness of the sampling and also the initial guess of the ligand binding mode. With recent improvements in computing performance, force fields [83] MD sampling [81, 82] and user interfaces [84] FEP is becoming a standard tool for medicinal chemistry. Combined with quantum mechanics it has the potential to provide the most accurate estimation of binding affinities [85]. QM/MM-FEP has also the advantage of eliminating force field errors, since in this method ligand force field parameters will no longer be needed.

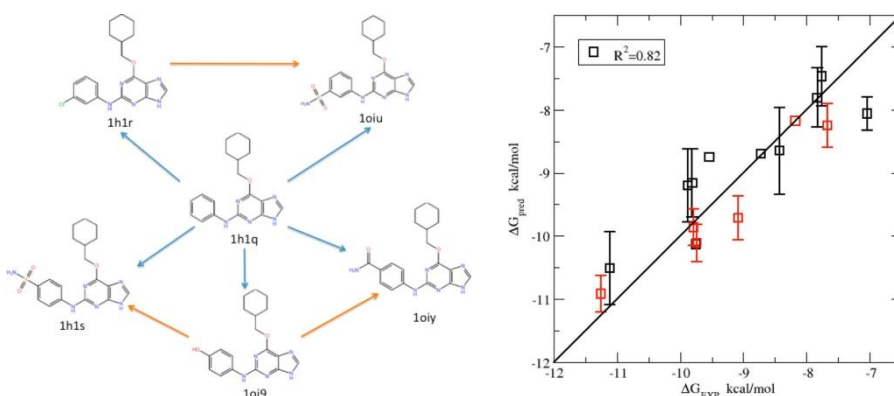


Figure 12. Alchemical transitions (left) and binding free-energy calculation accuracy (right) of CDK2 inhibitors by FEP [81].

High-throughput docking is routinely used in prospective virtual fragment screening campaigns. Rescoring methods – due to their increased computational resource requirements – are generally used in later phases

of fragment optimization. In the following several case studies of prospective fragment screening campaigns are collected from the literature. Some of these studies include also retrospective validation of the used methodologies. Table 3 summarizes the main features of the reported cases and prospective hit rates can be compared. Details of the virtual fragment screening methodologies in the specific case studies are described subsequently.

Table 3. Performance of reported virtual fragment screening campaigns.

Target	VFS method	Origin of fragments	Number of screened fragments	Number of hits	Hit-rate	Ref.
5 enzymes	general library, GOLD docking	ATLAS	500-1000	>7	0.5-10%	22
Thrombin	GOLD docking	ATLAS	80	>3	> 4%	86
BRD4	Glide docking	ZINC	41	9	22%	87
DPP-IV	FlexX docking	ACD	14	7	50%	88
AmpC β -lactamase	DOCK docking	ZINC	48	23	48%	61
CTX-M β -lactamase	DOCK docking	ZINC	69	10	14.5%	89
PTR1	DOCK docking	Uni. Dundee commercials	45	10	22%	90
6PGDH	DOCK docking	ACD	71	10	14%	91
AKR 1C1,1C3	FlexX docking	ZINC	70	24	34%	92
PI3K	Glide docking to homology model	AstraZeneca commercials	210	18	9%	93
MNK1,2	various ligand-based methods	CNIO in-house & commercials	1236	26	2%	94
nAChR α 7	similarity search	GDB-13	60	3	5%	95
H ₁ R	PLANTS docking and IFP	ZINC	26	19	73%	99
H ₃ R	structure- and ligand-based FLAP	ZINC	29	18	62%	100
A _{2A} R	DOCK docking	ZINC	22	14	64%	101
Arf1-Arno	Surflex docking	ChemBridge fragments	33	4	12%	102

2.2.4 VFS in high-throughput X-ray screening

Among the biophysical methods used frequently for fragment screening the heaviest restriction on the number of compounds in a screening campaign is imposed for X-ray crystallography. Even when fragments are

screened in cocktails and automated high-throughput detection is used, the number of fragments screened is in the several hundred range. It is thus not surprising that virtual screening to enrich fragments with a higher chance of binding to the target was first reported in combination with X-ray crystallographic screening. Astex reported the use of focused libraries in their Pyramid screening campaigns against 5 enzyme targets in 2005 [22]. They used different methodologies to assemble fragment libraries of 500-1000 against the five targets. They acquired a general 327-member set from frequent ring systems and linkers found in drug molecules, and used GOLD docking to identify target-specific sets. The in-house commercial compound library was filtered using fragment physico-chemical criteria and then docked to multiple crystal structures of the enzymes using pharmacophore constraints. Different scoring functions were analyzed and the one best reproducing known fragment binding modes for each target were used in fragment selection. The focused kinase set contained 116 fragments and the focused phosphatase set contained 264 compounds. Fragments were screened in cocktails of 4 and hit rates of 0.5-10% were reported. In another paper by Astex a screening campaign against thrombin was described in detail [86]. A similar virtual screening protocol was used as in the previous paper but additional pharmacophores were designed to reward the placement of hydrophobic groups in the S1 pocket. Finally 80 fragments were screened using X-ray crystallography and 3 of the hits were disclosed in the paper, two of which were found in the S1 pocket but one surprisingly occupied the S2-S4 region, while leaving the S1 pocket vacant. Two of the fragments were linked based on their binding mode to afford a 1.4 nM inhibitor.

Similar fragment enrichment for crystallization was performed using the Glide docking software against the BRD4 bromodomain in a recent publication [87]. The ZINC database was filtered for fragment criteria, clustered and cherry picked by medicinal chemists for a 487-member library. These compounds were docked with the single precision protocol in Glide to the crystal structure with conserved water molecules retained using also an H-bond constraint. After visual inspection of the results 60 co-crystals with 41 fragments were obtained and 9 showed clear electron density in the binding site.

2.2.5 VFS against other enzyme targets

As in the Astex papers, virtual fragment screening has been reported mostly against crystal structures of enzymes and specifically for kinases. In some cases homology models have also been used when the experimental structure was not available. More recently it has been applied also to new

target classes such as G protein-coupled receptors (GPCRs) and protein-protein interface (PPI) targets. FlexX was used to dock fragments to the crystal structure of dipeptidyl peptidase IV [88]. 10,000 small primary aliphatic amines were filtered for docking from the Available Chemical Directory (ACD). Two of four selected acceptor points were required to be engaged in H-bond contact and in addition a spatial constraint within the S1 pocket was defined. After visual inspection of the results 14 fragments were screened in a biochemical assay and 7 produced greater than 50% inhibition at 100 μ M.

Shoichet et al. were the first to compare the performance of virtual fragment screening to drug-like molecule screening and HTS. They used AmpC [61] and CTX-M β -lactamase [89] as model systems in their studies. They used crystal structures with the catalytic waters retained for docking of 137,639 and 67,489 fragments filtered from the ZINC database, respectively (in the former, restrictions on H-bond donor and acceptor numbers were relaxed). DOCK 3.5.54 was used for docking and the top 500 and 1000 poses were visually inspected for contacts to key catalytic residues and chemical novelty. For the AmpC β -lactamase 48 fragments were purchased and tested in both enzyme and SPR assays, of which 23 had K_i value lower than 10 mM. Also 8 crystal structures were determined, 4 provided good agreement with the docking pose, 2 had a larger RMSD but retained key contacts, and finally for 2 docking failed to identify the experimental binding mode. In this paper 20 random fragments were also screened, of which none showed inhibitory activity. For the CTX-M β -lactamase 69 fragments were purchased and out of the 10 validated hits in the enzyme assay, crystal structures for 5 were determined. 4 showed good agreement with the docking pose and one had a larger RMSD but key contacts were recovered. In this latter paper also a lead-like library of 1.1 million compounds was docked and out of the 37 compounds tested none showed activity in the enzyme assay. The authors conclude that fragment docking generally provides reliable binding modes and that docking is able to prioritize fragments for screening. However, the head-to-head comparison of hit rates to random screening was very limited.

DOCK 3.5.54 was also used to dock 26,084 commercially available fragments to the crystal structure of pteridine reductase 1 [90]. Results were also filtered by a pharmacophore hypothesis and for chemical novelty and subsequently clustered by their H-bonding patterns. Clusters were visually inspected and finally 45 compounds were tested of which 10 showed higher than 30% inhibition at 100 μ M. One crystal structure was obtained, which confirmed the predicted binding mode. The same group used DOCK 3.5.54 to dock 64,000 fragments from ACD to the crystal structure of 6-phosphogluconate dehydrogenase [91]. After a similar virtual

screening methodology 71 promising compounds were identified for purchase, of which 10 were true hits in the enzymatic assay at 200 μM but IC_{50} values were only determined for 3 providing higher than 50% inhibition at 50 μM .

More recently FlexX 3.1 was used in a virtual screening campaign against crystal structures of aldo-keto reductase 1C1 and 1C3 [92]. The ZINC database was filtered for trusted vendors and fragment likeness, which provided a library of 143,000 compounds to be docked to the two binding sites using an H-bonding constraint to the catalytic tyrosine. 37 available compounds for AKR1C1 and 33 available compounds for AKR1C3 were obtained and out of the 70 tested compounds 11 were insoluble at the assay conditions but 24 were discovered with low μM K_i values for AKR1C1, AKR1C3, or both, thus even selectivity could be pursued in this study, which is not always the case for fragments.

2.2.6 VFS without a target crystal structure

A homology model of phosphatidylinositide 3-kinase p110 β was constructed at AstraZeneca for virtual fragment screening, since the experimental structure of this enzyme was not available at the time [93]. The homology model was based on two crystal structures of the p110 γ isoform and constructed using MODELLER. 183,330 unique fragments from the AstraZeneca compound collection were docked using Glide 5.0 single precision protocol. Binding modes were analyzed for H-bonding interactions with 3 residues and hydrophobic contacts with 8 residues in the binding site, clustered and after visual inspection 210 compounds were selected for screening. 18 fragments belonging to 5 chemical families displayed measurable IC_{50} 's but no high selectivity against other PI3K isoforms.

Since only an apo crystal structure of mitogen-activated protein kinase-interacting kinase 1 was available, Bischoff et al. decided to use several complementary ligand-based virtual fragment screening methodologies to identify pharmacological tools for this enzyme [94]. They used the CNIO in-house library and a commercial compound library to filter fragments matching the models. 249 structures were selected using a staurosporine-derived pharmacophore, 140 molecules from similarity searches against known MNK1 and MNK2 ligands, 124 compounds using FTrees similarity, 231 compounds using 3D similarity eMaps plus 400 diverse compounds representing the CNIO compound library. Out of the 1236 compounds selected by these methods 26 were confirmed as hits with IC_{50} values less than 10 μM for MNK1. One was selective against MNK2, while another showed activity on MNK1 and MNK2 but selectivity against 24 other kinases and could be used as a pharmacological tool.

Blum et al. were the first to use the GDB-13 database of one billion virtually enumerated compounds containing up to 13 heavy atoms for virtual screening against the alpha-7 nicotinic acetylcholine receptor [95]. Structure based approaches were not considered since at the time of publication the closest homolog with known crystal structure was a snail acetylcholine binding protein and since docking of one billion compounds is not feasible. Instead they used the molecular quantum numbers (MQNs) and the city block distance metric for fast similarity searching against nicotine, an agonist of the alpha-7 nicotinic acetylcholine receptor. Out of the 31,504 hits 48 known actives were retrieved and only 692 were commercially available. Out of 60 commercials ordered 3 previously unknown inhibitors were identified.

2.2.7 The SAMPL3 challenge for VFS

The SAMPL3 challenge initiative by OpenEye provided opportunity to a head-to-head comparison of virtual fragment screening methodologies and experimental screening on a validated data set. The test data for SAMPL3 was provided by Newman et al. where 500 fragments from the Maybridge fragment library were soaked into crystals of bovine pancreatic trypsin and their structures were determined by X-ray crystallography [96]. Binding affinity data were also obtained by SPR, 20 of the 500 were designated as actives with a $K_D < 1\text{mM}$. Modelers could submit sorted lists of the 500 fragments and evaluate their results in the context of the full experimental data. One group used RosettaLigand for docking after selecting the best methodology on previously known trypsin ligand binding modes and affinities from the PDB [97]. They used multiple crystal structures for docking and rescoring by interaction fingerprints (IFPs), which methodology provided an area under the receiver operating characteristic curve (ROC AUC) of 0.843 (where 0.5 means random selection and 1 means perfect enrichment of actives). However, surprisingly for the prospective data set this method provided nearly random selection and an AUC of only 0.505 with no sign of early enrichment of actives in the sorted list of fragments. Analysis of the data showed that the use of a different scoring function and differently derived partial charges for the ligands might have provided better enrichment.

Another group also used the data from the PDB for selecting the best retrospective methodology [98]. They used a single high-resolution structure of trypsin for docking and evaluated five different protocols with GOLD 5.0 and four protocols with Glide 5.5 and found that GOLD with GoldScore was more reliable in pose prediction and affinity ranking than Glide. Using their three top ranked protocols they obtained high AUC values

of 0.776-0.787 for the prospective data set with substantial early enrichments. The four protocols using Glide showed inferior performance also on the prospective data set.

2.2.8 VFS on non-enzyme targets

With the advances in crystal structure determination of membrane embedded and transiently interacting proteins, recently virtual fragment screening has also been attempted on new target classes, namely G protein-coupled receptors (GPCRs) and protein-protein interface (PPI) targets. de Graaf et al. performed virtual fragment screening against the crystal structure of the histamine H₁ receptor [99] and a homology model of the histamine H₃ receptor based on the H₁R crystal structure [100]. In the former paper 108,790 fragments from ZINC containing a basic moiety were docked into the H₁R crystal structure using a protocol optimized retrospectively on H₁R binding data from the ChEMBL database. The PLANTS software was used for docking, binding modes were filtered for ionic interaction with the conserved aspartate residue and interaction fingerprints were used for rescoring calculating the similarity to the crystallographic doxepin binding mode. Out of the 354 fragments passing these filters 282 were chemically novel and after visual inspection 26 were screened in biochemical assay. The filtering process is shown in Figure 13. Of the selected fragments 19 had affinities ranging from 10 μ M to 6 nM for H₁R providing an unprecedented hit rate of 73%.

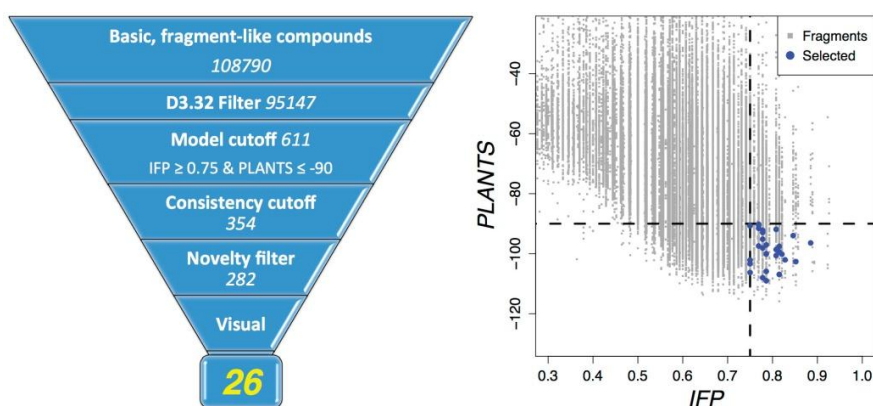


Figure 13. Virtual fragment screening workflow against the histamine H₁ receptor and selected fragments plotted in the space of calculated model scores [99].

In the virtual screening against H₃R both structure-based and ligand-based protocols were applied. Retrospective validation on in-house and ChEMBL data was carried out and FLAP methods (Fingerprint for Ligands

And Proteins) were found superior to both ligand-based methods such as ECFP-4 fingerprint based similarity metrics and shape-based ROCS similarity and structure-based methods such as docking by GOLD or PLANTS software. The FLAP method uses four-point pharmacophores to align molecules with known biological activity. Linear discriminant analysis is then used to identify a reference ligand for the alignment of molecules and derive a linear combination of probe scores that is capable of discriminating molecules with different biological activity. FLAP is trained on a similar number of active and inactive molecules and is thus not biased towards any biological activity range. 156,090 positively charged fragment-like compounds from ZINC were subjected to both structure-based and ligand-based FLAP models and 202 consensus hits and the top 200 molecules from the ligand-based model were visually inspected. 29 novel compounds were selected for testing, of which 18 were confirmed with affinities ranging from 0.5 to 10 μM for H_3R .

A head-to-head comparison of target immobilized NMR screening (TINS) and virtual screening was carried out against the adenosine $\text{A}_{2\text{A}}$ receptor by ZoBio [101]. In that study an in-house library of 500 chemically diverse fragments was docked using DOCK 3.6 to an antagonist-bound crystal structure of the $\text{A}_{2\text{A}}$ AR prior to experimental screening. The TINS screen resulted in 94 primary hits, but only 5 were confirmed in a radioligand displacement assay. 4 of these hits were found in the top 25 fragments by docking. To test whether docking identified false negatives of the NMR screen, five compounds with reasonable binding modes were selected from the top 50 fragments of the ranked library and screened in the radioligand displacement assay, three of which turned out to be inhibitors with high ligand efficiency. After these encouraging results 328,000 commercially available fragments from ZINC were docked using the same protocol to the $\text{A}_{2\text{A}}$ AR structure, the top 500 binding modes were visually inspected and 22 were ordered and screened. 14 molecules showed significant radioligand displacement and the K_i values ranged from 2 to 240 μM .

Finally, a paper by Chavanieu et al. described virtual fragment screening against a protein-protein interaction target, the Arno Sec7 domain regulating GDP/GTP nucleotide exchange by the Arf1 ADP-ribosylation factor [102]. They identified hot spots on the experimentally determined Arf1-Arno4M complex with a computational alanine scanning approach. Arno4M contains four mutations that allowed the crystallization of the complex. Surfex was used to dock the ~ 3000 fragments of the ChemBridge fragment library to four identified sub-sites at the computationally back-mutated wild type Arno surface. After visual inspection of the top solutions to identify bad contacts, 33 fragments were purchased together with 40 randomly selected fragments. Four of these fragments were confirmed

inhibitors that did not show aggregation-based effects. All four fragments were identified in the docking screen and none from the randomly selected set.

2.2.9 Concluding remarks on VFS

Taken together these results show that virtual fragment screening is a viable approach for enriching active fragments for experimental screening and hit rates as high as 73% could be achieved. It seems that workflows generally include docking with pharmacophore constraints or post-processing with pharmacophore hypotheses or interaction fingerprints and visual inspection of the predicted contacts with the target and some medicinal chemistry expertise to maximize the outcome of virtual screening.

2.3 Fragment optimization and *de novo* design

Once validated and well-characterized fragment hits have emerged from a screening campaign the hit-to-lead optimization can begin. As opposed to lead optimization from an HTS hit where usually large and lipophilic compounds need to be converted into smaller and less lipophilic ones while moderately increasing potency, fragment optimization needs a qualitatively different mindset, as a larger increase in potency is needed accompanied by a moderate increase in molecule size and maintenance of good physico-chemical parameters. While this is also a non-trivial task and examples of toilsome fragment optimizations are found in the literature, the entering speed of fragment originated candidates in clinical trials can be seen as a victory march of fragment-based drug discovery. Its success lies in the intrinsically higher potential of fragments for optimization, which stems from the thermodynamic and structural requisites of fragment binding. Computational methods applied in fragment optimization aim to predict modifications that simultaneously increase affinity and maintain these advantageous thermodynamic and structural features.

2.3.1 Optimization potential of fragments

While it had frequently been stated that fragment optimization has the potential to provide leads and drugs with better physico-chemical parameters, this advantage is not always fully exploited. For example Astex has reported 50 Da lower molecular mass and 1 clogP unit lower lipophilicity for their leads compared to literature HTS leads [103] (see Table 4) but it is at least as much the result of company culture as it is of the

favorable properties of fragments. In FBDD not only library design and screening campaigns have to be conducted in the most rigorous way, but control over the parameters needs to be maintained throughout the whole optimization process. If not optimized with sufficient care, fragments can also fall victims to molecular obesity and lose superiority over HTS derived leads [104]. Monitoring of various ligand efficiency (such as LE, BEI, SEI, SILE, %LE) and lipophilic efficiency metrics (such as LLE, LLE_{AT}, LELP) can help overcome the difficulty of hit prioritization for better optimization potential and maintaining the balance between potency and physico-chemical properties in the subsequent optimization process [105]. Compounds with favorable lipophilic efficiency values also have a higher chance of being more selective and having fewer ADMET and pharmacokinetics related problems, which might contribute to lower attrition rate of fragment derived candidates in later phases of development [106]. This is also in line with the finding that fragment binding is enthalpy driven as opposed to entropy driven binding of larger molecules [18] (refer to Figure 5). Enthalpic binding has also been associated with higher selectivity, lower attrition rates and a higher chance of finding a best-in-class drug [107].

Table 4. Comparison of the average physical properties of literature HTS leads, oral drugs and fragment-derived leads and hits from Astex [103].

	N	pIC ₅₀	MW (Da)	clogP
Astex fragment hits	39	3.8	173	1.4
Astex leads	39	7.5	366	3.0
Literature HTS leads	335	7.6	416	4.0
Oral drugs	592	7.3	357	2.6

2.3.2 Physical background of fragment optimization

The physical background of the superiority of fragment hits lies in their ability to form high quality interactions with the protein targets. Fragments can be seen as the minimal interaction pattern needed for binding to the respective target. In high throughput X-ray, NMR or SPR screening fragments with heavy atoms as few as 5-6 can be detected and can be progressed to optimization. An analysis of 1297 high resolution complex structures from the Protein Data Bank revealed that fragments form on average two H-bonds with near optimal geometry while also experiencing favorable hydrophobic embedding in the so-called hot spot of the protein target (refer to Figure 5). Hot spots are enclosed cavities of the protein with linear extent not exceeding 10 Å on average and their characteristic H-bonds are separated at an average of 5 Å. These characteristic H-bonds are

well conserved among different small molecules bound to the same protein. It has also been shown that larger compounds feature only one extra optimal geometry H-bond on average compared to fragment sized ligands [18]. While the findings of the study very well explain the efficiency of fragments for small molecule binding sites, interestingly FBDD is increasingly and successfully used for protein-protein interaction (PPI) targets as well, where usually large and surface exposed binding sites are involved. In these cases generally multiple fragments binding to different parts of the PPI binding site are identified and subsequently linked together to form high affinity inhibitors.

The conserved H-bonding pattern can also be regarded as the foundation stone for fragment optimization. For structure-based optimization and understanding of the SAR to be possible it is a prerequisite that initial fragment hits do not change their binding modes throughout the optimization process. Astex has indeed shown that for 39 of their fragment hit-lead pairs the average shift of the fragment binding pose was only 0.8 Å (RMSD) and for no individual pair the shift exceeded 1.5 Å (RMSD) [103]. These data are shown in Figure 14. Orita and co-workers have found a similar 0.7 Å mean shift for 25 fragment hit-lead pairs from the literature with a maximum of 1.7 Å [105]. While this might be generally true, there are examples of successful optimizations where the original fragment changed its binding mode. There are cases when despite the larger RMSD the specific interactions are maintained but also cases when the fragment adopts a totally different binding mode [108]. During optimization not only the fragment binding mode but the protein structure might change as well. Astex has reported essentially no fragment induced protein movements (maximal protein atom movement < 1 Å) in the fragment screening against one third of 25 protein targets while for half of the targets induced fit effects accompanied by a protein movement larger than 5 Å were found for specific fragments (see Figure 14). Examples include amino acid side chain movements, helix collapse, movement of the flap region in kinases or other loop rearrangements [103].

The conservation of the binding mode facilitates predictions based on the complex structure. In an ideal scenario the optimization process is monitored by crystallography or structural information from NMR is obtained. Using this information from the complexes modifications of the ligand can be evaluated in an iterative manner using hypotheses derived from medicinal chemistry knowledge or computational models and testing these hypotheses experimentally. As seen in fragment library design and fragment screening, computational tools can be used in every aspect of fragment optimization as well and form an efficient combination together with experiment. Such a workflow in general includes the enumeration of

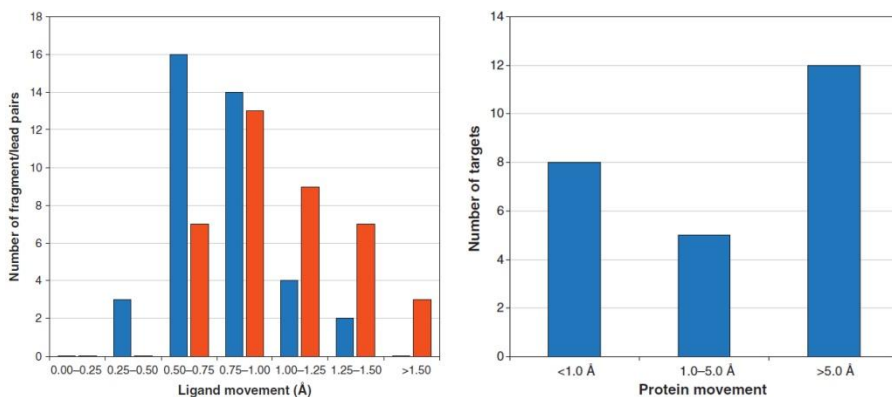


Figure 14. Root mean square (blue bars) and maximum (red bars) ligand movement (left) and maximum protein movement (right) in fragment optimization [103].

the chemical space around the fragment hit and then filtering the enumerated structures using predictive models for various desired properties. The top few idea compounds that fulfill the required criteria are then synthesized and tested experimentally, and structural information is used as a seed in the next round of iteration. The two basic steps in this workflow, namely enumeration and filtering can be done using medicinal chemistry knowledge, however, computers have the advantage of being able to enumerate a much larger chemical space than humans. Also models might suggest modifications that would otherwise elude human thinking thus contributing to the navigation in free IP space. When models with good predictive power are available, they can even entirely guide the optimization process.

2.3.3 *De novo* drug design

The terms *de novo* design and fragment-based design have recently been used interchangeably. *De novo* means to build something from the new, and is used for the design of new complex molecules from the assembly of their simpler structural constituents ranging from atoms through functional groups to fragments. While the concepts of *de novo* design and fragment-based design originated from different scientific communities (however, both started in the mid-1990's), they have so much in common that they converged and profited from the results of each other. Early examples of *de novo* design suffered from the purely computational set-up, which might have proposed compounds with improved potency, but these compounds would be too complex or having no drug-like properties or they would otherwise be an unsuitable idea. Recent improvements include better models for the prediction of affinity and selectivity, ADMET

properties, synthetic accessibility and structural novelty, etc. Also every computational tool has its own strengths and weaknesses. There is always a compromise between evaluating compounds with truly novel structures and predictivity, since computational models are trained on existing data. Also there is always a compromise between exhaustiveness of the method and need for computational resources. There will always be a more predictive model with higher computational cost. Thus it is seen, that best results are obtained when experiment and computation go hand in hand.

When complex crystal structures are not available for difficulties in crystallization or lack of resources but the protein structure is available with different binding partners or through homology modeling, structure-based and *de novo* computational tools can still be of help in guiding optimization and generating ideas for medicinal chemistry work. Though membrane proteins such as GPCRs require specialized techniques both in fragment screening and structural characterization, FBDD might be a promising tool for this target family as well. When no structure of the target or a close enough homologue is available, one can rely only on a combinatorial SAR expansion and possibly ligand-based *de novo* computational tools. Optimization without structure is considerably more challenging and will require more synthesis for hypothesis testing and establishing SAR and heavier investments in characterization of binding.

In the following different strategies for fragment optimization as well as structure-based and ligand-based computational methods applied in the process are summarized with focus on recent developments in techniques and methodologies. The various efficiency metrics and their potential in FBDD will also be discussed. Optimization possibilities on GPCRs and targets lacking crystal structures will shortly be presented. Finally a few fragment optimization case studies will be presented where computational tools played a crucial role. For further information the reader is referred to recent reviews discussing computational techniques in FBDD [52, 54, 108].

2.3.4 Strategies of fragment evolution

The two main strategies to optimize fragments into novel chemical entities are growing and linking. In growing a single protein-bound fragment is identified and new functional groups are one-by-one attached to this core fragment to exploit new interactions with the target (see Figure 6). As outlined earlier the anchoring fragment rarely changes its binding mode upon growing; however, the protein structure might undergo larger ligand-induced conformational changes, even new subpockets might open during fragment optimization [109]. The initial binding mode of the fragment can be available from experiment or docking studies. When the X-ray structure

of the protein-fragment complex is available, finding the best growing vectors and functional groups can be done automatically using computational *de novo* design tools.

In linking two or more protein-bound fragments are identified and joined together synthetically by suitable linkers that allow all of the fragments to retain their binding modes and specific interactions (see Figure 6). Fragments suitable for linking might come from co-crystallization of fragment cocktails with the target, second-site screening by SPR or NMR, particularly interligand Overhauser effect (ILOE) experiments, or virtual identification of simultaneously accommodated fragments in the binding site with tools such as multiple copy simultaneous search (MCSS) [110] or simultaneous docking of multiple fragments [111, 112]. In theory the linked compound should have binding free-energy greater than the sum of the binding free-energies of its constituting fragments because of the preorganization of binding elements. Though this approach might seem straightforward, it is often difficult to pursue synthetically, because of the high entropy loss of the linked fragments and the linker itself compared to the unlinked fragments [113]. Thus the selection of the ideal linker is not an easy task and computational tools can be of great help in it. De Esch et al. collected a remarkable variety of fragment optimizations from the literature including both growing and linking examples [114].

2.3.5 *De novo* design algorithms

De novo design tools have the same general workflow: enumeration of the possible chemical space using the fragment as a seed and scoring of the resulting virtual compounds using a suitable fitness function. They can differ in the implementation of these steps, namely the types of building blocks used in enumeration, the rules for attaching these building blocks to the core fragment, the algorithm used for optimization in the chemical space and the fitness function with respect to which the optimization is pursued. Building blocks can be atoms, functional groups or small fragments. Atom-based methods like LEGEND [115] have the advantage that they can theoretically enumerate the whole chemical space and find truly novel structures, however, these approaches consider too many possible molecules, many of which are problematic in terms of chemical stability, synthetic accessibility or druglikeness. If small fragments are used as building blocks the number of molecules to be considered is much lower and they are more probably synthetically accessible and drug-like. Fragment building block libraries can be assembled by methods described in the first section: filtering of public databases or proprietary building blocks as in AutoGrow [116], fragmentation of drug-like molecules as in COLIBREE [117],

Flux [118, 119], MEGA [120], PROTOBUILD [121] and using pharmacophore or bioisostere libraries as in Fragment hopping [122] and PhDD [123]. Such libraries may be categorized into ring systems, linkers and side chains if these specific subsets need to be used, e.g. a linker library for fragment linking in CONFIRM [124]. Modern *de novo* tools mostly use fragment libraries instead of atom-based build-up.

The simplest way of fragment assembly is the brute-force method, when all fragments are attached to all growing or linking vectors and unwanted chemistry or compounds not fitting in the binding site are filtered out. However, there are various ways of getting rid of the enumeration overhead. It is possible to identify possible growing vectors based on the crystal structures as in AutoGrow and to use retrosynthetic assembly rules to ensure synthetic accessibility already in the enumeration phase as in FlexNovo [125] and Flux. PROTOBUILD uses both approaches to reduce the search space. It is also possible to enumerate only those compounds that fulfill predefined min-max criteria of specific molecular descriptors like molecular weight, logP, rotatable bond count, etc. further reducing enumeration and evaluation costs [126]. Fragment assembly may also be biased towards drug-like compounds if the frequency of specific fragment linkings is matched to the frequencies in a drug-like or natural product database as is done in FOG [127]. Another method of fragment assembly is hybridization of molecules with known or predicted binding modes. The BREED algorithm identifies overlapping bond vectors in a set of compounds bound in the same binding site and swaps the fragments on the two ends of the bond [128]. If one of the bonded atoms is hydrogen, the method can be utilized as a fragment growing technique. A few novel methods inspired by the original BREED algorithm have been described: automatic tailoring and transplanting (AutoT&T) uses virtual screening hits for breeding taking into account also synthetic accessibility [129], while MED-Hybridise breeds multiple ligands in one iteration step using local similarity of protein surfaces from protein-ligand complexes from the whole PDB [130].

The choice of optimization algorithm is crucial in efficient sampling of the huge chemical space of drug-like molecules and in finding the appropriate regions which correspond to compounds with optimal affinity, chemical, physico-chemical and ADMET properties. Nature inspired algorithms such as genetic algorithms, evolutionary graph-theory, particle swarm optimization and ant colony optimization turned out to be especially useful in navigating the huge chemical space and guide the optimization against multiobjective constraints [131]. For example AutoGrow, Flux, MEGA, PROTOBUILD, GANDI [132] and LigBuilder 2.0 [133] use evolutionary algorithms in the search, while COLIBREE and MLSA use particle swarm optimization.

Fitness functions may include structure- or ligand based prediction of affinity using the previously presented scoring and rescoring methods or validated pharmacophore, QSAR and 3D-QSAR models in the lack of crystal structures. Synthetic accessibility is often assessed using the RECAP [55], SYNOPSIS [134], SYLVIA [135] or DOGS [136] algorithms. Further fitness parameters include diversity and novelty, druglikeness and ADMET properties, which all have a large number of models described in the literature.

Modern *de novo* tools have the advantage of integrating validated building block libraries, efficient enumeration algorithms and multiobjective scoring schemes. For example FlexNovo uses the incremental build-up strategy of the FlexX docking algorithm, large fragment libraries for enumeration and includes spatial, physico-chemical and diversity filters. FlexNovo has been integrated into the NovoBench platform [137], which also includes synthetic accessibility prediction and ligand-based (Ftrees-FS) search algorithms in order to be used in projects with different amount of structural information. AutoGrow uses the free AutoDock software to enumerate and redock evolved fragments into the protein binding site using an evolutionary algorithm. GANDI is a novel tool that is based on the linking strategy of predocked fragments from a user-defined fragment library. Its optimization scheme combines an evolutionary algorithm with taboo search simultaneously evaluating force field energy and similarity to known reference compounds. The relative weights of these terms can be tuned thus the method may be used in a purely structure- or ligand-based mode or in a combination of the two. Fragment hopping uses minimal pharmacophoric elements to find fragments from five different fragment libraries and places them in the preferred spatial orientation proposed by LUDI [138] and MCSS and joins them together. Evaluation of the virtual compounds includes diversity, isozyme selectivity, redocking and ADMET filters. LigBuilder 2.0 uses a genetic algorithm to grow or link fragments in an iterative scheme and uses the embedded SYLVIA tool for assessing synthetic accessibility. It also evaluates binding site complementarity, druglikeness and ADMET filters. MEGA is a new multiobjective optimization *de novo* design framework that combines evolutionary algorithms with graph-theory to design structurally diverse molecules satisfying one or more objectives. It uses ChillScore to score interactions with the target and also similarity to known reference compounds. MOEA [139] and LiGen [140] are among the latest reported integrated *de novo* design tools. Both feature a highly customizable workflow with both structure- and ligand-based fitness functions, ADMET predictions and efficient communication with external software. Synthetic accessibility prediction is part of LiGen but not of MOEA. As an example, MOEA's multiobjective design cycle is shown in Figure 15.

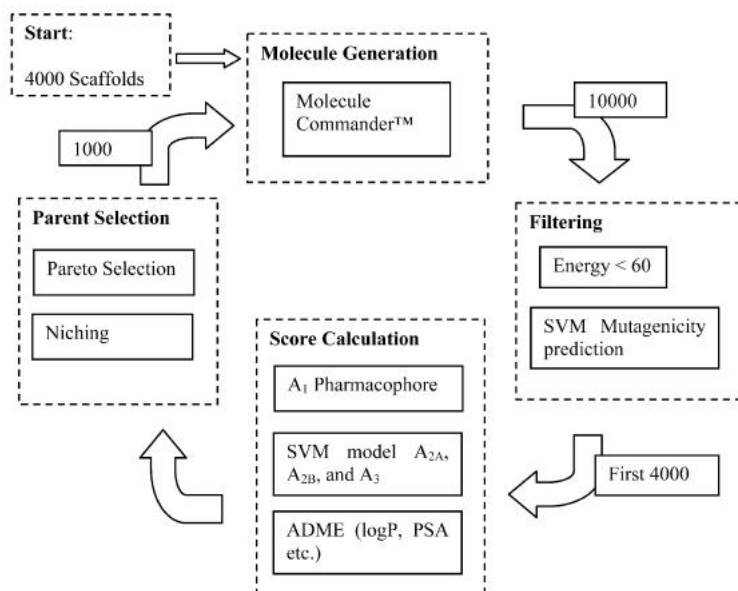


Figure 15. Flowchart of the multiobjective design cycle of MOEA [139].

2.3.6 Ligand-based *de novo* design

Ligand-based *de novo* design algorithms are useful when the structure of the protein-fragment complex is not available as is usually the case with membrane protein targets such as GPCRs and ion channels. COLIBREE, Flux, PhDD, NEWLEAD [141], SQUIRREL [142, 143], EA-Inventor [144] and Qsearch [145] are examples of pharmacophore-based *de novo* platforms. NEWLEAD was the first pharmacophore-based *de novo* design method; however, it can only process specific pharmacophoric functional groups rather than chemical features. Flux reassembles fragments obtained by the RECAP procedure using predefined assembly rules and an evolutionary algorithm evaluating the resulting compounds with topological atom-pair descriptors and similarity to reference molecules as fitness function. COLIBREE uses particle swarm optimization to vary linkers and side chains on a fixed scaffold evaluating topological pharmacophore similarity to reference ligands as the fitness function. This allows for positive and negative design to be performed simultaneously. SQUIRREL compares both molecular shape and potential pharmacophore features and can suggest bioisosteric replacement groups for a reference compound. PhDD is able to work with abstract pharmacophore models assessing also druglikeness, bioactivity, and synthetic accessibility. Tripos's EA-Inventor works on connection tables of structure populations using an evolutionary algorithm. Any user-defined scoring function can be used as the fitness function.

EASFD combines the EA-Inventor algorithm for structure evolution with Surflex-Dock for scoring [146]. EASFD has later been developed into the commercial product Muse [147]. Another approach called NovoFLAP combines the EA-Inventor algorithm with a powerful ligand-based scoring function that uses both molecular shape and pharmacophore features in a multiconformational context (FLAP) [148]. Qsearch is a fast algorithm that stochastically constructs new molecules from fragment spaces considering a three dimensional pharmacophore including not only feature addition steps but also undecoration of the compounds. Finally an interesting and surprising approach called the meta-structure approach can provide an alternative route for lead identification when no structural information of the target is available [149]. This method searches for protein targets with similar activity but possibly completely different fold based only on primary sequence and exploits structural information of known active ligands of the similar protein targets in *de novo* compound design.

Use of modern *de novo* design tools in the absence of structural information have been reported in the optimization of GnRH receptor, serotonin 5HT_{1B} receptor and selective adenosine A₁ receptor ligands. EA-Inventor was used by Neurocrine to select optimal side-chain combinations for a core identified by virtual screening for GnRHR [150]. Compounds were selected based on similarity to reference compounds, fitting to a 3D pharmacophore and property filters, but synthetic accessibility was checked by medicinal chemists. NovoFLAP was used by AstraZeneca to design the first non-basic 5HT_{1B} antagonist [148]. The basic amine moiety from a reference dihydrochromene ligand was redesigned to afford compounds with no hERG or phospholipidosis liabilities. Finally MOEA was developed and used by academic groups in the design of adenosine A₁ receptor ligands selective against adenosine A_{2A}, A_{2B} and A₃ receptors [139]. A 3D pharmacophore model for A₁ and three support vector machine (SVM) models for selectivities along with ADMET filters (Lipinski parameters, solubility and mutagenicity) were used in compound selection, however, also in this case synthetic accessibility was checked by medicinal chemists.

2.3.7 Fragment-based lead discovery on GPCRs

GPCRs constitute the largest target family in drug design, however, due to the complex nature of the membrane embedded dynamics their crystallization is not yet a routine task and usually requires heavy protein engineering investments as well. Besides the undruggable rhodopsin, β -adrenergic and adenosine receptors are the only GPCRs with multiple reported X-ray structures thus structure-based design efforts could be successfully undertaken mainly in these receptor sub-families so far.

Altogether X-ray structures of 21 out of the 779 distinct GPCRs have been solved, thus coverage is still small and for the majority of GPCR drug targets homology modeling with limited accuracy is the only possibility for structure-based studies. Fragment-based lead discovery on GPCRs has been reviewed by Visegrády and Keserű [151]. As mentioned earlier virtual fragment screening has been reported on histamine H₁ and H₃ and adenosine A_{2A} receptors [99-101]. Limited expansion of fragment hits has been pursued in the absence of structural information e.g. on adenosine A₃ [152] and melanocortin MC₄ receptors [153]. Structure-based optimization of several fragment-like adenosine A_{2A} receptor hits using Glide for docking has been reported by Heptares [154] and a complete *in silico* assisted lead discovery project has also been reported for the A_{2A} receptor by ZoBio and academic groups [101]. In this project NMR and docking-based virtual screening were run parallel and showed fair agreement, while also a larger fragment library was screened virtually, which provided further hits. Altogether 14 validated hits were identified and three of them were subsequently expanded guided by molecular dynamics simulations and free energy calculations (FEP) using the free GROMACS software (for an example see Figure 16).

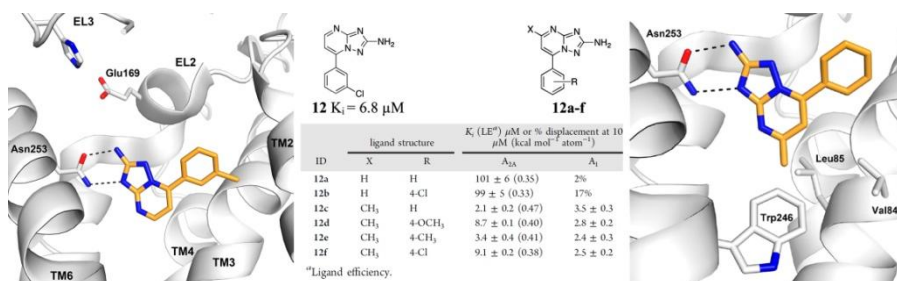


Figure 16. Structure-guided optimization of an A_{2A} fragment hit [101].

2.3.8 Ligand efficiency metrics in fragment-based design

Fragment-based optimization is a multiobjective task, where not only affinity to the target but selectivity, anti-target activity, pharmacodynamic and pharmacokinetic properties all have to be balanced. Fragments have the advantage of possessing favorable binding and physico-chemical properties from the start and the goal is to maintain these favorable properties during optimization. Ligand efficiency and lipophilic efficiency metrics provide an aid in navigating the complex multiparametric property space of compounds. The original LE metric as the binding free-energy per heavy atom of the ligand was introduced by Hopkins in 2004 with selection of HTS hits with better optimization potential in mind [19]. Ligands with LE

values greater than 0.3 kcal/mol are generally considered efficient binders. Alternative metrics with molar mass (in BEI) or polar surface area (in SEI) instead of heavy atom count were proposed by Abad-Zapatero [155]. Since then it was shown that the LE metric is size dependent and overemphasizes the effectiveness of very small fragments. Thus if fragments are prioritized solely based on LE, smaller ligands will stand a higher chance of good ranking. A ligand efficiency metric scaled by an exponential factor of heavy atom count was proposed by Reynolds and the percentage of the actual LE of the maximal achievable LE is called Fit Quality (FQ) [156]. Orita used a similar approach with a different exponential scaling function based on the golden ratio [157]. Nissink proposed an alternative solution for the problem, namely instead of the heavy atom count, the cubic root of the heavy atom count was used in the formula of SILE [158]. Though more simple than FQ, SILE has been debated to retain some size dependency. Formulae of the metrics are summarized in Table 5.

Table 5. Definition of ligand efficiency and lipophilic efficiency indices used in FBDD. Act may represent K_d , K_i , IC_{50} or EC_{50} , HA is the number of heavy atoms.

Name	Definition	Ref.
LE	$-RT \ln(K_d)/HA \approx 1.36 \cdot pAct/HA$	19
BEI	$pAct/MW$	155
SEI	$pAct/PSA$	155
FQ	$LE/(-0.064+0.873 \cdot e^{-0.026 \cdot HA})$	156
%LE	$100 \cdot LE/(\varphi^{\log_2(10/HA)}) \approx 27.6 \cdot pAct/HA^{0.3}$	157
SILE	$-RT \ln(K_d)/HA^{0.3} \approx 1.36 \cdot pAct/HA^{0.3}$	158
LLE	$pAct - \text{clogP}$	4
LLE _{AT}	$0.11 - (\Delta G - \Delta G_{lip})/HA \approx 0.11 - 1.36 \cdot (\text{clogP} - pAct)/HA$	159
LLEP	clogP/LE	104

Lipophilic efficiency metrics were introduced later in order to simultaneously consider binding efficiency and lipophilicity, which is known to have a great effect on compound quality and attrition. LLE (the difference between the negative logarithm of affinity and logP) was introduced by Leeson and Springthorpe to estimate the maximally accepted lipophilicity for a compound of given potency [4]. They proposed a separation of at least 5 log units between potency and lipophilicity. Astex defined a similar lipophilic efficiency index to LLE, which they named LLE_{AT} and reasoned that it is more suitable for comparing hits of different sizes [159]. Finally LLEP defined by the ratio of logP and LE was introduced by Keserú and Makara [104]. Though the LLEP function behaves undesirably for compounds with $\text{logP} \leq 0$, this is rarely a problem in lead discovery programs. It was shown

that compounds with LELP values lower than 10 have higher chances to be free of ADME and safety issues in terms of permeability, clearance, efflux transport, CYP induction, hERG inhibition and cell viability [106]. While LLE does not separate HTS and fragment hits, LELP has the advantage of discriminating preferred starting points effectively. The simultaneous application of the LLE > 5 and LELP < 10 cutoffs could select compounds advanced to Phase II clinical trials and approved drugs from other compound types. Orita [105] and more recently Hopkins et al. [160] reviewed the role of different ligand efficiency indices in drug discovery. According to an internet poll LE was the predominant metric used by the FBDD community in 2011 with lipophilic efficiency metric LLE coming up as second, while a multitude of other metrics are used by fewer groups as evident from Figure 17 [161].

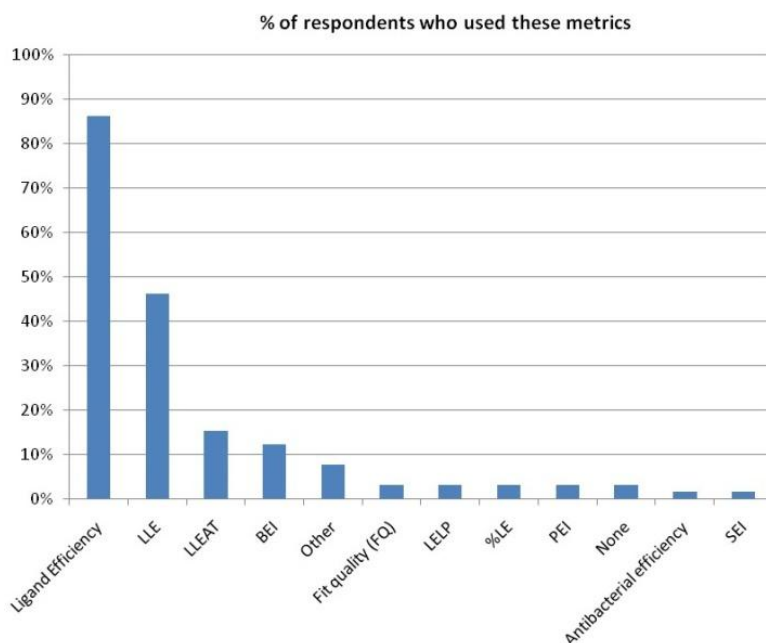


Figure 17. Ligand efficiency and lipophilic efficiency metrics used by the FBDD community in 2011 [161].

Ferency and Keserú analyzed trends in 145 fragment optimization programs and found that accompanying a median affinity increase of 3 and logP increase of 1.5 log units LE is generally unchanged, while SILE is preferably increased during fragment optimization [48]. LLE and LELP usually also increase but not in such a straightforward manner. Hence the authors propose the monitoring of SILE and LELP in the course of optimization in order to arrive to efficient and safe compounds that have a

higher chance of being successful. Distributions of these metrics for fragment hits and their respective optimized compounds are shown in Figure 18.

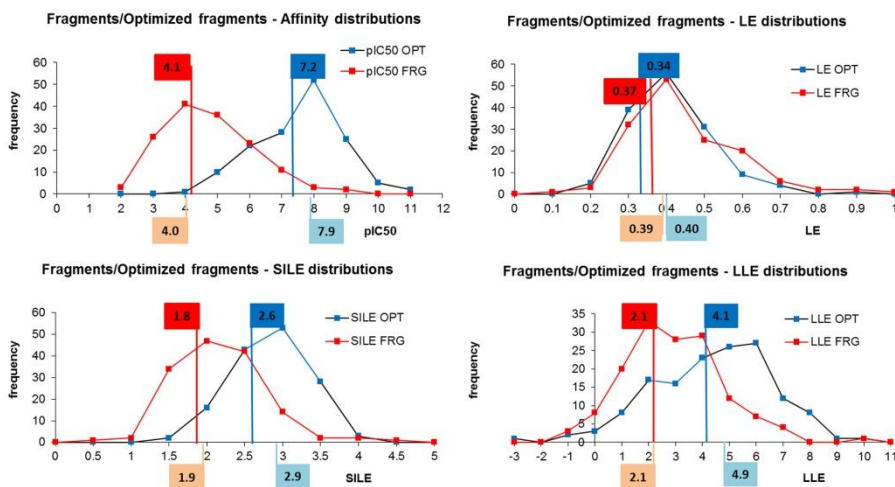


Figure 18. Distribution of affinity, ligand efficiency (LE), a size-independent ligand efficiency index (SILE) and a lipophilic efficiency index (LLE) of fragment hits and optimized compounds. Medians are indicated on the top, while medians for programs resulting in clinical candidates are indicated below the graphs [48].

Chapter 3 – Methods

In this chapter the methods used in primary site screening and secondary site modeling as well as the respective method development phases will be discussed.

3.1 Methods used in primary site screening

As stated earlier my aim was to evaluate different protocols for fragment virtual screening on GPCR targets. This work started with method development on small molecule data sets and the results were subsequently used in a fragment screening setup.

In the method development stage targets representing both aminergic and peptidergic GPCR subfamilies were selected, namely the dopamine D₃ and chemokine CXCR₄ receptors possessing X-ray structure as well as homology models. To evaluate a more general context, where no X-ray structure is available, comparative models of the histamine H₄ and the serotonin 5HT₆ receptors were also included among the targets. All-atom, explicit solvated MD simulations of the membrane embedded receptors were carried out to obtain different receptor conformations for docking. The use of initial X-ray structures, homology models, single structures from the trajectory and various ensembles were compared in retrospective virtual screening setups using the recently published GDD ligand collection in order to assess the performance of different virtual screening methodologies.

In the second stage prospective virtual fragment screening of the Gedeon Richter fragment library was performed on the available dopamine D₃ receptor crystal structure and the previously constructed homology model of the histamine H₄ receptor as well as on the ensemble of snapshots from the MD trajectory. Screening performances of the different protocols were compared by analyzing hit rates and hit compounds obtained by docking to the single structures and the conformational ensembles.

In the following the construction of the receptor homology models, the molecular dynamics simulation protocol, the compilation of the small molecule and fragment ligand sets, the preparation of the protein and the ligand structures for docking and the retrospective and prospective virtual screening protocols will be described.

3.1.1 Homology modeling of the H₄ and 5HT₆ receptors

The initial homology model of the human histamine H₄ receptor was constructed with Prime 3.0 [162] using the 3.1 Å resolution X-ray structure of the human histamine H₁ receptor (PDB code: 3RZE) and the sequence alignment in Appendix A. The N- and C-terminal peptides as well as the ICL3 were not modeled. The conformation of the Phe144^{4.54}–Gln147^{4.57} (amino acid numbering is given both according to Uniprot [163] and Ballesteros-Weinstein [164] as superscripts) kink sequence in TM4 was adjusted to resemble that of Gly162^{4.54}–Ser165^{4.57} from the 2.4 Å resolution X-ray structure of the human β₂-adrenergic receptor (PDB code: 2RH1) since the H₁ sequence is one amino acid shorter in this region than the other histamine receptor sequences. JNJ7777120 (hereafter JNJ, see Figure 19) was first manually docked into the receptor in the binding mode described previously, which is validated by site-directed mutagenesis data [165] and subjected to minimization of the 5 Å environment of the ligand with H-bonds between the protonated amine and D94^{3.32} and the indole NH and E182^{5.46} as constraints using the default settings in MacroModel 9.9 [166]. Then, JNJ was redocked into the minimized structure using Induced Fit Docking [167-169] in the Schrödinger Suite 2011 with the default settings and the same two H-bonds as constraints in both docking stages. Finally, the whole structure was subjected to the Impref minimization step in the Protein Preparation Wizard [170, 171].

The initial homology model of the human serotonin receptor 5HT₆ was built with Prime 3.0 [162] using the 2.7 Å resolution X-ray structure of the human serotonin receptor 5HT_{2B} (PDB code: 4IB4) and the sequence alignment in Appendix A. The N- and C-terminal peptides as well as the ICL3 were not modeled. All the extracellular loops were refined by Prime Loop Refinement [162] using extended sampling. The SB-742457 (hereafter SB, see Figure 19) ligand was docked to the binding site using Induced Fit Docking (IFD) [167-169]. The binding site was defined using the coordinates of the original ergotamine ligand of the template. The best IFDScore complex was visually inspected and was accepted for enrichment study and MD simulation.

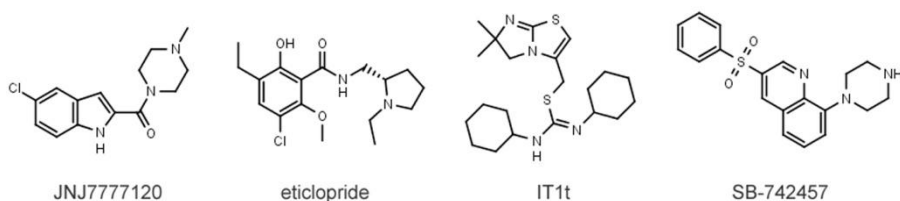


Figure 19. Formulae of the ligands used in GPCR modeling.

Furthermore state-of-the-art homology models of D₃ and CXCR₄ were downloaded from the GPCR Dock 2010 competition homepage [172].

3.1.2 Molecular dynamics simulations using NAMD

The X-ray structure of the dopamine D₃ receptor in complex with eticlopride (PDB code: 3PBL, eticlopride hereafter ETQ, see Figure 19), that of the CXCR₄ receptor in complex with the ligand IT1t (pdb code: 3ODU, ligand hereafter ITD, see Figure 19) as well as the two homology models were subjected to molecular dynamics simulation. The protein–ligand complexes were immersed into a POPC membrane bilayer [173] where the number of the lipid molecules was 99. For the protein atoms ff99SB [174], for ligand and lipid molecules GAFF [175] force field parameters were assigned. The system was solvated by water molecules described by the TIP3P [176] potential. JNJ had partial charges published in ref. 177; for ETQ, ITD, and SB the charges were calculated according to the *resp* protocol [178]. For ETQ, ITD, and SB, conformational analysis (gas phase and MMFF94x force field [179]) was performed using the Molecular Operating Environment (MOE) [180]. During partial charge calculations of the ligands, diverse conformations were selected and subjected to *ab initio* geometry optimizations at the HF/6-31G* level of theory using the Gaussian 09 software [181]. The molecular electrostatic potential was calculated at the same level of theory for each conformer, and atom centered charges were calculated by simple averaging using the *resp* module of AmberTools1.5 [182]. An appropriate number of Na⁺ cations and Cl⁻ anions (25/34, 34/43, 25/30, 25/40 for D₃-ETQ, CXCR₄-ITD, H₄-JNJ, 5HT₆-SB, respectively) were added in order to neutralize the system and mimic the ionic strength inside the cell. The force field parameters for these ions were taken from Joung and Cheatham [183, 184].

The molecular dynamics simulations were conducted with the NAMD 2.7 software [185] using the following protocol in order to equilibrate the membrane/water environment around the GPCR-ligand complexes:

(1) minimization (3200 steps) with restrained protein–ligand atoms (force constant was set to 10 kcal/mol Å²)

(2) minimization (3200 steps) without restraints

(3) heating in *NVT* ensemble from $T_i = 10$ K to $T_f = 310$ K (in 10 steps with $\Delta T = 30$ K and $\Delta t = 4$ ps) with restrained protein–ligand atoms (force constant was set to 10 kcal/mol Å²)

(4) 1-ns-long MD simulation in *Np_zVT* ensemble ($p_z = 1$ atm, $\gamma = 60$ dyn/cm, $T = 310$ K, restrained protein–ligand atoms (10 kcal/mol Å²))

(5) removing of the restraints in 10 steps with 100 ps duration of each, with linear scaling of the force constant from 1.0 to 0.0 ($Np_z\gamma T$ ensemble, $p_z = 1$ atm, $\gamma = 60$ dyn/cm, and $T = 310$ K).

After this equilibration for the D₃-ETQ, CXCR₄-ITD, and 5HT₆-SB systems, 20-ns-long simulations were conducted, which was followed by five independent (using different initial velocities), 5-ns-long MD simulations in the $Np_z\gamma T$ ensemble ($p_z = 1$ atm, $\gamma = 60$ dyn/cm, and $T = 310$ K). For the H₄-JNJ system, distance restraints were applied between the Asp94^{3,32}-JNJ and Glu182^{5,46}-JNJ parallel with removing the positional restraints (step 5) because without the restraints these interactions were disrupted. Thereafter, 20-ns-long unbiased dynamics were conducted as described previously. During the calculations, the Nosé–Hoover Langevin piston method [186, 187] was used; the cutoff was set to 10 Å, and a 2/2/4 fs multisteping scheme was applied. Long range electrostatic interactions were calculated via the particle mesh Ewald method [188] and the grid spacing was set to 1 Å. MD simulations were performed by Balázs Jójárt and subsequent analysis of the trajectories by Ferenc Bogár and Gábor Paragi.

3.1.3 Binding site clustering

For each trajectory point residues whose side-chain occurred in the 5 Å environment of the ligand were selected. Then, the number of occurrences was counted along the MD trajectory for selected residues and summed up providing the cumulative occurrences. Residues were sorted according to their contribution to the cumulative occurrences (number of occurrences of a residue divided by the cumulative occurrences). Starting from the top ranked residue, contributions were summed up until reaching 90%. Those residues were defined as interacting ones for a receptor which contributed to this sum. The advantage of the definition is that residues occurring only a few times in the 5 Å environment of the ligand were omitted.

Binding site clustering calculations were carried out with the ptraj program from the AmberTools [182] package. First, the structures were superimposed based on the side-chain heavy atoms of the interacting residues to the initial geometry of the trajectory concerned. Next, the “average linkage” algorithm was applied to generate clusters and representatives in each case. Clustering was based on the mass-weighted RMSD distance matrix of the same atoms as used for superposition. The number of clusters was controlled by using criteria for critical distances (ϵ), which was the same for all trajectories of a certain GPCR. This method provided 28, 30, 32, 28 representative conformations for the histamine H₄, dopamine D₃, chemokine CXCR₄ and serotonin 5HT₆ receptors, respectively.

3.1.4 Protein structure preparation

For ensemble docking calculations, two ensembles of receptor models were generated from the MD trajectories. On one hand, structures were systematically extracted from the trajectory at the beginning of the 5 ns threads after the effect of changing the velocities has equilibrated and then at the end of every nanosecond. On the other hand, receptor conformations were clustered along every individual MD trajectory, and a representative structure was selected for each cluster. The former method provides 30 models for each GPCR, while in the second case the freely adjustable parameter of the cluster selection was tuned accordingly to obtain approximately the same number of models as in the first case. Schrödinger Suite 2012 was used for protein preparation. All X-ray, homology model and ensemble receptor structures were prepared by the Protein Preparation Wizard [170], including Impref minimization.

3.1.5 Compilation of the ligand set for the CXCR₄ receptor

In the case of the H₄, D₃, and 5HT₆ targets, the recently published GDD ligand set was used [189], which contains 15, 317 and 36 actives, respectively, and the decoy to active ratio is 40 for all sets. Since a ligand set for CXCR₄ was not available in GDD, the same ligand selection method as described by Cavasotto and Gatica was reproduced [189]. CXCR₄ actives were retrieved from the Thomson Integrity [190] database, while the ZINC database [191] was used to find decoys. Finally, altogether 30 active and 1170 inactive ligands were collected.

3.1.6 Compilation of the in-house fragment library

12,905 fragment-like compounds from Gedeon Richter's in-house collection were collected complying with an extended version of the Rule of Three: having an MW \leq 300 Da, logP \leq 3, number of H-bond donors and acceptors \leq 3 at pH 7.4, number of rotatable bonds \leq 6, PSA $<$ 130 Å², containing 1-3 rings and no reactive functionalities (see property distributions in Figure 20 and diversity assessment in Appendix B). Properties were calculated using the cxcalc utility by ChemAxon [192].

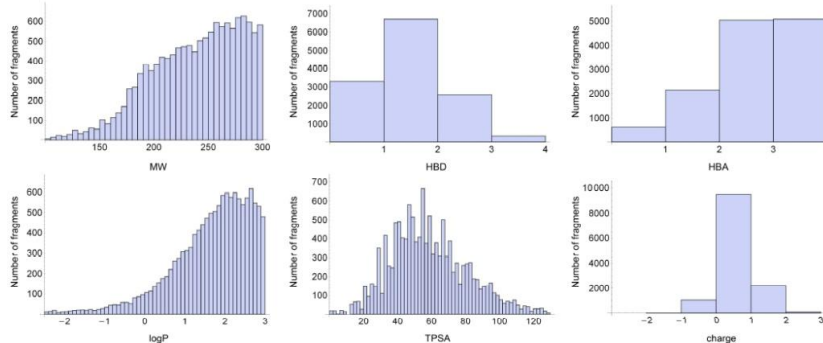


Figure 20. Property distributions of the Gedeon Richter fragment collection (molecular weight, hydrogen bond donor and acceptor count, calculated water-octanol partition coefficient, total polar surface area and charge of major microspecies at pH 7.4).

3.1.7 Ligand structure preparation

Ligands were prepared by LigPrep 2.5 [193] in the Schrödinger Suite 2012 with default settings. Major tautomer and protomer states were generated by the Epik module at pH 7.4 [194-196].

3.1.8 Docking using Glide

Grids were centered on the centroid of the interacting residues. The size of the grid box – which contains all ligand atoms during docking – in the retrospective small molecule virtual screening was defined by the maximal ligand size of 25 Å. The dimension of the inner box – where the midpoint of the ligand must be located – was set to 14 Å along the three coordinate axes. On the other hand grids for the initial homology model and crystal structure, as well as for the representatives from the MD trajectories were centered on the ligand centroids in the case of prospective fragment virtual screening, and had dimensions of 14 × 14 × 14 Å for the inner box and 44 × 44 × 44 Å for the outer box to ensure that sampling of the binding mode was not biased by the grid size.

Retrospective docking calculations were performed by Glide 5.8 [197-200] using the single precision (SP) calculation method. The default values were applied for the docking parameters except for the maximum number of minimization steps, which was set to 400. As a brief verification of the docking protocol, the original ligands were redocked into the crystal structure. These dockings provided 0.3 and 0.8 Å RMSD values considering the heavy atoms of the ligands for the D₃ and the CXCR₄ crystal structures, respectively. The performance of virtual screening was assessed by

enrichment factor (EFx%), ROC, and AUC. The enrichment factor was defined as $EFx\% = (n_{actx\%}/n_{allx\%})/(n_{act}/n_{all})$, where $n_{actx\%}$ is the number of active ligands in the top x% of the ranked ligand library, $n_{allx\%}$ is the number of ranked ligands in the top x%, n_{act} is the number of all actives, and n_{all} is the total number of ligands. ROC is the plot of actives percentage versus decoys percentage in the ranked list, while AUC is the area under the ROC curve.

Glide 5.7 [197-200] was used for docking of the fragment library. Docking calculations were conducted using the single precision (SP) mode, with post-dock minimization performed for 15 poses. Only the top pose for each fragment by the Emodel scoring function was saved, which were ranked by the GlideScore scoring function for each individual receptor conformation. For single structure docking to the D₃ X-ray structure and the H4 homology model, the top 50 compounds from the GlideScore ranked list were chosen for biological testing. In the ensemble docking approach mean ranks and their standard deviations calculated over the ensemble were used for evaluating each individual compound. Compounds having a mean rank lower than 500 were selected for biological testing. This cutoff gave a similar number of compounds to be tested as for the single structure case: 56 for the dopamine D₃ receptor and 50 for the histamine H₄ receptor.

3.2 Methods used in secondary site modeling

In this part of the work my aim was to study computational methodologies applicable for finding starting points for fragment linking. The performance of a sequential docking protocol for identifying fragments bound in possible secondary sites of proteins was evaluated. This work also started with method development on a small molecule data set and the performance of the protocol was tested subsequently on a fragment data set. The protocol was finally used to identify fragments for linking inside the binding pocket of the D₃ dopamine receptor and also the selectivity of the synthesized compounds against the D₂ dopamine receptor was assessed on a structural basis.

In the method development phase a simple sequential docking protocol using the commercial docking software Glide was tested for reproducing experimental binding conformations of multiple ligands. A set of 129 X-ray crystal structures was collected from the Protein Data Bank (PDB) containing at least two non-cofactor type ligands in close proximity. Ligands were docked sequentially to their respective structure in a self-docking setup and the performance of the methodology was then analyzed. Results obtained for the pharmaceutically relevant subset of cytochrome P450 enzymes and structures coming from HSP90 fragment screens were further investigated.

Encouraged by the results I intended to investigate the performance of the reported methodology on ternary protein-fragment complexes to provide a docking-based computational tool for identifying suitable starting points for the fragment linking approach. Both self-docking and cross-docking performance was assessed and possible reasons for misdocked cases were investigated.

Finally this methodology was applied for fragment docking and linking to GPCR targets, namely the D₃ crystal structure and a D₂ homology model and assess the subtype selectivity of the compounds on a structural basis. A similar methodology was also used in [201] with dopamine as the fixed primary site ligand and no subsequent linking of the identified fragments.

In the following details of the compilation of the data sets, homology modeling of the D₂ receptor, protein and ligand preparation and the docking protocols will be discussed.

3.2.1 Compilation of the protein-ligand complex data set

Crystal structures of protein–ligand complexes were selected from the PDB. Initial filters included a resolution of at least 2.5 Å, protein structures excluding DNA and RNA binding, and no appearance of words associated

with photosynthesis or the words MEMBRANE and IMMUNE in the HEADER section of the pdb files. The number of non-covalently bound ligands in each structure was determined excluding water, common cations and anions, common solvents and crystallization agents including PEGs, buffer constituents, lipids, disulfide bond reducing agents etc., cofactors, common carbohydrates and carbohydrate-amines (e.g. NAG), modified residues, and the unknown species (UNL and UNX). Pairwise minimal interatomic distances (MIDs) between the ligands were calculated and clusters with 2–6 ligands having an MID within 6.0 Å were identified. At least two ligand centroids were required to fall within the 14 × 14 × 14 Å cube centered on the common ligand centroid. Finally structures that did not contain cations, anions and cofactors except for heme in the 6.0 Å neighborhood of such a cluster were saved.

Protein binding sites were characterized using SiteMap [202] version 2.4 in single binding site region evaluation mode with a 6.0 Å buffer around the ligand cluster. Structures without a SiteMap recognized binding site were discarded. The remaining structures were finally visually inspected to eliminate cases with incorrectly defined connectivity or atom types not parametrized in the OPLS-2005 force field. This filtering of the PDB resulted in 129 structures as of 1 October 2011 (see Appendix C for PDB ID codes). These structures thus have good resolution and contain a cluster of at least two and at most six ligands in close proximity to each other suitable for docking. Two of these protein–ligand complexes (PDB codes: 1e7c and 3g35) had two distinct, non-symmetry equivalent sites where multiple ligands were present. The docking procedure in these cases was performed for both binding sites increasing the total number of sites to 131 representing 54 targets. These sites contain a total of 294 ligands to be docked, meaning an average of 2.24 ligands per binding site. Binding sites were then classified as sites containing multiple copies of the same ligand and those containing different ligands. Since in the latter case ligands can be docked in different orders the total number of docking calculations was 324.

3.2.2 Compilation of the protein-fragment complex data set

The above described protocol was applied to the PDB again in 2012 May and structures with fragment-like ligand clusters were carried on to this study as well. Then the literature was searched for successful examples of the linking strategy and ternary fragment complexes with structures available in the PDB. In line with the finding of the previous work – that sequential docking of more than two ligands is significantly less reliable – examples where more than two fragments were linked were not pursued.

Finally 32 synthetically linked or tethered (linked in situ using disulfide bonds) examples representing 18 targets were collected, of which one was an NMR structure. For eight examples the linked compounds were not synthesized, only the ternary complex is available. Additionally three examples were included where the hit elaboration strategy was actually growing, but a well-defined second fragment was attached through a linker. Two examples are from ligand deconstruction experiments where the deconstructed fragments were shown to bind the target in a similar fashion as in the linked ligand. X-ray structures of either the two fragments (for 14 structures) or the linked compound (for 18 structures) complexed with its target were retrieved, whichever was available (see Appendix D for PDB ID codes and SMILES representation of ligands).

3.2.3 Homology modeling of the D₂ receptor

The human dopamine D₂ receptor amino acid sequence from the UniProt server [163] was aligned to the sequence of the template, chain A of the 2.89 Å resolution X-ray structure of the human dopamine D₃ receptor crystallized with the D₂-D₃ dual antagonist eticlopride (PDB code: 3PBL) using Prime 3.2 [162] and the sequence alignment in Appendix A. The third intracellular loop was not modeled and the eticlopride ligand was included in homology model building to prevent the collapse of the binding site. Finally the whole structure was subjected to Impref restrained minimization in the Protein Preparation Wizard [170] in the Schrödinger Suite 2013.

3.2.4 Protein structure preparation

The most completely modeled biological assembly in the unit cell was retained from the crystal structures. If the biological assembly contained crystal mates, only chains in the vicinity of the docked ligands were added. In cases where there were more identical chains in the unit cell, the first chain containing the multiply ligated site was selected. Further phases of the work were automated using the Schrödinger Python API available in Schrödinger Suite 2010 (version 3.8). The structures were prepared for docking with the Protein Preparation Wizard [170] that includes assigning bond orders, adding hydrogens, treating metals, creating disulfide bonds, converting selenomethionines, deleting distant waters, assigning the H-bond network with water sampling and finally minimizing the structure up to 0.3 Å RMSD with the OPLS-2005 force field. All waters and ligands were then deleted from the structures before grid generation.

In the second case study of HSP90 complexes structure preparation included retaining six conserved crystallographic water molecules in the

structures, since these waters are known to play an important role in HSP90 binding [203]. Retained water molecules were selected by aligning the five HSP90 structures and identifying those present in all structures. Orientation of their hydrogens and protonation states of nearby residues were automatically assigned by the Protein Preparation Wizard. They form hydrogen bonds with the Asn51, Asp93 and Trp162 side chains, backbone carbonyls of Leu48 and Gly97, backbone NH of Gly137 and with each other. They all form two or three hydrogen bonds and have a relative B-factor of 0.4-0.9. In the fragment data set structural water molecules were additionally retained in the thrombin structure with PDB code 2c8w. In the last part of the work chain A of the dopamine D₃ crystal structure was subjected to the full Protein Preparation Wizard workflow in the Schrödinger Suite 2013 with default settings.

SiteMap was used to estimate binding site volumes and enclosure. The enclosure parameter ranges from 0.5 to 1, a higher value means a more buried site. The average value for tight-binding sites is 0.78 [204].

3.2.5 Compilation of the fragment libraries for linking

An in-house focused library of 196 fragments was collected containing a basic amine moiety in an aliphatic ring connected directly or through a short linker to a substituted aryl or hetaryl moiety. Such compounds were believed to function as primary binding site ligands of the D₂ and D₃ receptors. It has been shown that the primary binding sites of the two receptors are nearly identical and selectivity can be achieved by modulation in the secondary binding pocket [205]. Another in-house focused library of 266 fragments were collected containing a cyclohexyl or piperidine ring as these fragments were believed to function as secondary binding site ligands based on known D₃ antagonists such as SB-277011 [206] suitable for modulating selectivity.

3.2.6 Ligand structure preparation

Docked ligands were prepared by converting them first to 2D structures with the ChemAxon molconvert plugin [207] and then back to 3D with the Schrödinger LigPrep [193] version 2.4 retaining the configuration of the chiral centers. This procedure eliminated the conformational bias of using experimental binding modes. Epik [194-196] version 2.1 was used to generate tautomers and protomers at pH 7 ± 2. For proteins crystallized outside of this range we verified that LigPrep found no additional ligand protomers on the pH of crystallization. LigPrep version 2.6 [193] and Epik version 2.4 [194-196] were used in the GPCR modeling part of the work.

Physico-chemical properties, namely molecular weight, logP, number of H-bond donors and acceptors, number of rotatable bonds, molecular volume, hydrophobic and total accessible surface area (ASA) of the ligands were calculated with the ChemAxon cxcalc plugin [192] and their druglikeness was assessed using Lipinski's rule (MW \leq 500 Da, logP \leq 5.0, hydrogen bond acceptor count \leq 10, hydrogen bond donor count \leq 5). Figure 21 shows the distributions of crystallographic and calculated properties of binding sites and ligands considered in the small molecule dataset. In the fragment data set linked ligands were first split at the linker, free valences were capped with hydrogens and then submitted to the preparation workflow. Due to the presence of metalloproteins in the dataset, Epik was set to generate additional metal binding states during ligand preparation.

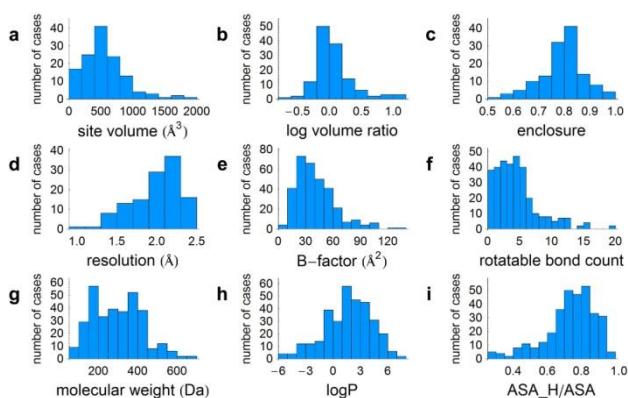


Figure 21. Distribution histograms of binding site (a–d) and ligand (e–i) properties calculated with SiteMap (a–c), obtained from crystallographic data (d–e) and calculated with cxcalc (f–i). Log volume ratio is the logarithm of total ligand volume divided by the site volume. ASA is the accessible surface area and ASA_H is the hydrophobic accessible surface area.

3.2.7 Docking using Glide

Docking of the small molecule data set was performed by Glide 5.6 [197-200] using Single Precision (SP), Extra Precision (XP) and SP hard modes. The latter represents SP calculations without scaling down the van der Waals radii of nonpolar ligand atoms (using a scaling factor of 1.0 instead of the default 0.8). A docking run for a particular structure consisted of at most as many consecutive grid generation and docking steps as the number of ligands in the docked ligand cluster. The maximum available grid size (36 \times 36 \times 36 Å outer and 14 \times 14 \times 14 Å inner box) was used. The grid was always centered on the common centroid of all the heavy atoms of the ligand cluster that allowed positioning the grid in the same way in each step

of a docking run. The number of poses entered to post-docking minimization and saved was set to 30, other sampling parameters were set to their default. RMSDs between docked and experimental ligand conformations were calculated for heavy atom positions.

The sequential docking protocol used in the study contained multiple grid generations depending on the number of ligands evaluated for a particular binding site. The first grid was generated for the ligand-free receptor. In the first docking step each tautomer and protomer of the first ligand was docked. When two different ligands were bound, both docking permutations were evaluated. The 30 saved poses were ranked by their respective Emodel scores. If any of the top three poses of any protomer or tautomer had an RMSD less than 2.0 Å to any of the experimental ligand conformations, that pose was selected and merged with the ligand-free starting structure (first poses had priority over second ones and second poses had priority over third ones; lower RMSDs had priority among different protomers and tautomers). If none of the top three poses had an RMSD less than 2.0 Å, but a higher ranked pose had, then the pose with the minimal RMSD was merged with the ligand-free starting structure, and the rank of the merged pose was recorded. If no poses with RMSD less than 2.0 Å were found, then the docking run was terminated since no satisfactory pose was generated. In the second step a new grid was generated for the merged structure and all protomers and tautomers of the second ligand were docked. The pose to be merged with the one-ligand containing structure was selected the same way as in the first step and its rank was recorded. If the cluster contained more than two ligands, this procedure was repeated until all ligands were docked or the run was terminated because of no satisfactory RMSDs. After the docking run the 30 saved poses were also re-ranked by GlideScore and Glide Energy scoring functions and the ranks of the first pose with RMSD less than 2.0 Å were also calculated in the re-ranked lists. The workflow is shown in Figure 22.

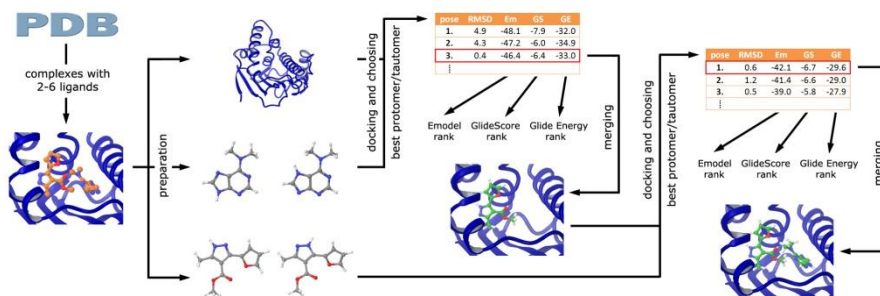


Figure 22. The sequential docking workflow used in secondary site modeling.

RMSD values and Emodel, GlideScore and Glide Energy ranks of the merged poses were assigned. RMSDs of the first docking steps were analyzed in order to compare sequential multiple ligand docking to single ligand docking benchmark studies. Median and mean RMSDs and standard deviations were calculated for top scoring and lowest RMSD poses. Success rates are defined as the ratio of ligands where any pose had an RMSD less than 2.0 Å. Top pose rates were calculated as the ratio where the top pose had an RMSD less than 2.0 Å. RMSD and rank distributions of all docking steps for the different docking modes were subjected to Kolmogorov–Smirnov statistical analysis using STATISTICA 10.

The docking workflow for the fragment data set was identical to the one described above, only the updated Schrödinger Suite 2011 (LigPrep 2.5 [193] and Epik 2.2 [194-196] for ligand preparation and Single Precision (SP) Glide version 5.7 [197-200] for docking) was used. Fragments were docked in the order of their binding, where such information was available, i.e. the first-site binders were docked first and second-site binders after. Where this information was not available (PDB codes: 2c8w, 3img, 3le8, 4a7i, 4dm3), the fragment accommodated deeper in the binding cleft was docked first. This consideration is based on the finding of the previous work that the reverse order docking provided similar or poorer results. Glide version 5.9 [197-200] was used in the last part of the work for docking to the D₃ and D₂ receptor structures.

Docking results are reported as the heavy atom graph RMSDs (considering symmetry) of the first and second ligands compared to their experimental binding modes, and the ranks by the Emodel scoring function of the ligand poses merged with the protein structure from among the top 30 saved poses. In the case of the 1nny structure it was noted that the naphthyl ring of the first fragment was flipped compared to the single fragment bound structure 1no6, thus the RMSD in this case was calculated to the latter binding mode after fitting the two protein chains onto each other.

3.3 Experimental methods

Synthesis of **19**, **20** and **21** was performed by Éva Ágainé Csongor and details are given in Appendix E. Receptor binding assays were performed by Éva Schmidt and Ferenc Horti and details are given in the following.

3.3.1 Human recombinant H₄ binding assay

Membranes from CHO-K1 cells expressing human histamine H₄ receptors were purchased from PerkinElmer Life and Analytical Sciences (Cat. No. ES-393-M400UA). Frozen membrane aliquots were thawed at room temperature and diluted 200-fold (15 µg protein/500µL diluted membrane/well) with binding buffer (50 mM TRIS-HCl pH 7.4, 5 mM EDTA).

The assay was performed according to the PerkinElmer assay protocol for human H₄ receptor: 500 µL diluted membrane suspension (15 µg protein/assay) was incubated with [³H]histamine as radioligand. Final reaction volume was 550 µL and final radioligand concentration was 4-7 nM. 10 µM histamine was used for determination of non-specific binding. The samples were incubated at 27°C for 30 min and binding was terminated by vacuum filtration through Whatman GF/B glass fiber filters, pre-soaked in 0.5 % PEI. The filters were washed 3 times with 4 mL ice cold binding buffer. Filters were transferred to vials, 4 mL Optiphase HiSafe scintillation cocktail (PerkinElmer) was added and radioactivity was determined by Packard TriCarb 2900 TR (PerkinElmer) liquid scintillation counter.

SEM was lower than 15% for single concentration measurements and lower than 7% for the hits. The ligand displacement by the compounds was determined using a minimum of six concentrations in duplicate or triplicate, and experiments were repeated at least two times. The specific radioligand binding is defined as the difference between total binding and the non-specific binding determined in the presence of an excess of unlabelled ligand. IC₅₀ values (i.e. concentration of compound giving 50% inhibition of specific binding) were determined from concentration-displacement curves by sigmoidal fitting using Prism Software 4.0 (GraphPad, San Diego, CA, U.S.A.). K_i values (i.e. inhibition constants) were calculated using the Cheng-Prusoff equation: $K_i = IC_{50}/[1+([L]/K_D)]$, where [L] is the free radioligand concentration and K_D the affinity of the labeled ligand for receptor. K_D was determined from the Scatchard plot.

3.3.2 Human recombinant D₂ and D₃ binding assay

Cell cultures (HEK 293 Gα15 and CHO-K1) expressing human D₂ and D₃ receptors (purchased from HD Biosciences, China and Euroscreen Fast,

Belgium, respectively) were homogenized in buffer solution (composition: 50 mM Tris, 5 mM MgCl₂, 1 mM EGTA for hD₂ and 15 mM Tris, 2 mM MgCl₂, 0,3 mM EDTA, 1 mM EGTA for hD₃, pH=7.4 at 25°C) in 4x v/w with a Dounce tissue grinder and centrifuged at 40,000 g at 4°C for 10 or 25 min, respectively. The supernatant was removed and the pellet was resuspended in 4x v/w buffer and recentrifuged. This process was repeated twice more and the pellet was resuspended in buffer (the composition see above for hD₂; for hD₃ as follows: 75 mM Tris, 12,5 mM MgCl₂, 0,3 mM EDTA, 1 mM EGTA, 250 mM sucrose, pH=7.4 at 25°C) at a volume of 12.5 mL/g original weight. The preparations were then aliquoted and stored at -70°C.

The aliquoted membrane was thawed and washed once in binding buffer containing 50 mM Tris-HCl; 5 mM MgCl₂, 5 mM KCl; 1 mM CaCl₂, 120 mM NaCl, 1 mM EDTA. In the same buffer 5 (hD₂) or 3.3 (hD₃) µg protein/assay was incubated with 2 nM [³H]raclopride in the presence or absence of test compound (to determine the binding inhibition of the test compound or the total binding, respectively) for 120 minutes at 25°C at a volume of 250 µL in 96 Deep Well plate. Non-specific binding was determined in the presence of 10 µM haloperidol. After incubation, samples were filtered over UniFilter® GF/BTM using PerkinElmer Harvester and washed with 4x1 mL ice-cold binding buffer. The plate was dried at 40°C for an hour and 40 µL Microscint scintillation cocktail (PerkinElmer) was added to each well. The radioactivity was determined in MicroBeta 2450 microplate counter (PerkinElmer).

SEM was lower than 15% for single concentration measurements and lower than 7% for the hits. The ligand displacement experiments were repeated at least two times. The specific radioligand binding is defined as the difference between total binding and the non-specific binding determined in the presence of an excess amount of haloperidol. IC₅₀ values (i.e. concentration of compound giving 50% inhibition of specific binding) were determined from concentration-displacement curves by sigmoidal fitting. The inhibition constants (K_i) were calculated using the Cheng-Prusoff equation: $K_i = IC_{50}/[1+([L]/K_D)]$, where [L] is the free radioligand concentration and K_D the affinity of the labeled ligand for receptor. K_D was determined from the Scatchard plot. GraFit 6.0 (Erithracus Software, Horley, UK) software was used for curve fittings.

Chapter 4 – Results

4.1 Virtual screening against GPCRs

GPCRs adopt multiple conformations ranging from the fully inactive to the active state that has crucial functional relevance from a pharmacological point of view, since partial, full and inverse agonists or neutral antagonists have different therapeutic effects. Moreover, high affinity compounds of different chemotypes may show similar functional efficacy, suggesting that a functional state can also cover multiple protein conformations in terms of the extracellular binding pocket. The scope of this work was to investigate the potential of using multiple receptor conformations for structure based drug design purposes. Therefore receptor conformations selected from MD trajectories were generated. The quality and the potential applicability of receptor conformations were assessed by retrospective enrichment studies.

The key goal was to compare high quality models that represent an optimized ligand–protein conformation (X-ray or comparative model) to multiple MD frames that exhibit broader conformational variability. Four prototypic targets were investigated: CXCR₄, D₃, H₄ and 5HT₆. CXCR₄ is a peptidergic GPCR with a large, open binding site, while D₃, H₄ and 5HT₆ are aminergic receptors representing more closed binding pockets. Among them, D₃ and CXCR₄ have small-molecule bound X-ray structures. Both CXCR₄ and D₃ were assessed in the GPCR Dock 2010 competition, therefore the best models of the modeling community are available, and the models are entirely unbiased, since they were built before the structures were disclosed [188]. The other two targets were the H₄ and the 5HT₆ receptors, with no reported X-ray structure. In these cases, close homologues, the H₁ [209] and the 5HT_{1B} and 5HT_{2B} [210, 211] receptor–ligand complexes are available, which were used as templates to build comparative models.

Explicit-solvent molecular dynamics simulations of the holo receptors were carried out using the X-ray structures (CXCR₄ and D₃) or in the case of H₄ and 5HT₆ the homology models on a nanosecond time scale. Holo complexes were used instead of apo forms to prevent the collapse of the binding pocket and to preserve the steric availability of the interaction pattern of the ligand. Binding site RMSD-based clustering and systematic sampling were used to generate approximately 30-30 receptor conformations for each target. In case of MD, single receptor and consensus scoring evaluation was carried out. Protein flexibility was measured in terms of per residue RMSD values compared to the initial structure.

It should be noted that quality assessment of the different docking algorithms or the ligand sets was out of the scope of this work. Therefore,

the focus was only on the preparation of the receptor models, from a methodological aspect. The models are summarized in Table 6.

Table 6. Main features of the receptor models used in this work.

target	Receptor models					
	homology model	X-ray structure	MD details			
			system (ligand)	length (ns)	number of frames cluster	number of frames systematic
CXCR ₄	VU-MedChem	3ODU	3ODU (IT1t)	20+5×5	32	30
D ₃	PompeuFabra	3PBL	3PBL (eticlopride)	20+5×5	30	30
H ₄	this work	-	homol. mod. (JNJ7777120)	20	28	21
5HT ₆	this work	-	homol. mod. (SB-742457)	20+5×5	28	30

4.1.1 The impact of the structure source

The primary objective of the work was to survey the source of receptor models. The quality of receptor models was assessed by retrospective enrichment studies that measure the feasibility of models to select active compounds from decoys. Enrichment factor, receiver operating characteristic (ROC), and area under the ROC curve (AUC) values were calculated. It was investigated whether the X-ray structure is the paramount representation of the protein conformation and the MD simulation only perturbs the protein framework and reduces its validity, or if one could find a single conformation among the MD ensemble that can outperform the experimental structure. The second objective was to assess the quality of homology models, since most of the pharmaceutically relevant GPCRs have not been crystallized to date. The H₄ and 5HT₆ targets were selected as a real-life scenario, where no X-ray structure is available; thus the MD simulation is based on the homology model. During this specific assessment, the best snapshot (highest enrichment factor EF) was selected from the MD simulations regardless of whether it was found with clustering or systematic sampling. The EF and AUC results are presented in Figure 23 and in Appendix F.

In the case of CXCR₄, the homology model and the X-ray structure did not result in significant enrichment. The EF1% was equal to zero (the random case produces EF1% = 1); in contrast the best MD snapshot resulted in EF1% = 6.7. Considering the aminergic D₃ receptor, the EF1% of

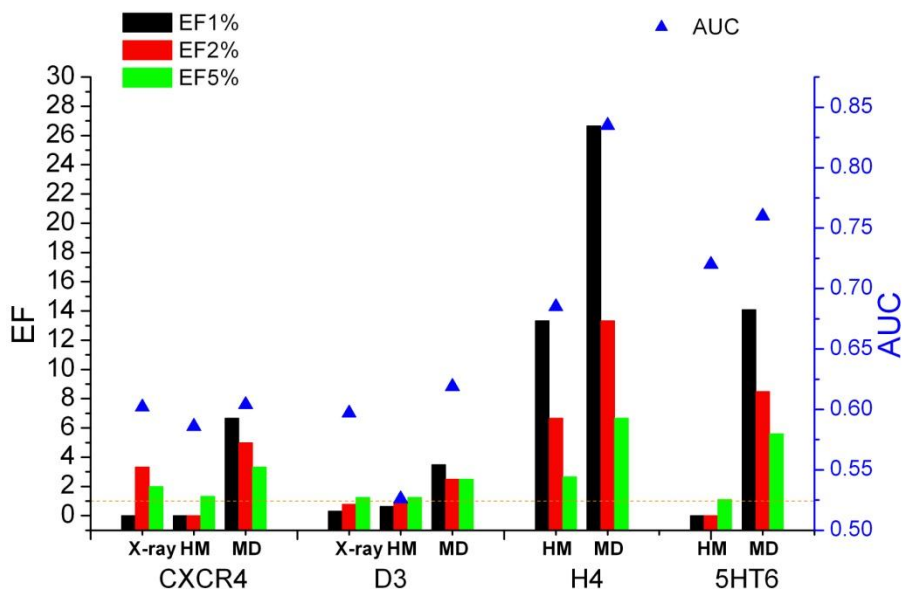


Figure 23. Enrichment factors (colored bars) and AUC values (blue triangles) for the CXCR₄, D₃, H₄, and 5HT₆ targets obtained with X-ray, homology model (HM), and the best molecular dynamics frame (MD). The orange dotted line represents EF = 1. It should be noted that the y axis starts from EF = -1 in order to enable the representation of EF = 0 bars.

the homology model and the X-ray was 0.63 and 0.32, respectively. In contrast, the best snapshot from the MD trajectory resulted in EF1% = 3.5. The H₄ homology model and the best MD frame yielded 13.3 and 26.7 EF1% values, respectively. In the case of the 5HT₆ target, the homology model and the best MD frame resulted in zero and 14.1 EF1% values, respectively. The AUC values were found to be 0.72 and 0.76 for the homology model and the best MD frame, respectively. In line with the previous results, the homology model was significantly outperformed by the best MD receptor model. It is interesting to note that the MD-based docking ranked three actives among the top five compounds and five actives among the top 10; thus the performance of the MD-optimized structure was found to be very promising for prospective screening.

The results of the enrichment studies (depicted in Figure 23) can be summarized by stating that the best single structure from the MD simulation was superior to the initial model, regardless of the target and the evaluation method (EF or AUC). This observation suggests that during the MD simulations, a “consensus” binding pocket is formed that is able to outperform the homology model or experimentally observed conformation of the protein in terms of enrichment factor. It is suggested that during MD

simulation of the protein–ligand complex various low-energy protein conformations are sampled, and this ensemble contains such conformations that are not entirely refined around the original ligand, but they correctly represent the interaction pattern of the binding site. Such a protein conformation is not committed to the original ligand and therefore can host and score multiple diverse active chemotypes. This hypothesis is exemplified with the four top ranked actives in Figure 24. The top ranked active compound in case of the X-ray or homology model structures has approximately the same rank as the MD frame, but the MD frame can host multiple active compounds with similar low ranks unlike X-ray or homology models. This hypothesis is in line with the theory of the consensus binding site refinement protocol (cIFD) that has been recently published [212]. In the case of the cIFD method, the binding site is refined around multiple active compounds simultaneously by using Locally Enhanced Sampling (LES) to preform a specific binding pocket that can host diverse actives, without steric clashes. According to the results of this work, similar “multipotent” binding sites can be captured during MD simulation of the ligand–protein complex.

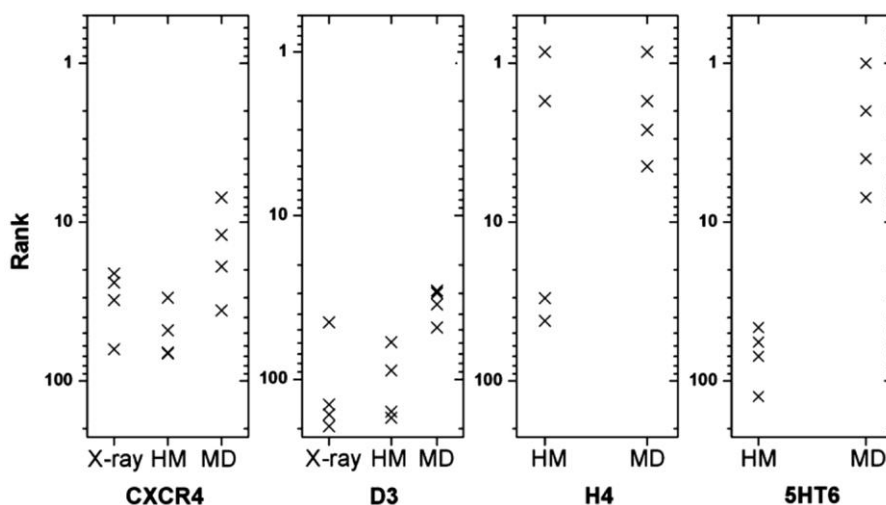


Figure 24. The ranks of the top four actives for the CXCR₄, D₃, H₄, and 5HT₆ targets in X-ray, homology model (HM) and the best molecular dynamics frame (MD).

Next, the robustness of the enrichment study was tested to challenge the consensus binding site hypothesis. Because of the large number of MD frames that were included in the enrichment study, chance correlation might have occurred. In rare cases, a good enrichment might be obtained simply due to occasional scoring of some active compounds, but the whole model is not able to accommodate the actives better than inactives on

average. In order to carry out statistical evaluation, the original ligand set was divided into small random subsets containing one third of the actives and one third of the decoys, and these subsets were generated 10 times for each target. During this approach, 10 enrichment studies were simulated using reduced ligand sets. However, these sets are not independent from the original; thus these statistical results are approximate. The enrichment of these small subsets was calculated, and the 10 EF1%, EF2%, EF5%, and AUC values were compared with two sample t-tests among the homology models, X-ray structures, and best MD models. It was found that the difference between homology models and X-ray structures compared to the best MD snapshots was significant ($p < 0.05$, MD was superior) for the D₃, H₄, and 5HT₆ cases using either EF or AUC values. In the case of CXCR₄, the difference between the homology model and the MD frame was significant ($p < 0.05$). Comparison of the X-ray structure and the MD frame in the case of CXCR₄ revealed that the difference is not significant for EF1%, EF2%, EF5%, and AUC.

Considering another aspect and assessing the applicability of comparative modeling on GPCRs, these results suggest that in the case of CXCR₄ and D₃, neither the X-ray nor the state of the art homology model yielded acceptable enrichment. In the cases of H₄ and 5HT₆, where close X-ray structures were used as a template, significant enrichments were observed. The H₄ and 5HT₆ homology model-based MD simulations resulted in a similar outcome to that of the D₃ and CXCR₄ cases – the MD ensemble comprised a protein model with the utmost EF – that underlines the usefulness of comparative modeling and subsequent MD simulation on GPCRs.

It should be noted that a characteristic difference was observed between the investigated targets in terms of the overall enrichment: CXCR₄ and D₃ were similar to each other, but H₄ and 5HT₆ were different. X-ray and homology models of CXCR₄ and D₃ resulted in lower enrichments than those of the random sampling (EF1% < 1), while the MD frames were somewhat better. Limited AUC values were observed on these targets. Planesas recently published virtual screening results using Glide with a different ligand set from that of the present study for CXCR₄ and achieved similar results, EF1% = 2.8 and EF5% = 4.6 [213]. Cavasotto and Gatica carried out an enrichment study on D₃ using the same ligand set and obtained EF2% = 0.3, which is also similar to the present results [189]. Therefore, CXCR₄ and D₃ might be considered as challenging targets from a structure-based virtual screening aspect. In contrast, both the homology model and the MD model of H₄ yielded promising EF and AUC values. This finding is in line with the literature data; the H₄ receptor can be considered as a more tractable target yielding promising enrichments [214, 215]. 5HT₆ shows a somewhat

different picture. Although the EF value of its homology model is very poor, similarly to CXCR₄ and D₃, the best MD model performs considerably better.

4.1.2 The impact of the binding site character

In order to assess the relationship between the binding site properties and enrichment values, SiteMap [202] descriptors were generated for all the MD frames for CXCR₄, D₃, and H₄ targets. In the case of CXCR₄ and D₃, no significant correlation was found between the binding site properties and the generally low enrichment factors. Only in the case of H₄, the *exposure*, *size*, *contact*, and *philic* properties had significant correlation with EF1%, EF2%, and EF5% (correlation matrix and descriptor definitions are given in the Appendix G). The *exposure*, that measures how opened the binding site is, showed the highest linear correlation (0.53, 0.48, and 0.59 for EF1%, EF2%, and EF5%, respectively). Overall, the SiteMap parameters were not in a strong relationship with the enrichment values, although in the case of H₄ the *exposure* might be indicative. Thorough testing of this relationship was out of the scope of this work.

4.1.3 The impact of the frame selection method

Next, the two frame selection methods were compared, namely, the clustering by the binding site RMSD and the systematic sampling approaches. These collections were compared with two sample t-tests over their EF1%, EF2%, EF5% and AUC values independently to assess the general differences. No statistical difference was observed in the case of CXCR₄ and 5HT₆. With regard to the D₃ target, the difference was significant for EF1%. In this case, the clustering method was found slightly better, although the EF values are unacceptable (EF1% < 1). Considering EF2% and EF5% values calculated for H₄, systematic sampling performed better with statistical significance. Comparing only the best structures and using EF1% for evaluation, CXCR₄ enrichment values were identical (both EF1% = 6.7). For D₃, the clustering outperformed the systematic sampling (EF1% values were 3.5 and 2.5, respectively), and for H₄ and 5HT₆, the systematic sampling surpassed the clustering (EF1% values were 27.7 and 13.3 for H₄ and 14.1 and 8.4 for 5HT₆, respectively). Overall, clustering and systematic frame selections showed similar performance. This observation might be due to the fact that the systematic approach covered the most populated clusters, and the best frames were selected from those. The limited internal diversity of the clusters resulted in the centroid selection having a similar performance to the approximately random selection of the representatives provided by the systematic approach.

4.1.4 The impact of MD ensembles

Finally, protein conformations collected from MD simulations by systematic and cluster-based sampling were used to assess their usefulness in ensemble docking. The histogram of enrichment factors achieved at single structure evaluation revealed that for two of the targets, multiple conformations had similar high EF values among the best structures, implicating that the combination of these rankings might be beneficial. Based on literature data, ensemble docking has typically better performance using a few carefully selected protein conformations rather than including each and every structure available [216-218]. Therefore, average ranks of the ligands were calculated for all the possible receptor combinations to an ensemble size up to 6. The number of enumerated ensembles is shown in Figure 25.

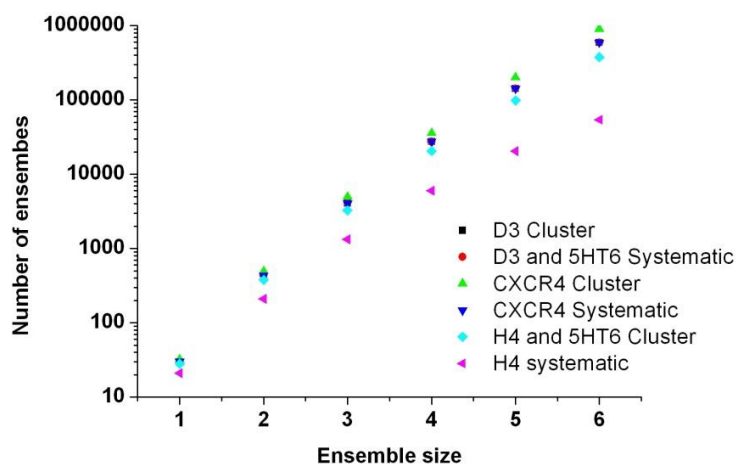


Figure 25. Number of calculated ensembles as a function of the ensemble size.

In the case of CXCR₄, the EF1% was better for ensemble evaluation compared to single receptor evaluation for cluster-based frame selection, but for the AUC values, no significant improvement was observed (Figure 26). Considering the D₃ and H₄ targets, the single structure enrichments could not be outperformed by ensemble evaluation. EF values obtained for 5HT₆ suggest some limited improvement achieved by rank average ensemble evaluation. Overall, no serious difference was observed between cluster-based and systematic MD frame selection, similarly to previous analyses. In summary, the rank average-based ensemble evaluation did not have an unambiguous positive effect on enrichment; however, in the cases of CXCR₄ and 5HT₆, positive effects were observed considering the enrichment factor values.

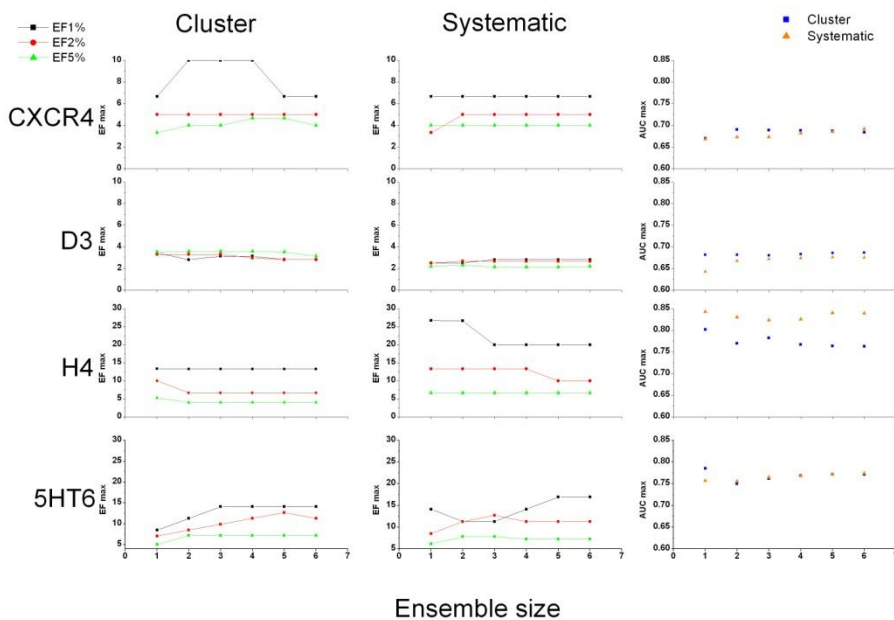


Figure 26. Best enrichment factors (EFs) and AUC values for a given ensemble size for ensemble evaluation based on rank averages.

4.1.5 Application domain of the proposed methodology

The consensus receptor models that resulted in increased enrichment in this work had been captured by membrane-embedded MD simulations of the receptor–ligand complex. Therefore, the accuracy of the initial receptor–ligand complex has a fundamental impact on the outcome. During the MD simulations the binding site preserves its ligand interaction pattern while it is equilibrated close to the energy minimum. Concurrently, several protein conformations are generated that are less biased toward the original bound ligand but projects its interaction surface properly. It is therefore suggested that this methodology be used on high-quality X-ray structures (holo-form) and on homology models that have accurately modeled complex conformation.

The GPCR Dock 2010 assessment highlighted that modeling of the D₃ receptor having 41% sequence identity with the transmembrane (TM) domain of the template β_1 AR satisfied the accurate modeling criteria (ligand RMSD is 0.96 Å and 58% of the contacts are reproduced) [188]. In contrast, the best model of the CXCR₄-IT1t complex (target-template sequence identity in the TM domain is 25.5%) has a ligand RMSD of 4.88 Å, and only 36% of the contacts could be predicted correctly. In the latter case, the time scale of the MD simulations applied here cannot ensure that the complexes

find their equilibrium conformations (the backbone RMSD for the second extracellular loop of CXCR₄-IT1t complex was 7.42 Å for the best model). It should be noted that Shaw and co-workers have shown that homology models – in most cases – drift away from the native structure during extreme long (100 μs) MD simulations [219]. In the present work, these considerations were used selecting the histamine H₄ as a modeling target, since the histamine H₁ receptor satisfied the sequence identity (~40%) for homology modeling.

Self-docking into X-ray structures and systematically built GPCR homology models yielded similar results. Aminergic GPCRs could be successfully modeled, but homology models for peptidergic GPCRs did not result in acceptable binding poses [220]. In addition, peptidergic GPCRs represent a higher level of complexity for structure-based virtual screening, as it is exemplified by hit rates for aminergic homology models compared to peptidergic ones [99]. Previous experience suggests that experimental data (X-ray or NMR) or high-quality homology models are preferred for sampling protein conformations for virtual screening applications. The protocol is thus not recommended for more complex homology modeling cases such as peptidergic GPCRs with low quality templates.

The GPCR Dock 2010 assessment also emphasized the utility of biochemical and ligand pharmacophore information for the accomplishment of the best models. Thereby targets without known ligands (orphan receptors), or without biochemical characterization such as site directed mutagenesis, possess difficulties similar to the prediction of the correct holo complex.

In theory, the proposed methodology is not biased toward antagonist ligands and can be adapted for agonist structures as well. Because of the complexity of the functional responses of GPCRs, the level of protein flexibility incorporated in this work does not cover changes related to the activation process. Given the limited understanding of GPCR structure and function relationships to date [210, 211] it is assumed that structure based virtual screening can recognize ligands with high affinity to the receptor structure that should be validated first in a binding assay *in vitro*.

The MD simulation increases the CPU time (in this case, 4 ns/day simulation time could be achieved on 32 CPUs) resulting in the total 45 ns simulation requiring at least 10 days. According to the proposed methodology, 20–30 receptor structures must be tested in enrichment studies that also consume computational resources. However, the computational costs of the retrospective enrichment studies for 20–30 test conformations are still acceptable – orders of magnitude lower compared to prospective screening – considering that typically millions of compounds are virtually screened during the prospective campaigns. Although the

available computational resources increased significantly during the past decade, and the MD simulations as well as the docking studies are highly parallelized, careful design of simulations still remains a principal requirement. The cost and benefit ratio should be evaluated thoroughly, but according to the present work, the changes of EF1% values are encouraging: for the four targets studied here, the initial model compared to the best, single MD frame resulted in EF1% 0 to 6.7, 0.32 to 3.5 (10×), 13.3 to 26.7 (2×), and 0 to 14.1 improvements. This enhancement can be exploited in prospective virtual screening; therefore docking into one appropriately selected consensus receptor can replace a large number of ensemble calculations. The positive results of the most recent example, 5HT₆, highlight the applicability of the proposed methodology in a real-life drug discovery scenario: a convincing improvement in virtual screening performance could also be achieved on a target with no experimental structure.

4.2 Virtual fragment screening against GPCRs

In this part of the work prospective virtual fragment screening on the available dopamine D₃ receptor crystal structure and the previously described homology model of the histamine H₄ receptor was performed. Snapshots from the all-atom membrane-embedded MD simulations were also used for ensemble virtual screening of the same fragment library. Screening performance of the different protocols were compared analyzing hit rates and hit compounds obtained by docking to the single structure and the conformational ensembles.

4.2.1 Analysis of receptor binding sites

While the histamine H₁ and H₄ receptors share 40% amino acid identity in the transmembrane region and they recognize the same endogenous ligand, there are substantial differences in their binding sites. For example Asn147^{4.57} in H₄ corresponds to Trp158^{4.56} in H₁, Leu175^{5.39} to Lys191^{5.39}, Glu182^{5.46} to Asn198^{5.46} and Gln347^{7.42} to Gly457^{7.42}. Also, mutation of Asn147^{4.57} and Glu182^{5.46} showed significant alteration to JNJ7777120 inhibition constants [165]. Thus the initial homology model featured two specific H-bonds of JNJ7777120 to Asp94^{3.32} and Glu182^{5.46} as shown in Figure 27. In the course of the molecular dynamics simulation the H₄ receptor binding site appears to be relatively rigid based on side chain χ_1 and χ_2 angles of the interacting residues (see Figure 28). Met150^{4.60} is quite flexible and Leu175^{5.39} assumes two different rotameric states, but these variations don't alter the binding pattern of the ligand. However Glu182^{5.46}

also adopts two main rotameric states, which causes some variability in the ligand position within the binding site. The ionic interaction to Asp94^{3,32} is mostly uninterrupted and surprisingly Gln347^{7,42} also formed an H-bond with the carbonyl group of JNJ7777120 in some of the representative frames.

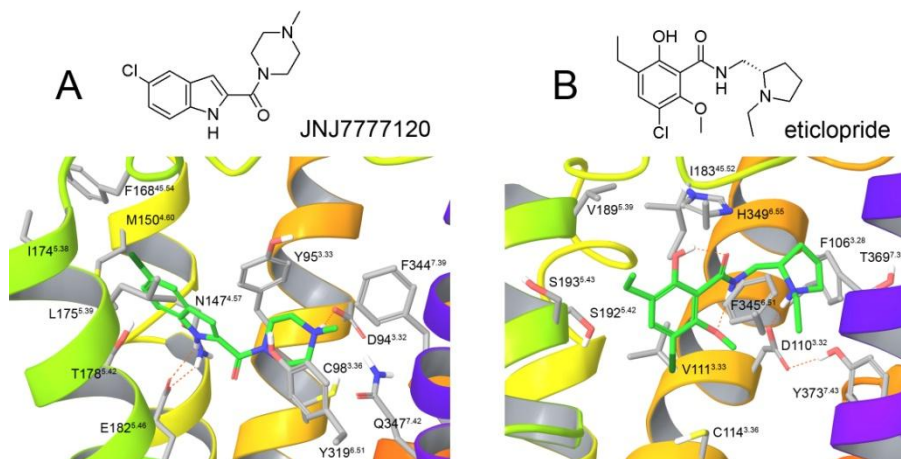


Figure 27. Ligand structures and binding pockets of the initial receptor structures. A) Homology model of the human histamine H_4 receptor in complex with JNJ7777120; B) X-ray structure of the human dopamine D_3 receptor in complex with eticlopride. Receptors are represented as ribbons (helix 6 omitted for clarity) with interacting amino acids and ligands in grey and green skeletons, respectively and H-bonds in orange dash line.

The D_3 receptor binding site is also quite rigid, only Cys114^{3,36}, Ser196^{5,46} and Thr369^{7,39} assume an alternative rotamer state featuring alternative H-bonds in a few representative structures (Figure 28). Interestingly, His349^{6,55} was rather flexible, which seems to be in a tight H-bond network in the crystal structure. The ligand interaction pattern changed little; the highest RMSD from the crystal binding mode was 2.4 Å after superposition of the proteins, the ethylpyrrolidine part of eticlopride was able to move somewhat without losing the ionic interaction with Asp110^{3,32} (shown in Figure 27).

4.2.2 Single structure and ensemble docking results

In the case of the H_4 receptor the Gedeon Richter fragment library was docked to the homology model and to the 28 representative conformations collected from the molecular dynamics simulation, while for the D_3 receptor docking has been carried out to the prepared X-ray structure and the 27

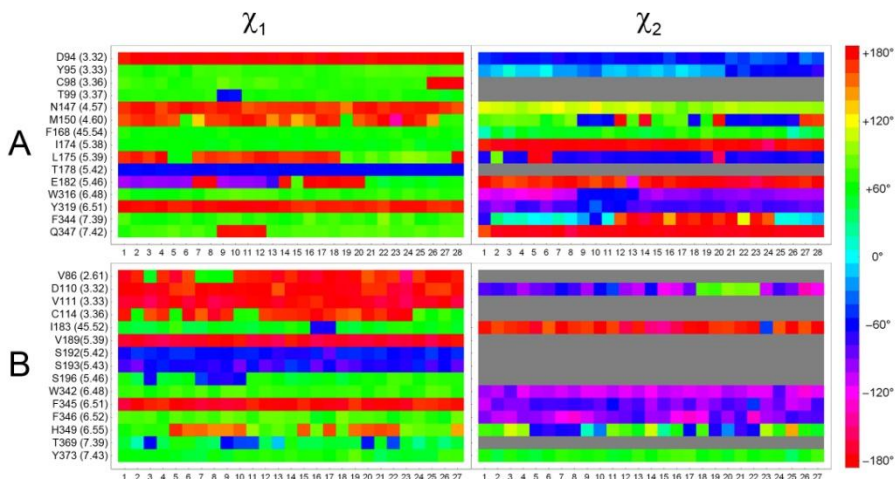


Figure 28. Conformational variability of the binding sites: χ_1 and χ_2 side chain angles of binding site amino acids for each representative MD frame in A) the H_4 receptor and B) the D_3 receptor. Angles are color coded according to the legend.

representative conformations from simulation. In both cases individual structural models provided a wide range of docking scores (GlideScore) but the single starting structure provided lower scores overall than the selected frames from MD (note that MD frames were only partially minimized). For example the docking scores of the top scoring fragments in each of the H_4 frames ranged from -8.093 to -9.920 but it was -10.686 for the homology model. Similarly for the D_3 receptor top scores ranged from -8.063 to -9.514 but it was -9.796 for the X-ray structure. Since binding sites appeared to be quite rigid during the MD simulation, these differences in the docking scores can be attributed to little variations in side chain geometries, indicating that specific interactions in the X-ray structure and homology model are in the optimal geometry with their respective ligands, while they loosen up during MD. Thus the distribution of the top scores indicate that X-ray structures and homology models have optimized protein-ligand interaction patterns while MD snapshots represent more diverse conformations, which are able to select more chemotypes than those optimized structures.

For the single structures it was straightforward to select the top 50 fragments by GlideScore ranking for biological testing. For ensemble docking two different data fusion methods were considered. The rank-by-rank and rank-by-number consensus scoring schemes were investigated; the rank-by-vote method was shown to provide poorer results [221]. In the rank-by-rank scheme ligands are finally ranked by the mean of their rank numbers in each docking run to the representative structures. It was also investigated whether low standard deviation of ranks accompanies low

mean ranks and a strong correlation was confirmed between average rank and its standard deviation for fragments having mean rank lower than 500 (see Figure 29). These fragments also fell in the top 1% of the ranked database in more than 3 representative frames both for the D₃ and the H₄ receptor. The correlation becomes less pronounced for higher mean ranks and eventually turns around for compounds ranked high by all MD frames. In the rank-by-number scheme ligands are finally ranked by the mean of their docking scores. It has been shown that using the mean of standardized Z-scores outperforms the average of the original scores; hence in this work the standardized GlideScores were evaluated. However, non-normal distribution of the GlideScores was observed for the fragment library and since there was two-thirds overlap between the top 50 selected by the rank-by-rank and rank-by-number schemes, the first one was finally used to select fragments for biological testing.

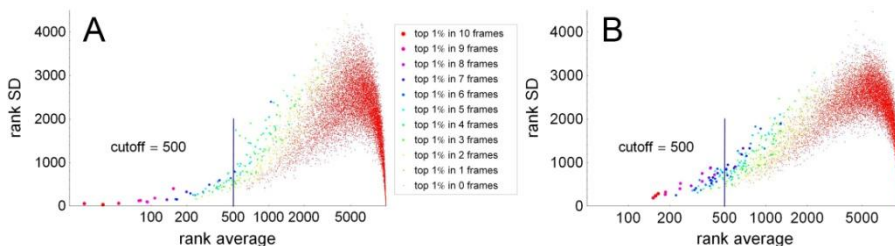


Figure 29. Log-linear plot of fragment rank averages and standard deviations of ranks in the ensemble docking approach for A) the D₃ receptor and B) for the H₄ receptor. Rank standard deviation is plotted against rank average calculated from the ranks obtained in the representative receptor structures for the 12,905 fragments. Markers are size and color coded by the number of receptor frames in which the fragment fell within the top 1% of the ranked library.

4.2.3 Pharmacological activities

In the case of the D₃ receptor 50 fragments from the X-ray structure docking run and 56 fragments from the ensemble docking run were selected for biological testing. These lists had 14 compounds in common, thus altogether 92 fragments were tested for D₃ binding affinity in 10 μM concentration. In the case of the H₄ receptor 50 fragments from the initial homology model docking run and also 50 fragments from the ensemble docking run were selected for biological testing. These lists had 15 compounds in common, thus altogether 85 fragments were tested for H₄ binding affinity in 10 μM concentration. The only 30% overlap between the different methods is not altogether surprising since the crystal structure and the homology model select compounds that bind to a specific receptor

conformation while ensemble docking selects compounds that have reasonably good interaction patterns with multiple receptor conformations. It has also been shown that the overlap of hits picked up by different screening paradigms likewise might be very low [222].

Table 7. Hit rate statistics for the two receptors considered in this study. Hits are defined as showing higher than 20% inhibition in the D_3 and H_4 radioligand binding assays.

	D_3	H_4
combined hit rate	25/92 (27%)	15/85 (18%)
single structure hit rate	9/50 (18%)	11/50 (22%)
ensemble docking hit rate	18/56 (32%)	8/50 (16%)
overlap between hit sets	2/25 (8%)	4/15 (27%)

In the case of D_3 25 virtual hits provided higher than 20% inhibition in the biological assay, corresponding to a combined hit rate of 27% (hit rates are summarized in Table 7). Out of these 9 came from the crystal structure docking run (18% hit rate) and 18 from the ensemble docking run (32% hit rate) with only 2 overlapping compounds. Binding affinity was determined for the 8 best compounds exhibiting higher than 75% inhibition at 10 μ M concentration (see Table 8 and appendix K). K_i values were in the range of 0.17 to 2.8 μ M. Besides binding affinity various ligand efficiency metrics are applied in fragment-based lead discovery in order to prioritize fragment hits. These metrics incorporate molecule size either in terms of molecular mass or heavy atom count and lipophilicity usually represented with the calculated octanol-water partition coefficient clogP . In this work ligand efficiency ($\text{LE} = -\text{RTln}(K_i)/\text{HA}$) and lipophilic ligand efficiency ($\text{LELP} = \text{clogP}/\text{LE}$) were considered. Since the D_3 ligands identified here are very tight binders, LE values much higher than the usually accepted lower limit of 0.3 were obtained. As they are also on the lower side of lipophilicity, LELP values mostly below 5 were found, compounds **2** and **4** being the most favorable.

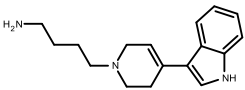
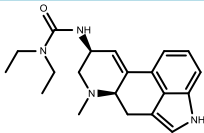
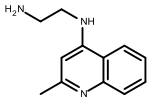
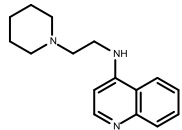
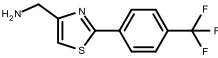
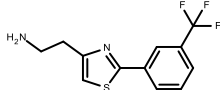
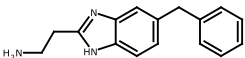
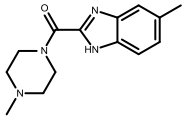
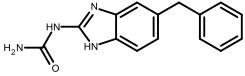
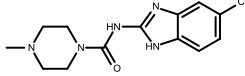
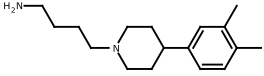
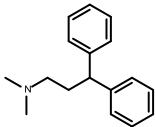
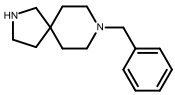
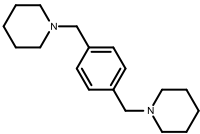
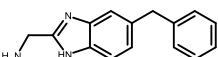
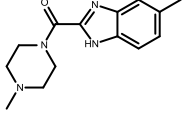
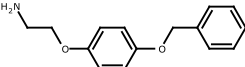
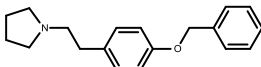
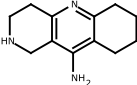
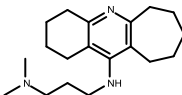
In the case of H_4 somewhat fewer, 15 virtual hits provided higher than 20% inhibition in the biological assay, corresponding to a combined hit rate of 18%. Out of these 11 came from the homology model docking run (22% hit rate) and 8 from the ensemble docking run (16% hit rate) with 4 overlapping compounds. Five of them were unavailable in the compound collection in sufficient quantity for binding affinity measurement but K_i values were determined for the remaining 10 compounds (see Table 9 and Appendix K). These were in the range of 8.4 to 75 μ M, an order of magnitude higher than the hits for the D_3 receptor. The lower hit rate and

Table 8. Experimental binding affinities of selected fragment hits of the D₃ receptor and their LE and LELP values. The origin of the hit is indicated in the XRD and MD columns with + meaning the fragment was a virtual hit in the crystal structure docking or in the ensemble docking, respectively. Closest structural analogs from ChEMBL with measured binding affinity or functional activity against any of the five dopamine receptors are also indicated.

cpd	Structure	K _i / μM	LE	LELP	XRD	MD	Closest known D ₁₋₅ R ligand
1		0.17	0.66	3.7		+	
2		0.50	0.57	1.2	+	+	
3		0.59	0.61	4.4		+	
4		1.1	0.63	0.7		+	
5		1.1	0.74	2.7	+		
6		1.6	0.66	4.2		+	
7		2.8	0.47	5.6	+		
8		2.8	0.40	4.2		+	

the lower binding affinities indicate a difference in the chemical tractability of the two receptors. LE values of the H₄ ligands were correspondingly not as high as for D₃ but still above the 0.3 limit up to 0.45. Also, the H₄ ligands were somewhat more lipophilic resulting in higher LELP values, though still below 10. Especially fragments **10** and **18** showed favorable LE and LELP

Table 9. Experimental binding affinities of selected fragment hits of the H_4 receptor and their LE and LELP values. The origin of the hit is indicated in the HM and MD columns with + meaning the fragment was a virtual hit in the homology model docking or in the ensemble docking, respectively. Closest structural analogs from ChEMBL with measured binding affinity or functional activity against any of the four histamine receptors are also indicated.

cpd	Structure	$K_i / \mu\text{M}$	LE	LELP	HM	MD	Closest known $H_{1-4}R$ ligand
9		8.4	0.35	6.4	+	+	
10		12.6	0.45	2.1	+		
11		14.3	0.39	7.1	+		
12		20.6	0.34	8.3	+		
13		21.9	0.32	9.3	+		
14		32.0	0.31	7.4	+		
15		32.9	0.36	5.4	+	+	
16		58.4	0.32	8.0	+	+	
17		58.7	0.32	8.1	+		
18		75.1	0.37	2.3		+	

values. Taken together, these fragments would be suitable starting points for medicinal chemistry optimization; however, the scope of this work was to analyze the impact of different virtual fragment screening methodologies on hit finding.

When hit-to-lead programs are initiated, novelty of the hits is also a crucial point. To assess this, substructure and similarity searches were conducted in the ChEMBL bioactivity database ([35], accessed 21 January 2014). D₃ hits were checked against all compounds with bioactivity data measured on the five dopamine receptors, while H₄ hits against compounds with bioactivity data measured on the four histamine receptors. Exact substructure searches provided hits for **10** and **17**, and similarity searches revealed additional similar known structures (see Table 8 and Table 9). Compounds **2**, **4**, **8**, **15** and **18** proved to be truly novel ones, and others might also suggest potential unexplored growing vectors.

Comparing the hit rates it can be seen that both X-ray structure and homology model were capable of providing useful hits in virtual screening, and in this particular case the homology model performed even better than the crystal structure. The superiority of the ensemble docking approach is not witnessed in this work. While for the D₃ receptor the latter provided a substantially higher hit rate, the homology model performed best for the H₄ receptor even though it was not preliminarily optimized in retrospective enrichment studies. Based on these results it can be concluded that both single structure and ensemble docking is useful for virtual fragment screening and seem to be complementary as the overlap between hit sets was low. Consequently a combined approach would maximize the outcome of hit finding efforts.

4.2.4 Binding modes

While no H-bond or pharmacophoric constraints were applied during docking the majority of the virtual hits in all four hit lists were basic amines forming ionic or H-bond interactions with the conserved Asp110^{3,32} in D₃ and the homologous Asp94^{3,32} in H₄ or the other acidic residue Glu182^{5,46} also known to play an important role in the recognition of histamine in H₄. In the case of the D₃ receptor it was found that docked poses of the in vitro active fragments provided very similar binding modes in multiple representative receptor conformations obtained by molecular dynamics simulation. Also the fragment binding modes from the X-ray structure docking were pretty much similar to the ensemble binding modes further strengthening the probability of their biological significance [105].

For example the thiazolemethanamine **1** produced nine very similar binding modes in ensemble docking with the basic amine interacting with

Asp110^{3.32}, the thiazole ring encased between Phe346^{6.52} and Val111^{3.33} and the chlorophenyl moiety facing His349^{6.55} and Val350^{6.56} with the chlorine substituent preferably pointing to the former, though in three poses pointing to the latter. The docked pose for the crystal structure is similar, though a bit shifted towards Asp110^{3.32} and the chlorophenyl moiety rotated by 90 degrees and the chlorine pointing to Val350^{6.56} (Figure 30). The tricyclic D₃ fragment **2** is quite rigid and produced eleven very similar binding modes and also the binding mode in the crystal structure was almost identical. The basic amine group again forms an ionic H-bond to Asp110^{3.32} and the aromatic ring almost overlaps with the chlorophenyl moiety of fragment **1**. In a few structures an H-bond between the fragment amide N-H and the hydroxyl group of Ser196^{5.46} or the backbone carbonyl of Ser192^{5.42} is perceptible (Figure 30).

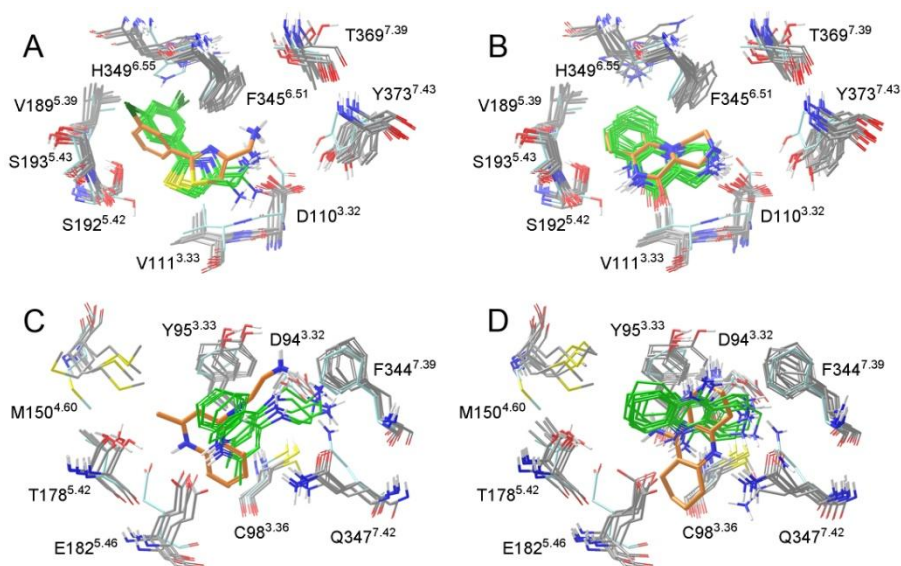


Figure 30. Interaction modes of selected fragment hits obtained by single structure and ensemble docking. A) **1** in the D₃ binding pocket; B) **2** in the D₃ binding pocket; C) **10** in the H₄ binding pocket; D) **18** in the H₄ binding pocket. Selected interacting amino acids of the crystal structure and the homology model are shown in light blue skeleton, those of the representative MD frames in grey, single structure docked fragment poses in orange and ensemble docked poses in green skeletons. In A) and B) Phe346^{6.52}, Val350^{6.56} and Ser196^{5.46} are omitted for clarity. In C) and D) Tyr319^{6.51} and Leu175^{5.39} are omitted for clarity.

In the case of the H₄ receptor the picture was not as clear as for D₃. There was substantially higher variability among docked poses in the ensemble approach and binding modes from docking to the homology

model produced different results in more cases. The major cause for this was probably the different rotameric state of Glu182^{5,46} in the homology model and in most of the representative frames from MD. Compound **9** for example produced a variety of binding modes probably because of its multiple H-bond donor sites, though it got good docking scores both in the homology model and in the representative receptor conformations. Several similar poses were obtained for aminoquinoline **10**, in which the primary amine forms an ionic H-bond to Asp94^{3,32}, a cation- π interaction with Phe344^{7,39} and the protonated quinoline nitrogen forms another ionic H-bond to Glu182^{5,46}. In the homology model the fragment is shifted towards the extracellular side of the pocket because of the greater distance between the two acidic sites, the quinoline ring is flipped and the anilinic N-H forms an additional H-bond to the phenolic OH of Tyr319^{6,51} (Figure 30). Since this fragment was in the hit list from the homology model docking, the latter binding mode appears to be more feasible.

For the tricyclic **18** seven similar poses were found in which the aliphatic amine group interacts with Asp94^{3,32} and the carboaliphatic ring is encased between Tyr95^{3,33}, Met150^{4,60} and Leu175^{5,39}. However, in four of these poses the protonated pyridine, while in three poses the anilinic N-H forms an H-bond with Glu182^{5,46}. The pose found in the homology model differs from both of them: it is rotated by 90° with the aliphatic amine again interacting with Asp94^{3,32}, the anilinic N-H with Glu182^{5,46} the protonated pyridine with Gln347^{7,42} and the carboaliphatic ring pointing towards the intracellular cavity of the binding site (Figure 30). Since this fragment was in the hit list from ensemble docking, the former binding mode appears to be more feasible.

These findings underpin the superior hit rate for D₃ and the inferior hit rate for H₄ of the ensemble approach against the single structure hit rates. Also the higher binding affinities of D₃ fragments correspond to the lower variability of their predicted binding modes [105].

4.3 Multiple ligand docking

In this part of the work performance of a sequential docking protocol was evaluated for modeling cooperatively bound ligands in the binding sites of proteins. The work was carried out on a small molecule data set of 129 ternary and higher order complexes compiled from the PDB crystallographic database. During model development two potentially interesting applications emerged, namely the prediction of cytochrome P450 enzyme activators and the application to virtual second site fragment screening.

4.3.1 Docking performance for the first ligand

Sampling efficiency of docking programs is most often assessed by RMSD values calculated between docking poses and experimental binding modes. The RMSD distribution of top scoring poses and ranks of the best poses are informative of scoring performance. Evaluating the sampling efficiency of Glide in multiple ligand docking first the median and mean RMSDs were calculated for the top scoring and the best pose of the first ligands and compared the results to those obtained in single ligand docking for 68 high resolution X-ray complexes [223] (see Table 10). It was found that median and mean RMSDs of top poses were typically higher in this data set than those for single ligand docking as expected for docking ligands significantly smaller than their respective binding sites.

Table 10. Statistical results for docking the first ligands to multiple ligand binding sites and for single ligand docking.

RMSD	This work			Cross et al. [223]		
	median (Å)	mean (Å)	std. dev. (Å)	median (Å)	mean (Å)	std. dev. (Å)
SP top pose	1.31	2.42	2.49	1.22	2.08	2.49
SP best pose	0.54	1.23	1.50	0.72	1.30	1.40
XP top pose	1.90	2.96	2.93	1.15	1.97	2.13
XP best pose	0.76	2.16	2.56	0.79	1.34	1.53
SP hard top pose	1.34	2.40	2.48	-	-	-
SP hard best pose	0.49	1.29	1.66	-	-	-

Although XP mode is usually considered being more precise, the difference in top pose median RMSDs is smaller for the SP protocol than that for the XP (0.09 Å and 0.75 Å, respectively). Best pose median RMSDs were, however, somewhat smaller than those of Cross et al. (0.18 Å and 0.03 Å for SP and XP, respectively). This might not be specific to multiple ligand docking but might even be attributed to the difference in Glide versions. Standard deviations for the SP protocol are pretty much similar to those reported for single ligand docking, while for XP significantly higher values were obtained (with the difference of 0.8 Å and 1.0 Å for top poses and best poses, respectively). SP and SP hard protocols performed similarly when docking the first ligand. Although the top pose rates (the percentage of top poses within 2.0 Å RMSD relative to the experimental binding mode) reported by Cross et al. were identical for SP and XP protocols (69.1%) [223], for the present dataset it was found that SP based protocols outperformed XP (top pose rates were 58.0 %, 51.1 % and 58.0, for SP, XP and SP hard protocols, respectively). Other parameters such as the

resolution of the X-ray structure, relative B-factors (the ligand's mean B-factor divided by the whole structure's mean B-factor) and physico-chemical descriptors of the ligands showed virtually no impact on docking accuracy (data not shown).

4.3.2 Docking performance for further ligands

The objective in this step was the evaluation of the sequential docking methodology. To achieve this goal the number of successful docking steps (defined by any docking pose within 2.0 Å RMSD) among the 30 saved poses and the impact of the number of consecutively docked ligands was investigated. Analysis of the expectation values revealed that the successive docking of more than two ligands is highly unlikely to give reliable results (Table 11). The calculated expectation values of the number of successful docking steps were 1.37, 1.03 and 1.40 for SP, XP and SP hard protocols, respectively, reflecting that the chance to recover at least two experimental binding conformations is 55%, 37% and 57%, respectively. In conjunction to that observed for docking the first ligand, it was found that SP and SP hard performed similar and much better relative to the XP protocol in multiple docking situations.

Table 11. Number of successfully docked ligands (RMSD < 2.0 Å) per binding site using SP, XP and SP hard protocols as the function of the number of ligands.

number of ligands at the site	number of sites	number of docking runs with n successful consecutive docking steps											
		SP				XP				SP hard			
		n=0	1	2	3	n=0	1	2	3	n=0	1	2	3
2	110	20	28	62	-	37	31	42	-	23	25	62	-
3	13	4	2	3	4	6	4	3	0	3	1	4	5
4	6	3	1	1	1	1	2	2	1	2	1	2	1
5	1	0	0	1	0	0	1	0	0	0	0	1	0
6	1	1	0	0	0	1	0	0	0	1	0	0	0
total	131	28	31	67	5	45	38	47	1	29	27	69	6

RMSD distributions for all docking steps and rank distributions for all successful (RMSD < 2.0 Å) steps were analyzed by Kolmogorov-Smirnov statistics (see Figure 31). RMSD distributions were significantly higher for the XP protocol as compared to that of SP and SP hard ($p < 0.005$). Rank distributions obtained by the default Emodel scoring function showed the reverse trend; XP provided significantly lower ranks relative to the other two protocols ($p < 0.05$), while SP and SP hard were similar. Rank distributions obtained by the three different scoring functions (Emodel,

GlideScore and Glide Energy) showed no statistically significant differences in any of the docking protocols (SP, XP, SP hard). In successful docking steps RMSDs were usually similar or lower for XP than that of the SP. However, it was interesting to see that the higher the rank of the selected pose (typically if larger than the 6th), the more challenging successful docking was for XP. Thus it seems that XP typically sorts out high-scoring poses only, and is unable to score better than SP in docking multiple ligands. RMSDs of the second docking steps were somewhat higher than those of the first docking steps; however their distributions were not significantly different from that of the first steps. Median RMSDs of second docking steps were 0.26 Å, 0.59 Å and 0.28 Å higher than first ones for SP, XP and SP hard, respectively. It was found that if the first ligand was docked successfully ($\text{RMSD} \leq 2.0 \text{ \AA}$), then the second docking step was also successful in 70% of the cases. If the first RMSD was over 2.0 Å, 86% of the second ligands also failed to dock successfully (in the SP protocol when the docking run was not terminated after an $\text{RMSD} > 2.0 \text{ \AA}$).

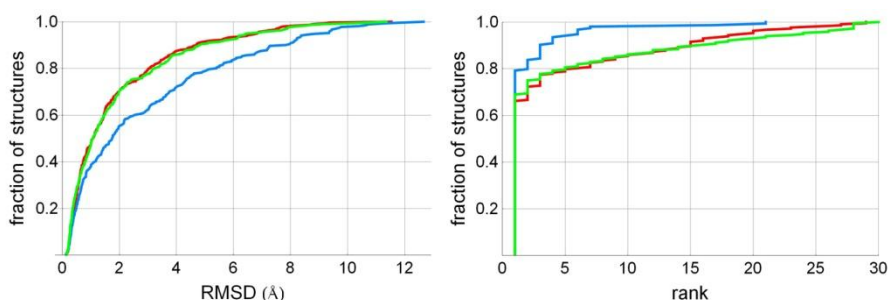


Figure 31. RMSD (left) and rank distributions (right) of all docking steps using the Emodel scoring function in the SP (red), XP (blue) and SP hard (green) protocols.

4.3.3 Performance on drug-like ligands and closed sites

Finally, the impact of ligand and binding site properties were investigated. Considering that scoring functions were typically optimized against a set of known binders of pharmaceutical targets and decoys with drug- and lead-like features [198-200], it was expected that multiple docking of drug-like ligands would be more efficient. This hypothesis was tested by ligands which did not violate any of the Lipinski's rules providing a 110-member drug-like subset. Using the SP protocol with Emodel scoring success rate calculated in at least two consecutive and successful ($\text{RMSD} < 2.0 \text{ \AA}$) docking steps increased from 55% to 59% (see Figure 32 and numerical data in Appendix H). The number of cases where the selected pose was actually the top ranking pose (top pose rate) was also increased

from 31% to 33%. There was a visible but in Kolmogorov-Smirnov statistics not significant difference between the RMSD distributions of Lipinski compliant and non-compliant ligands. It can be concluded that drug-like ligands performed only slightly better in multiple docking settings. XP and SP hard protocols showed similar characteristics as for the whole dataset. The success rates increased from 37% to 40% and 57% to 61%, respectively, while only marginal improvements were seen in top pose rates (from 25% to 26% and from 34% to 35%, respectively). Success rates and top pose rates obtained by all the protocols with GlideScore and Glide Energy score were slightly lower.

It was also expected that docking to shallow and open binding sites would be more challenging than to the closed sites. Since in the former case ligands can exploit less binding interactions, scoring would be more difficult. Binding sites were therefore classified using their enclosure values calculated by SiteMap as 48 open and 83 closed sites. Out of the 83 closed sites 53 (64%) provided a docking pose within 2.0 Å RMSD relative to the experimental binding conformation in at least two successive steps. Docking to 29 out of the 48 open sites (60%), however, was unsuccessful yielding poses with RMSD larger than 2.0 Å. Finally combining the enclosure and drug-like filters docking drug-like ligands to closed sites was investigated. Evaluating at least two consecutive docking steps in this subset of 68 complexes success rates of 68%, 47% and 71% were obtained for the SP, XP and SP hard protocols with Emodel scoring, respectively. Top pose rates were 37%, 29% and 43%, respectively.

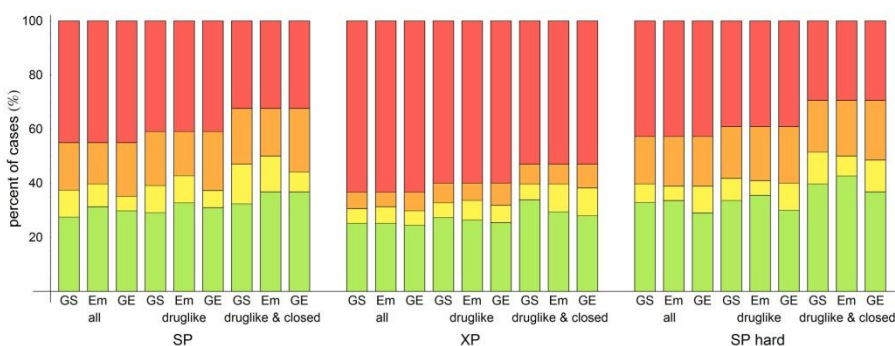


Figure 32. Cumulative success rates obtained in at least two successful consecutive docking steps for SP, XP and SP hard protocols combined with GlideScore, Emodel and Glide Energy scoring functions and filters (all sites, sites with druglike ligands and closed sites with drug-like ligands). From bottom to top: fraction of cases where both of the top ranking poses had RMSD < 2.0 Å (green), where any of the top three poses had RMSD < 2.0 Å (green+yellow), where any of the poses had RMSD < 2.0 Å (green+yellow+orange) and all structures in the subset (green+yellow+orange+red).

Independent analysis of each docking step required the selection of a near native binding mode for the first ligand that mimics the best case scenario in a real life screening situation. Since typically this information is not available in prospective applications the binding mode of the first ligand should be selected based on docking scores to merge with the receptor for the next round of docking. The simplest method is to merge the top pose identified by a single scoring function. Top pose rates calculated in two consecutive steps for the present dataset show the usefulness of this method. Thus using the SP hard protocol with Emodel scoring on drug-like ligands and closed binding sites binding modes obtained for 43% of the compounds are expected to be accurate. A computationally more demanding method would be to merge multiple (N) poses of the first docked ligand with the receptor and perform the second docking step on all of the acquired complexes saving multiple (N) poses again. However, in this method the selection of the best complex from the resulting $N \times N$ pool is not trivial. Instead, the performance for $N=3$ was evaluated by considering well-docked poses among the top three binding modes. This estimates the upper limit of the performance since the second docking steps usually failed when the first merged pose had an RMSD over 2.0 Å. Selecting the well-docked poses from a 30×30 pool would provide significant improvement on the expense of 31 grid generation and docking steps.

4.3.4 Case study: application to cooperative CYP binding

Cytochromes P450 (CYPs) are promiscuous metabolic enzymes with the ability to bind multiple ligands in their active site as demonstrated by X-ray crystallography [224]. *In vitro* CYP assays are generally used to predict *in vivo* pharmacokinetic properties and drug interactions of compounds. Determination of binding constants, however, is sometimes not straightforward as these assays often show non-Michaelis-Menten kinetic profiles [225] indicating the cooperative binding of substrates. There is a large body of evidence published on cooperative binding to CYP3A4 [226] and CYP2C9 [227] but similar findings have been reported for other isoforms as well. Heterotropic cooperativity in these isozymes may lie in the background of drug-drug interactions, though only a few studies were able to connect *in vitro* and *in vivo* observations [228-230]. Predicting drug interactions or metabolic activation by computational methods is a challenging task since metabolic enzymes have broad substrate specificities and their hetero-activation profile is substrate dependent. Up to now only two CYP3A4 and CYP2C9 heteroactivator pharmacophore models [231, 232] have been published and a single structure based docking method was developed to predict activators of CYP2C9-mediated flurbiprofen hydroxylation [233].

Since the present data set contained seven CYP structures it was straightforward to evaluate the performance of the sequential docking protocol on this set of pharmaceutically relevant enzymes. Two further CYP structures (human CYP2C8 with two bound retinoic acids with a resolution of 2.60 Å and human CYP3A4 with two bound ketoconazole molecules with a resolution of 3.80 Å) were added to this assembly as they fulfilled all but the resolution criterion, that were set up in the compilation of the data set. The resolution of the latter is worse than typically required for docking but here the structure was used since double occupancy is evident from the electron density map, however, the binding mode of the distal ligand may be ambiguous. The CYP dataset contained six bacterial and three mammalian CYP isoforms. Crystallographic properties are summarized in Table 12.

Table 12. Crystallographic and docking data of cytochrome P450 structures with multiple bound ligands. res. = resolution, vol. = site volume calculated by SiteMap, encl. = enclosure calculated by SiteMap, lig. ID = ligand number, B-fact. = mean B-factor of the ligand, Em = rank by Emodel.

PDB ID	CYP iso-form	res. (Å)	vol. (Å ³)	encl.	lig. ID	B-fact. (Å ²)	RMSD (Å) SP	Em	RMSD (Å) XP	Em	RMSD (Å) SP hard	Em
1egy	107	2.35	490	0.93	1	25.73	0.19	1	0.18	3	0.20	1
					2	35.40	0.36	3	0.32	1	0.33	2
1eup	107	2.10	615	0.91	1	29.95	0.57	1	0.68	4	0.45	1
					2	47.27	0.73	1	0.62	1	0.93	1
2whf	130	1.58	645	0.76	1	43.67	0.77	2	>2.00	-	1.97	2
					2	38.02	0.68	5	>2.00	-	1.25	1
2d0e	158	2.15	563	0.91	1	47.45	0.50	3	0.76	3	0.25	12
					2	71.84	0.42	1	>2.00	-	0.35	1
1t93	158	1.62	358	0.95	1	16.50	0.48	3	0.48	4	0.45	2
					2	16.22	0.52	9	>2.00	-	0.27	8
2z3u	245	2.40	353	0.91	1	14.79	0.20	1	0.22	1	0.18	1
					2	33.02	0.40	1	0.40	1	0.34	1
3g5n	2B4	2.50	633	0.67	1	64.48	0.25	1	0.53	1	0.94	1
					2	40.36	0.48	1	>2.00	-	0.41	1
					3	73.21	>2.00	-	>2.00	-	>2.00	-
2nnh	2C8	2.60	772	0.87	1	57.23	0.49	1	0.39	1	0.40	1
					2	54.19	0.52	14	1.94	1	0.55	1
2v0m	3A4	3.80	1247	0.81	1	34.35	0.89	1	0.86	1	1.17	1
					2	71.84	1.94	2	1.20	6	1.54	30

It can be seen that except for the triple occupancy 3g5n structure, all other CYP sites are characterized closed due to high enclosure values. Calculated site volumes confirm that bacterial CYP isoforms comprise much more compact sites, while mammalian CYPs exhibit more spacious ones that can accommodate compounds of various sizes. The ligands present in the bacterial and the rabbit 2B4 isoforms fulfill Lipinski's rule of druglikeness, while in human CYPs a logP value of 5.01 was calculated for retinoic acid and ketoconazole has a molecular weight of 531 Da, both rather close to corresponding Lipinski limits. Most B-factors of the ligands are relatively low indicating that the experimental binding modes are realistic. Based on previous experience these observations suggested good docking results. In fact, SP and SP hard protocols with Emodel scoring provided successful poses in all cases but one that was the third ligand in the only triple ligand complex, being superior to the performance on the full data set. Again, the performance of the XP protocol was inferior; 6 of the 19 docking steps were unsuccessful. SP provided 6 of the 9 structures with good poses found among the top three poses in both steps, while XP performed similarly for only 3 complexes (see Table 12 for docking results).

The aminophenanthrene ligand coordinating the heme iron in 1egy was docked perfectly as the top pose by both SP and SP hard protocols. The top pose of XP had the aromatic rings flipped but occupied almost the same space. The second ligand made apolar contacts with the aromatic and aliphatic side chains of the active site and its amino group was not involved in any hydrogen bonds in the crystal structure. Interestingly, Glide identified a hydrogen bond in most of the top ranked poses to the hydroxyl group of Tyr75 or to the backbone carbonyl of Phe86. As a result a flipped pose or even an irrelevant binding mode was predicted.

The proximal androstenedione in 1eup forms a hydrogen bond with both of its carbonyl groups. One of them is with Asn89 that was lost in the docking runs due to flipped asparagine side chain created by the Protein Preparation Wizard when optimizing the H-bond network. Despite this Glide identified the experimental binding mode as top. Many misdocked poses featured a perpendicular orientation of the androstenedione molecule to the heme probably because of the overemphasized electrostatic interactions between the heme iron and one of the carbonyl groups. The distal ligand was well-docked with all docking protocols.

In 2whf the scoring function ranked a flipped iron coordinating pose to the top thus rendering the well-docked distal pose second. It was interesting to see that the distal ligand could penetrate deeper into the active site with its aromatic end, retaining only one of its hydrogen bonds that resulted in a high RMSD (see Figure 33). Surprisingly no heme iron coordinating pose could be found with the XP protocol.

2d0e and 1t93 are structures of the same isoform cocrystallized with very similar ligands, thus the two binding sites are nearly identical. Flaviolin and hydroxynaphthoquinone molecules form multiple hydrogen bonds. Active site Arg288 anchors the ligands in both experimental and docked poses in addition to aromatic stacking with the heme and each other. Interestingly this was not preserved in the top ranking poses of the first docking steps instead a binding mode with three hydrogen bonds was found for both compounds. For the second docked flaviolin molecule the stacking interaction was captured well but poses involved in more hydrogen bonds were still enforced for hydroxynaphthoquinone even at the expense of distorting the planarity of its rings.

In 2z3u the two chromopyrrolic acid residues (the natural substrate of CYPStaP) are held very firmly by multiple hydrogen bonds, π - π and cation- π interactions that were predicted successfully as the top ranked pose in all docking protocols.

3g5n was one of the cases where the inner grid box contained only two out of the three ligand centroids. Two molecules were correctly docked by SP based protocols (see Figure 33). The semi-distal ligand forms contacts mostly with aromatic and aliphatic side chains that were correctly identified in the first docking step. Its imidazole part is encased in a polar environment but is not involved in specific interactions. The iron coordinating binding mode was found second by the SP protocols, but XP missed the iron coordinating pose again. The binding conformation of the third ligand, which is partially exposed to the solvent with its imidazole ring, could not be reproduced by either of the protocols. Instead poses exhibiting aromatic stacking with the iron coordinating ligand and involved in a hydrogen bond with the amide hydrogen of Gly99 were obtained.

The retinoic acid molecules in 2nnh are both involved in two strong hydrogen bonds with the backbone amides of Gly98 and Ser100 for the proximal and with Asn204 and Arg241 for the distal ligand. These interactions were recovered in all docked poses that resulted in good ranks in the first docking step. On the other hand, however, the ring of the distal ligand was flipped in many poses in the second docking step that was responsible for RMSDs greater than 2.0 Å, though the binding motif is essentially the same (see Figure 33).

The binding mode of the proximal ketoconazole molecule in 2v0m was remarkably well reproduced with all docking protocols. The acetyl piperazine moiety of the distal ligand was positioned well in the second step; however, the dichlorophenyl and imidazole rings were typically misdocked that increased the RMSDs significantly (see Figure 33). The chlorine atom of the distal ligand forms interactions with the backbone amide of Leu216 and the aromatic ring of Phe213 while its imidazole ring faces a polar environment

in the crystal structure. These interactions were replaced by a hydrogen bond between the backbone of Asp217 and the rotated imidazole ring in many of the docked poses resulting high ranks in the second step. It should be noted, however, that the electron density at the head region of the distal ligand was poorly defined [224] and the experimental binding mode might also be questionable.

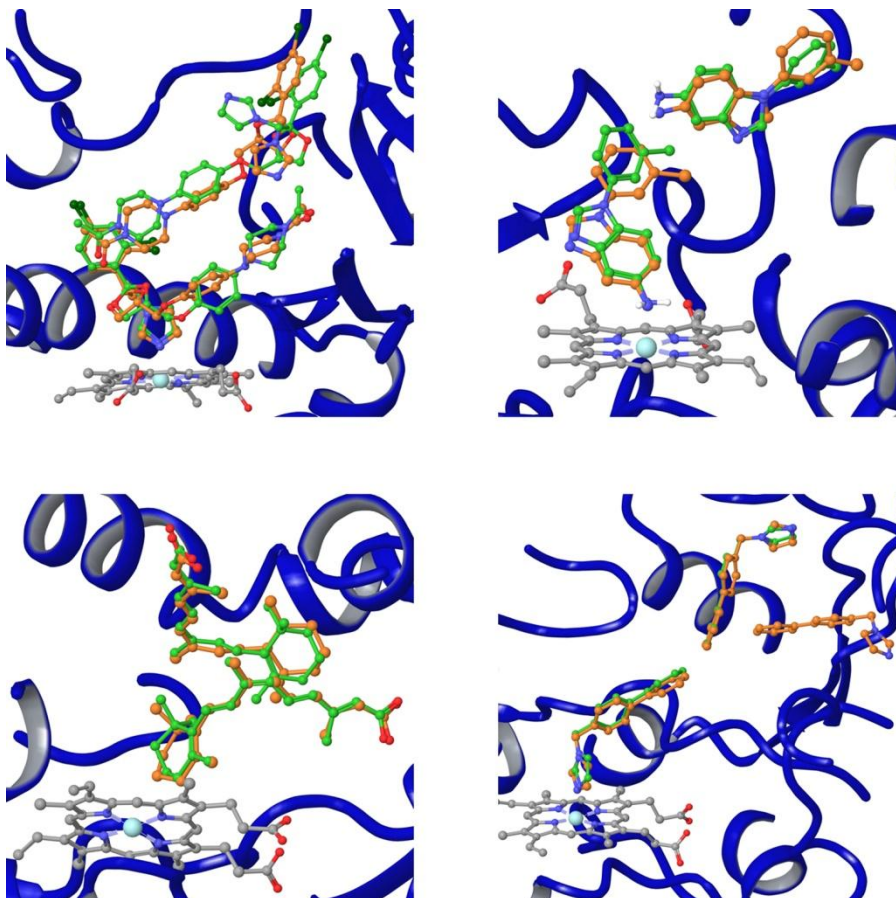


Figure 33. Representative binding modes found in cytochrome P450 complexes with multiple ligands by the SP protocol and Emodel scoring. Top left: 2v0m, top right: 2whf, bottom left: 2nnh, bottom right: 3g5n. Heme carbon, docked ligand carbon, docked ligand polar hydrogen, co-crystallized ligand carbon, oxygen, nitrogen, chlorine and iron atoms are colored grey, green, white, orange, red, blue, dark green and cyan, respectively.

4.3.5 Case study: application to fragment binding to HSP90

One of the most important drug discovery applications of multiple ligand docking can be fragment based hit identification. The present approach provides the virtual equivalent of experimental second site screening in order to find fragments suitable for linking. Demonstrating this capability five complexes of the heat shock protein 90-alpha (HSP90) were picked up from the dataset that were obtained in fragment based discovery programs [203, 234-236]. Each of these complexes contains two different fragments mostly with low B-factors and fulfilling Lipinski's criteria by definition. The binding site of the protein is quite small and closed as indicated by the corresponding enclosure values. Crystallographic properties are summarized in Table 13. These features implicated successful docking but high RMSDs and ranks were obtained. With the exception of the 2xdu complex, protocols were able to reproduce experimental binding modes, but poses within 2.0 Å RMSD were typically not ranked into the top three poses (the average rank was 8.3). However, structural waters are known to play an important role in ligand binding to HSP90 [203]. Visual inspection indeed revealed that top ranked high RMSD poses overlap with conserved crystal water molecules that were omitted by the Protein Preparation Wizard in the original protocol.

Table 13. Crystallographic and docking data of HSP90 complexes with multiple fragments. Conserved waters were included in all docking runs. *res.* = resolution, *vol.1* = site volume calculated by SiteMap without waters, *vol.2* = site volume with waters, *encl.* = enclosure calculated by SiteMap, *lig. ID* = ligand number, *B-fact.* = mean B-factor of the ligand, *Em* = rank by Emodel.

PDB ID	res. (Å)	vol.1 (Å ³)	vol.2 (Å ³)	encl.	lig. ID	B-fact. (Å ²)	RMSD (Å) SP	Em	RMSD (Å) XP	Em	RMSD (Å) SP hard	Em
2qfo	1.68	388	325	0.76	1	15.95	0.38	1	0.38	1	0.43	1
					2	17.41	0.16	1	0.16	1	0.26	1
3hz1	2.30	476	365	0.80	1	25.84	0.46	1	1.10	1	0.29	1
					2	18.53	0.47	1	1.25	1	0.38	1
2xdu	1.74	412	351	0.81	1	24.60	0.21	11	0.21	1	0.20	1
					2	33.47	0.29	1	0.30	1	0.24	1
2yei	2.20	419	362	0.80	1	47.47	1.04	1	0.28	1	1.14	3
					2	42.31	0.90	1	1.13	1	0.95	1
2yej	2.20	447	347	0.78	1	53.74	1.02	1	1.02	1	1.04	1
					2	82.07	0.42	1	0.40	2	0.25	1

A total of six conserved water molecules were identified that form hydrogen bonds with the Asn51, Asp93 and Trp162 side chains, backbone carbonyls of Leu48 and Gly97, backbone NH of Gly137 and with each other as described in the methods section. Repeating the docking runs with the six conserved waters included, yielded top ranked poses with RMSDs less than 2.0 Å for all of the docking steps in the SP protocol, and most of the docking steps in the XP and SP hard runs (see Table 13 for docking results). These results were again far superior to the performance on the full data set. The binding site volumes calculated with SiteMap decreased by 60-110 Å³ while enclosure values did not change significantly. The better ranks of the well-docked poses, however, are probably not only the results of the decreased site volumes and different binding site shapes. Instead without waters included, docked fragments interact with the same side chains of the receptor that form hydrogen bonds in the water mediated complex.

Docking the phenylaminofuranone first to 2qfo without waters the top pose forms direct hydrogen bonds with Asp93 and Asn51 taking the place of the pyrimidinamine moiety. In 3hz1 and 2yej top poses of all ligands form direct hydrogen bonds with the carbonyl of Leu103 without waters while in the crystal structures the pyrazole ring forms a water mediated bridge with the same amino acid. In top poses identified in 2yei direct hydrogen bonds to Leu103 and Trp162 were found without considering structural waters. Thus the region around the Leu103 carbonyl group is a docking hot spot of HSP90. Examples of docking results are shown in Figure 34. In this system the SP protocol with Emodel ranking proved to be the best in binding mode reproduction but even the XP and SP hard protocols failed at the ranking of only one well-docked pose.

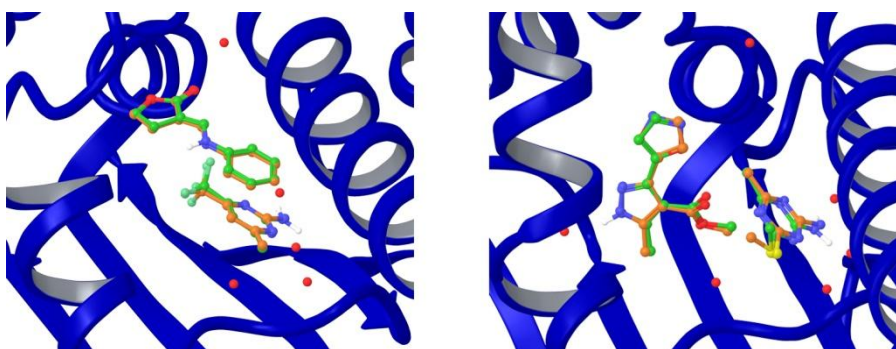


Figure 34. Representative binding modes of ligands in HSP90 complexes obtained with the SP protocol using Emodel scoring with conserved waters included. Left: 2qfo, right: 2yej. Docked and experimental ligand binding modes are shown in green and orange skeleton, respectively, waters as red spheres.

4.4 Multiple fragment docking

Encouraged by the finding in the previous stage of the work, I intended to investigate more thoroughly the performance of the reported methodology on further ternary protein-fragment complexes to provide a docking-based computational tool for identifying suitable starting points for the fragment linking approach. 32 complex structures of cooperatively bound or synthetically linked fragment examples were collected from the literature and the sequential docking protocol was applied to the two fragment ligands.

4.4.1 Self-docking results

Docking results are shown in Figure 35. Details of the PDB structures, structures of the docked ligands and numeric docking results are given in Appendix I. The structures have reasonably good resolution ranging from 0.95 to 2.60 Å, only two having resolution over 2.5 Å, the cutoff used in the previous stage of the work. Targets among others include proteases, kinases, phosphatases and metalloproteins, and are implicated in the pathomechanisms of cancer, diabetes, Alzheimer's disease, etc.

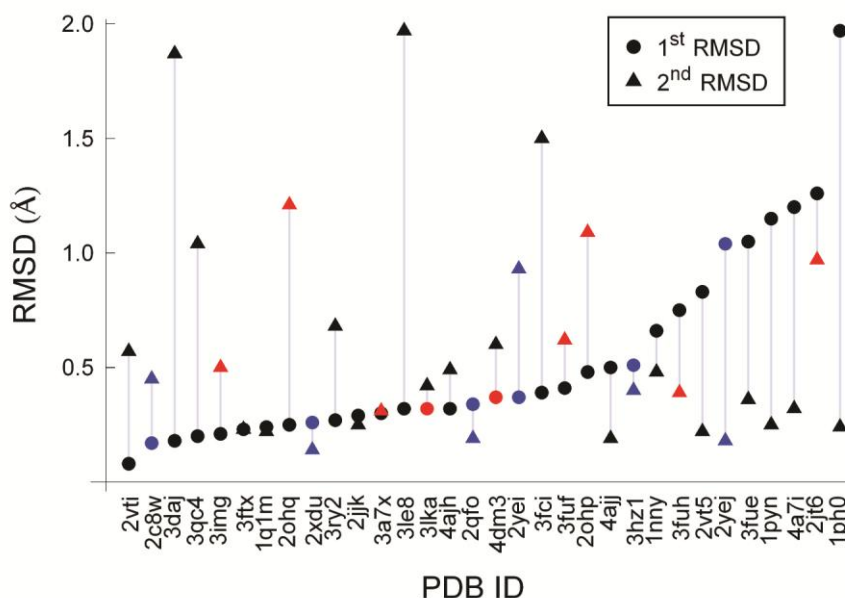


Figure 35. Multiple fragment docking results obtained by sequential Glide docking. Plot markers are colored red for docking steps with scoring errors (*Emodel* rank > 1) and blue for complexes where structural waters were included in grid generation.

As can be seen, the default sampling of Glide SP was sufficient in all of the examples: a pose was always found with RMSD < 2.0 Å to the experimental binding conformation among the top 30 saved poses. Furthermore, in 49 out of the 64 docking steps (77%) a pose with RMSD < 1.0 Å, and in 39 cases (59%) a pose with RMSD < 0.5 Å were found, the distribution of whose did not depend on whether the first or the second docking steps are in question. This result is especially important, since the accurate prediction of the binding poses is a precondition for the successful structure based design of appropriate linkers. The linker length is approximately 1.3 Å for a methylene group in the extended conformation, and even if both predicted binding modes have only a 0.5 Å uncertainty, the sum of errors can be in the range of an extra linker atom. Hence, the generally low average error of Glide posing is encouraging for *in silico* FBDD.

There are reports in the literature stating that conventional docking scores underperform for fragments, however, studies of Sándor et al. [59] and Verdonk et al. [60] revealed no significant difference in docking performance between fragments and drug-like molecules with success rates ranging from 50% to 90%. Similarly, in the present case the overall scoring was satisfactory, though in a few cases Glide had difficulty in identifying the experimental binding conformation from among the 30 saved poses. Considering the first docking stage only 2 fragments were not ranked top out of the 32 examples (6%). In the second docking step, the rate was somewhat higher, and in 7 cases (22%) was the Emodel scoring function unable to score the experimental binding mode as top.

It is hypothesized that this lower success rate in the second docking step can originate from two factors. One is the inaccuracy of the prediction of the first fragment's binding mode, which can in turn enlarge the error in the second docking step if the first docked fragment partially overlaps with the experimental binding conformation of the second. Such an effect was seen for the sequential docking of drug-like ligands previously, though it is not evident for the present dataset. Another possible reason is that only the first-site fragments can exploit specific interactions of the hot-spot, while the second site is usually less attractive and identifying the correct binding mode at these sites is intrinsically more difficult. The latter hypothesis is exemplified by 3 out of the 7 scoring errors, where top poses had extra or alternative H-bonds compared to the experimental binding modes. In 2ohp the indole fragment formed an H-bond to the Phe108 backbone carbonyl instead of the Gly230 backbone carbonyl. In 2ohq the methoxybiphenyl moiety was flipped to form an H-bond with Tyr71. In 3img the carboxyl group of benzofurane-2-carboxylic acid occupied the place of the sulfate ion between His44, Lys160 and Ser197, which belongs to the hot spot, since in 3le8 the carboxyl group of the indolyacetic acid also resides there.

4.4.2 Case studies: HSP90, PTP1B and HTX

Heat shock protein 90-alpha (HSP90) structures from the previous work stage were evaluated again using the newer versions of the software. Though significantly more accurate than before, docking to these structures without waters was still unsuccessful in the sense that poses within 2.0 Å RMSD to the experimental binding modes had an average rank of 6.4. Also, for the thrombin structure 2c8w the RMSD of the first docked ligand was 5.04 Å and thus the docking workflow was terminated. Only when structural waters were retained could a top ranked solution be found. For these six structures the docking results with waters are indicated in Figure 35.

Protein tyrosine phosphatase 1B (PTP1B) has been a difficult target pursued in the research for type II diabetes and obesity therapeutics. Since its catalytic site is identical to that of T-cell protein tyrosine phosphatase, achieving selectivity is a very challenging task. Moreover, PTP1B inhibitors tend to be large and highly charged with low membrane permeability. NMR-based second-site screening and linking of fragments was able to successfully overcome these obstacles and provided selective inhibitors with lower charge density [237-240]. Thus the docking results for these fragments were particularly interesting. In the four crystal structures of PTP1B the first-site fragments are *N,N*-diaryloxamic acids, phenoxymalonic acid and an isoxazole carboxylic acid anchored by Arg221, Gln266 and backbone NHs. Second-site fragments include a naphthoic acid and methyl

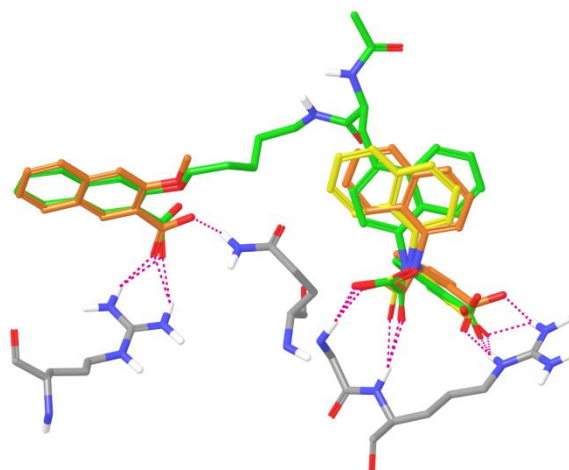


Figure 36. Top ranked docked binding conformations of the linked fragments (orange) overlaid with the experimental binding conformation of the linked compound from 1nny (green) and the first-site fragment binding conformation from 1no6 (yellow) in the binding pocket of PTP1B. Key interacting residues from 1nny are shown in gray and H-bonds in magenta.

salicylate based fragments interacting with Tyr20, Arg24, Arg254 and Gln262. The evolution from triacidic antagonists to monoacidic ones markedly improved their druglikeness. In the case of this target both binding sites seem to encompass specific interaction points. Docking results confirm this finding as low RMSD top ranked poses were obtained for all 8 fragments. However, the RMSD close to 2.0 Å for the *N,N*-diaryloxamic acid in the 1ph0 structure is a consequence of the misplacement of its unsubstituted phenyl ring, while the specific interactions could be predicted successfully. Similarly in the case of the 1nny structure the naphthyl ring of the first-site ligand was flipped in the top ranked poses compared to the experimental one (having an RMSD of 1.65 Å), and only after checking the other structures deposited together with 1nny was it noticed that this flip can also be seen experimentally. The RMSD calculated to the original binding mode in 1no6 was 0.66 Å. Figure 36 shows the top ranked binding modes compared to the 1nny and 1no6 experimental structures. Thus docking actually drew attention to a phenomenon that otherwise might have had been overlooked.

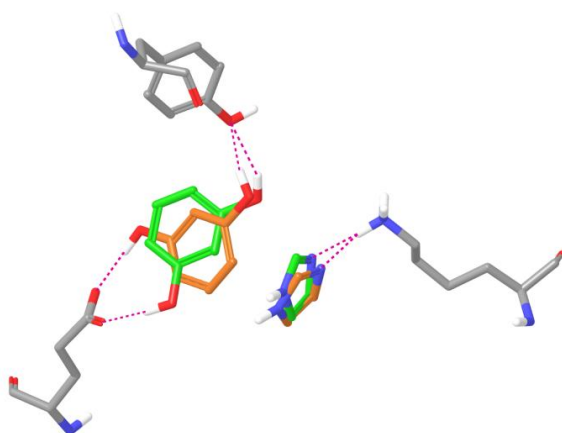


Figure 37. Top ranked docked binding conformations of the cocktail fragments (orange) overlaid with their experimental binding conformations from the 4dm3 structure of PNMT (green). Key interacting residues from 4dm3 are shown in gray and H-bonds in magenta.

High-throughput X-ray crystallography may be prone to experimental errors as shown by Mark et al. in a recent article, where they examined the validity of phenylethanolamine *N*-methyltransferase (PNMT) complexes acquired by fragment cocktail screening [241]. For one cocktail they found that the modeled 6-chlorooxindole binding mode was not stable in a molecular dynamics (MD) simulation. Instead, re-refinement of the electron density and subsequent MD confirmation revealed that two other

fragments of the cocktail were bound. In fact, resorcinol and imidazole bind together to PNMT forming specific interactions with Tyr35, Lys57 and Glu219, instead of only π -stacking interactions for 6-chlorooxindole. Glide was able to identify the binding modes of the two ligands with RMSDs of 0.37 and 0.61 Å. However, the experimental resorcinol binding mode was recovered only as the 5th in the Emodel rank order. Top poses formed H-bonds with the same amino acid side chains, but the aromatic ring was flipped (Figure 37). The imidazole binding mode was reproduced as a top ranked pose. Docking of 6-chlorooxindole to the alternatively modeled structure 3kpy provided RMSDs of 2.02–4.75 Å and various different binding modes. These findings implicate that docking could aid high-throughput X-ray crystallography in identifying multiple fragment binding from cocktails.

4.4.3 Cross-docking results

Cross-docking simulations were performed in order to assess the robustness of the sequential docking methodology with respect to small deviations in binding site geometry. The dataset contained two structures of *M. tuberculosis* pantothenate synthetase, lactate dehydrogenase A, fructose-1,6-bisphosphatase 1, and beta-secretase 1, four structures of protein tyrosine phosphatase 1B and leukotriene A4 hydrolase and five structures of the heat shock protein 90-alpha, which afforded altogether 52 cross-docking cases. Structures of the same protein were aligned using the Protein Structure Alignment tool in Maestro and the docking methodology was repeated for all combinations of protein–ligand pairs. The RMSD was calculated between the docked poses and the experimental binding conformations of the aligned pairs.

Docking performance for the first fragments was only slightly poorer compared to self-docking cases (shown in Figure 38, numeric docking results are given in Appendix J): there were two unsuccessful docking runs, where no pose with RMSD < 2.0 Å could be found, but for 41 out of the 52 docking steps (79%) a pose with RMSD < 1.0 Å, and in 23 cases (44%) a pose with RMSD < 0.5 Å were found. Scoring failed for 6 out of the 50 successful docking steps (12%). Docking of the second fragments in cross-docking situations proved to be more challenging: there were 13 unsuccessful docking runs (25%) and for 24 out of the 52 docking steps (46%) a pose with RMSD < 1.0 Å, and for 12 cases (23%) a pose with RMSD < 0.5 Å were found. A near-native second-site binding pose was ranked top in 21 out of the 52 cases (40%).

While for most structures of the same proteins the binding sites were very similar, there were two problematic cases, where larger protein movements were encountered, and which produced most of the posing and

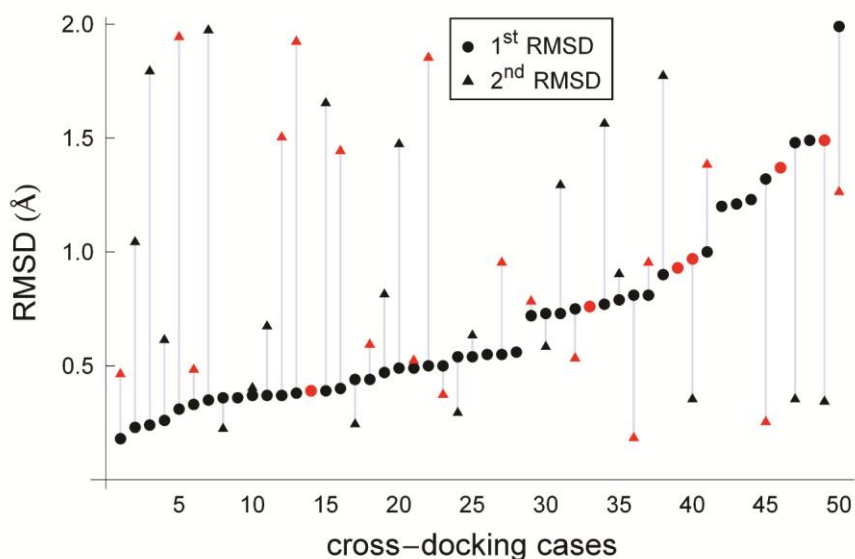


Figure 38. Multiple fragment docking results obtained in cross-docking experiments. Plot markers are colored red for docking steps with scoring errors (*E*model rank > 1).

scoring errors. The 1q1m structure of PTP1B represents a closed Pro180-Gly183 loop, while the other three complexes have an open loop. Also the key interacting residue Arg221 adopts a different rotamer, which precludes well-docked poses for oxamic acid and malonic acid ligands. The 2qfo structure of HSP90 similarly shows a closed Asp102-Gly114 stretch, while this sequence is helical in the other complexes. Thus docking of the 2qfo second-site fragment to the other structures and docking the other second-site ligands to the 2qfo structure both failed.

4.5 Fragment linking for dopamine D₃ receptor ligands

Recent clinical evidence supports the effectiveness of dual dopamine D₂ and D₃ antagonists or partial agonists in schizophrenia, depression and bipolar mania [242]. Finding the balance between D₃ and D₂ affinities is essential for a beneficial effect and safety profile. Dual acting compounds should show higher affinity to the D₃ than to the D₂ receptors due to different expression levels of the two receptors in specific brain areas. Since the elucidation of the dopamine D₃ crystal structure in complex with eticlopride in 2010 [243], much attention has been directed towards the structure-based screening and design of D₃ ligands. In the present part of the work the sequential docking methodology was applied for fragment

docking and linking to the D₃ crystal structure and a D₂ homology model. The subtype selectivity of the compounds was also assessed on a structural basis. A similar methodology was also used in [201] with dopamine as the fixed primary site ligand and no subsequent linking of the identified fragments.

4.5.1 Primary site docking results

Docking of the first focused library of basic fragments (see chapter 3.2.5) resulted in similar binding modes as in [205]. All of the 196 fragments could be docked into the inner binding site of the D₃ receptor, of which 145 produced an ionic hydrogen bond to the characteristic Asp110^{3,32} in the D₃ crystal structure and the aromatic moiety encased between hydrophobic residues Phe345^{6,51}, Phe346^{6,52}, Val111^{3,33} and Ile183^{45,52}. Binding modes of the four top ranked compounds are depicted in Figure 39. The top 15 fragments in D₃ docking also achieved high ranks when the same library was docked to the D₂ crystal structure, particularly the highest scoring 1-(3-cyano-5-trifluoromethylphenyl)piperazine was identical in both

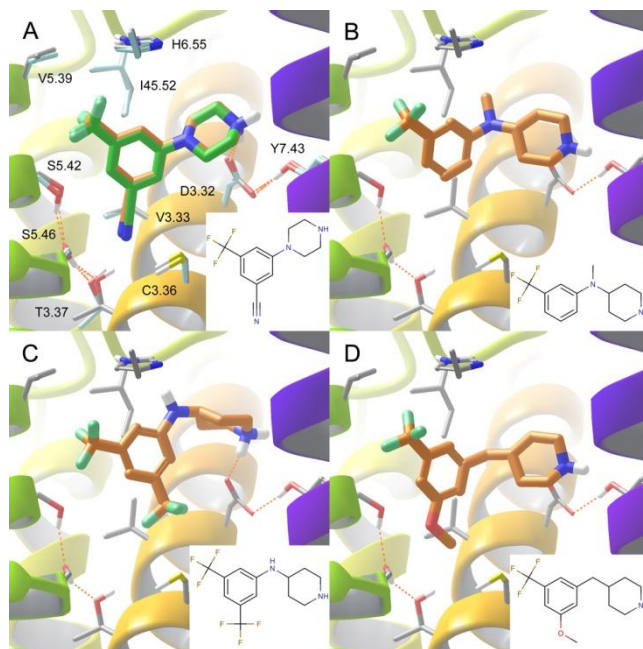


Figure 39. Binding modes of the top four fragments (from A to D) in D₃ primary site docking. In A) the D₃ and D₂ binding sites are overlaid in grey and light blue carbons respectively, as well as docked poses of the ligand in orange and green carbons respectively. From B) to D) only D₃ results are shown. Helix 6 is omitted for clarity. Compound structures are shown as insets.

receptors providing good docking scores (-8.576 for D₃ and -8.745 for D₂) and identical binding modes. This is in line with the highly conserved nature of the primary binding site. Docking seemed to favor a *meta*-trifluoromethyl substituent in further high ranking fragments as well.

4.5.2 Secondary site docking results

The 145 well-docked fragments were merged with the apo D₃ structure allowing for 145 new grids to be constructed and the second focused fragment library was docked to all of these new grids of partially occupied binding site. Docking scores of the 266 fragments in all 145 D₃ grids were averaged and the fragments were ranked by this mean docking score. The single best primary site ligand was also merged with the apo D₂ homology model and the second library was docked into this partially occupied structure to assess structural determinants of selectivity. Top ranking secondary site binders in the D₃ receptor and their binding modes in the D₂ receptor were visually inspected. The binding modes of the top three fragments by mean D₃ docking score in ten D₃ grids and the single D₂ grid are shown in Figure 40. It can be seen that these fragments produce extensive H-bonding patterns in the secondary binding site of the D₃ crystal structure. Carbonyl groups of the cyclohexylurea (mean docking score: -6.574) and the cyclohexyl-glycinamide (mean docking score: -6.230) and one of the S=O groups of the cyclohexylaminosulfonamide (mean docking score: -6.087) act as acceptors for Thr369^{7,39} in D₃ and the homologous Thr412^{7,39} in D₂. Two NH groups of all three ligands interact as donors to Glu90^{2,65} and Ser366^{7,36} in D₃ as well as the same Glu95^{2,65} and Ser409^{7,36} amino acids in D₂. The only interaction different between the two receptor subtypes is the second S=O group of the cyclohexylaminosulfonamide fragment, which acts as an acceptor for Tyr36^{1,39} in D₃, while in the homologous position of D₂ Leu41^{1,39} can be found incapable of forming a hydrogen bond with the ligand.

Furthermore, these ligands were found to produce robust binding modes in most of the 145 D₃ grids. As can be seen from Figure 40 the predicted binding modes of the second-site ligands in the grids containing the top ten primary site ligands are almost identical in the case of the urea and the sulfonamide fragment and show little variability for the glycinamide derivative. Robust ensembles of docking poses have been associated with higher fidelity of the predicted binding mode [244] and a higher entropy change upon binding [245]. Further fragments produced less robust binding modes. Therefore these top three fragments predicted to bind the secondary site were selected for linking with the top primary aryl-piperazine fragment. Docking suggested possible linking of the basic aryl-piperazine

nitrogen with either the para or the meta position of the cyclohexyl rings of the secondary fragments. The distance of the para positions in the various docking poses ranged from 3.8 to 4.5 Å while the distance of the meta positions ranged from 3.4 to 3.6 Å, thus both seemed to be suitable linking points. Because of synthetic accessibility and fewer possible stereoisomers, linking was carried out at the symmetric para position.

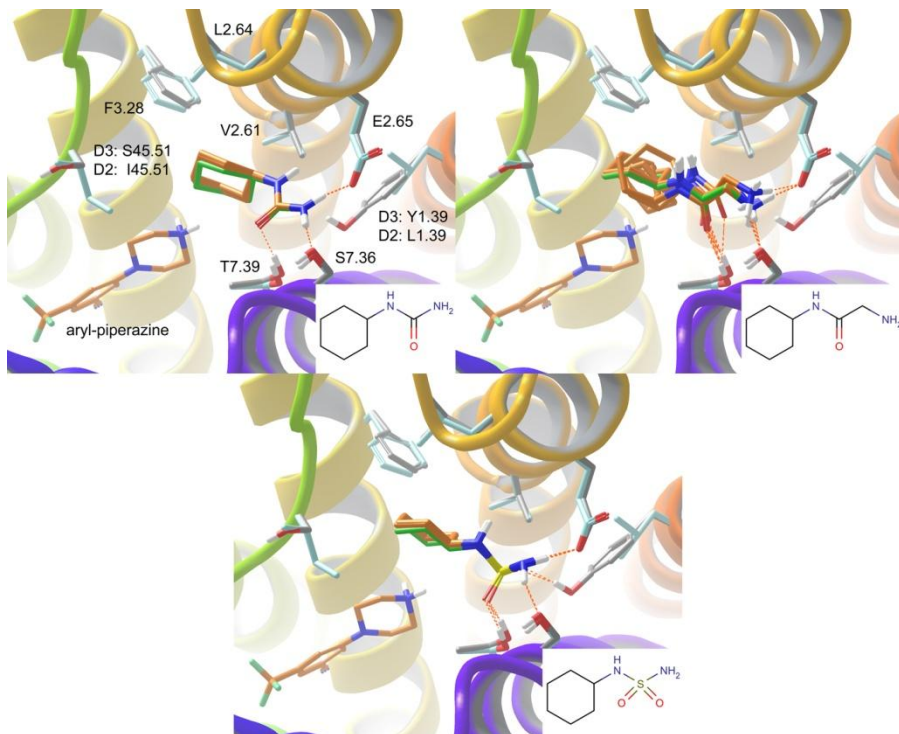


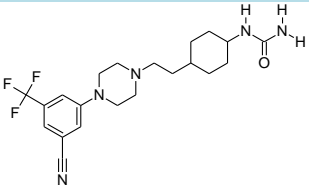
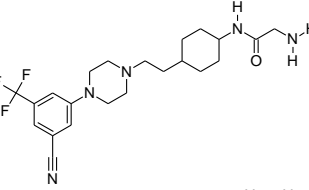
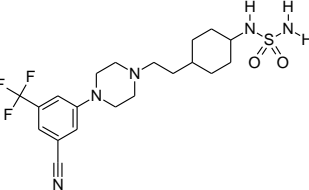
Figure 40. Binding modes of the top three fragments in D_3 and D_2 secondary site docking. The D_3 and D_2 binding sites are overlaid in grey and light blue carbons respectively, as well as an ensemble of 10 docked poses of the ligand in D_3 in orange carbons and a single docked pose of the ligand in D_2 in green carbons. Only the top ranked primary site ligand is included for clarity. Compound structures are shown as insets.

4.5.3 Biological activities

Linked compounds **19-21** were synthesized and tested in *in vitro* [^3H]raclopride binding experiments against recombinant human D_2 and D_3 receptors. The ligand displacement experiments were repeated at least three times. K_i values and derived selectivities of the compounds are shown in Table 14, dose-response curves in Appendix K. The linked compounds possessed subnanomolar activities against the D_3 receptor and low- to mid-

nanomolar activity against the D₂ receptor. The very high affinity towards the D₃ receptor is generally beneficial for achieving a low dosage in clinical settings. The selectivity of compound **20** was lowest, only 9 times higher K_i was measured for D₂ than for D₃, which is in line with the higher flexibility and less robust predicted binding mode of the secondary site fragment. On the other hand, compound **21** showed a 55 times higher K_i for D₂ than to D₃, which is also supported by the docking results. Higher selectivity has been shown to be beneficial for the desired pharmacological profile of dual dopamine D₂ and D₃ antagonists or partial agonists. This was the only compound featuring an extra D₃ specific interaction, namely the H-bond with Tyr36^{1,39}, which is not present in D₂. Docking of the linked compounds to the apo structures provided similar binding modes and the same H-bonding pattern as the original unlinked fragments (data not shown). Only a small upward shift of the aryl-piperazine fragment was evident in the primary binding site (RMSD: 1.7 Å) and very small deviations were seen in the secondary fragment binding modes (RMSD: 0.57 Å for the urea, 1.06 Å for the glycinamide and 0.84 Å for the sulfonamide fragment). The docking scores of the linked compounds were very high, and in this particular case

Table 14. *In vitro* binding data obtained experimentally on recombinant human D₂ and D₃ receptors with calculated selectivities and docking scores of synthesized compounds. The data are derived from at least three independent experiments; the standard error of the mean is indicated.

#	Compound structure	hD ₃ R K _i (nM)	hD ₃ R docking score	hD ₂ R K _i (nM)	hD ₂ R docking score	Sel.
19		0.75 ± 0.10	-10.39	30 ± 11	-10.66	39×
20		0.62 ± 0.23	-10.49	5.4 ± 0.2	-11.21	9×
21		0.67 ± 0.15	-10.51	37 ± 9	-10.83	55×

the relative values of compounds at both receptors were in accordance with the experimental data. However, the relative scale of the two receptor scores was wrong: D₂ docking scores were always lower than D₃ scores (see Table 14). Nevertheless it has been shown that multiple fragment docking can provide starting points for linking even for GPCR targets with elucidated 3D structures, and subtype selectivity has been achieved by virtual secondary site fragment screening and fragment linking.

Chapter 5 – Conclusions

The present work aimed at reviewing existing and developing new *in silico* methodologies for the aid of fragment-based drug discovery, a recently emerged but very promising field of pharmaceutical research. Methodologies useful in primary and secondary site virtual fragment screening were devised and evaluated on retrospective data sets and in prospective applications.

The objective of the first part of the study was to assess the potential of single structure models and ranking-based ensemble validation to guide the selection of receptor conformations for virtual hit finding. Explicit solvent membrane dynamics simulations of four protein–ligand complexes from the GPCR family (CXCR₄, D₃, H₄, and 5HT₆) were carried out by collaborators at the University of Szeged to generate discrete protein conformations representing the intrinsic flexibility of the binding site. RMSD-based clustering and systematic frame selection were utilized to obtain representative conformations, and these structures were compared to X-ray structures and homology models. Best single snapshots from the MD trajectory considerably outperformed X-ray as well as the homology models. Both frame selection methods produced improved enrichments compared to the X-ray and homology model, while the ranking-based ensemble evaluation could not further increase the performance. The H₄ and 5HT₆ cases highlighted the usefulness of homology models for MD-based receptor conformer generation. On the basis of this observation, the use of MD simulation is encouraged to explore the conformational space of the initial GPCR–ligand complex to create an ensemble of possible models and test their performance to find the best model for prospective screening.

Subsequently prospective structure-based virtual screening methodologies were evaluated on two of the previously studied targets, the dopamine D₃ and the histamine H₄ receptors and a fragment library of 12,905 compounds. For both targets single structure and ensemble docking screens were performed. 50 virtual hits from both methodologies for both receptors were measured *in vitro* at the Pharmacology Department in Gedeon Richter and confirmed hit rates ranged from 16% to 32%. The reported hits provided high LE and low LELP values and are suitable starting points for hit-to-lead optimization. Analysis of the obtained binding modes provided insight to the variation in hit rates of the different methodologies. It was found that the X-ray structure, the homology model and structural ensembles are all suitable for docking based virtual screening of fragments against these GPCRs. However, there was little overlap among their hit sets

and were thus complementary to each other. Combined approaches should provide valuable starting points for fragment-based lead discovery for other GPCRs as well if an X-ray structure or a good quality homology model is available.

The objective of the second part of the study was to propose a computational methodology for identifying starting points for fragment linking. First the performance of Glide was investigated on 129 multiple ligand bound protein complexes in a sequential docking setup with three different protocols and three different scoring functions. On average 36 % of the whole set of structures with at least two well-docked ligands ranked among the top three poses were obtained. The introduction of the druglikeness filter for ligands and closeness filter for binding sites resulted in higher performance, and the ratio of well-reproduced structures increased to 50% for the SP hard protocol. XP was found to provide lower success rates but with a higher probability of the top scoring poses being well-docked. Three ligands could be docked in only a few cases. Two pharmaceutically relevant subsets, that of cytochromes P450 and HSP90 complexes from fragment screens, were examined in more detail. In these cases higher success rates were observed than in the drug-like and closed site subset. These results show the limitations of large-scale screening applications in the sequential docking of multiple ligands but indicate their utility in screening against drug interactions and in virtual fragment screening.

Next this simple sequential docking protocol was evaluated on a data set containing structures from successful fragment linking examples and ternary protein-fragment complexes. It was able to correctly predict the binding modes of multiple fragments. Cross-docking experiments also provided reasonably high success rates, though proteins with mobile structural elements near the binding site impose a greater challenge for docking. Sampling on this dataset was found to be sufficient; however, cross-docking data suggest some opportunities to improve the scoring functions further. This methodology could be useful in generating promising starting points for fragment linking and supports the identification of suitable linking strategies in fragment based drug design. Furthermore, in combination with high-throughput X-ray crystallography, it might prevent the misinterpretation of diffraction data.

Finally the reported sequential fragment docking methodology was applied to identify fragments to link in a GPCR target, namely the dopamine D₃ receptor binding site. A homology model was also built for the D₂ receptor subtype and docking of the fragments as well as the full linked compounds was carried out to both receptors in order to assess the structural basis of subtype selectivity of the predicted binders. Three linked

compounds were synthesized by Éva Ágai-Csongor and experimental results were in line with docking predictions. Thus it has been shown that multiple fragment docking can provide starting points for linking for GPCR targets with elucidated 3D structures, and subtype selectivity has been achieved by virtual secondary site fragment screening and fragment linking.

The results of the research can be summarized in the following thesis points:

1) I have shown that single frames selected by systematic sampling or clustering from all-atom POPC membrane-embedded unbiased ns timescale molecular dynamics simulation trajectories using the ff99SB+GAFF force field outperform X-ray structures and homology models in virtual screening against G protein-coupled receptors (GPCRs) and that ensemble evaluation does not further improve virtual screening performance [246].

2) I have shown that GPCR X-ray structures, homology models and structural ensembles from molecular dynamics trajectories can be used in prospective virtual fragment screening. I have identified novel GPCR fragment starting points for medicinal chemistry optimization with good physico-chemical properties and ligand efficiencies using virtual fragment screening [247].

3) I developed and validated a novel sequential docking methodology for identifying starting points for fragment linking using a data set of 129 X-ray structures with multiple bound ligands. In the best protocol 68 % of the experimental structures could be reproduced and even better performance was achieved for pharmacologically relevant cytochrome P450 structures and fragment-bound structures of the HSP90 protein [248].

4) I found that the developed sequential docking methodology has outstanding performance on fragments using a data set of 32 X-ray structures with cooperatively bound or linked fragments. I have shown that sampling performance is sufficient for multiple fragment docking but fragment scoring could be improved for less specific second site binders, in line with the 'hot spot' hypothesis [249].

5) I demonstrated the applicability of the sequential fragment docking methodology in a prospective setup and identified fragment hits for linking inside the binding pocket of a GPCR, namely the human dopamine D₃ receptor. The three synthesized linked compounds have high affinity to the D₃ receptor and their selectivity against the dopamine D₂ receptor subtype could be explained on a structural basis [250].

References

1. Paul, S.M., Mytelka, D.S., Dunwiddie, C.T. et al. How to improve R&D productivity: the pharmaceutical industry's grand challenge. *Nat. Rev. Drug Discov.* **2010**, 9, 203-214.
2. Kola, I., Landis, J. Can the pharmaceutical industry reduce attrition rates? *Nat. Rev. Drug Discov.* **2004**, 3, 711-715.
3. Leeson, P.D., St-Gallay, S.A. The influence of the 'organizational factor' on compound quality in drug discovery. *Nat. Rev. Drug Discov.* **2011**, 10, 749-765.
4. Leeson, P.D., Springthorpe, B. The influence of drug-like concepts on decision-making in medicinal chemistry. *Nat. Rev. Drug Discov.* **2007**, 6, 881-890.
5. Lipinski, C.A., Lombardo, F., Dominy, B.W., Feeney, P.J. Experimental and computational approaches to estimate solubility and permeability in drug discovery and development settings. *Adv. Drug Deliv. Rev.* **2001**, 46, 3-26.
6. Hann, M.M. Molecular obesity, potency and other addictions in drug discovery. *Med. Chem. Commun.* **2011**, 2, 349-355.
7. Rees, D.C., Congreve, M., Murray, C.W., Carr, R. Fragment-based lead discovery. *Nat. Rev. Drug Discov.* **2004**, 3, 660-672.
8. Jencks, W.P. On the attribution and additivity of binding energies. *Proc. Natl. Acad. Sci. USA* **1981**, 78, 4046-4050.
9. Andrews, P.R., Craik, D.J., Martin, J.L. Functional group contributions to drug-receptor interactions. *J. Med. Chem.* **1984**, 27, 1648-1657.
10. Lauri, G., Bartlett, P.A. CAVEAT: a program to facilitate the design of organic molecules. *J. Comput. Aided Mol. Des.* **1994**, 8, 51-66.
11. Mattos, C., Ringe, D. Locating and characterizing binding sites on proteins. *Nat. Biotechnol.* **1996**, 14, 595-599.
12. Shuker, S.B., Hajduk, P.J., Meadows, R.P., Fesik, S.W. Discovering high-affinity ligands for proteins: SAR by NMR. *Science* **1996**, 274, 1531-1534.
13. Nienaber, V.L., Richardson, P.L., Klighofer, V., Bouska, J.J., Giranda, V.L., Greer, J. Discovering novel ligands for macromolecules using X-ray crystallographic screening. *Nat. Biotechnol.* **2000**, 18, 1105-1108.
14. Tsai, J., Lee, J.T., Wang, W. et al. Discovery of a selective inhibitor of oncogenic B-Raf kinase with potent antimelanoma activity. *Proc. Natl. Acad. Sci. USA* **2008**, 105, 3041-3046.
15. <http://practicalfragments.blogspot.com/2013/01/fragments-in-clinic-2013-edition.html>
16. Hann, M.M., Leach, A.R., Harper, G. Molecular complexity and its impact on the probability of finding leads for drug discovery. *J. Chem. Inf. Comput. Sci.* **2001**, 41, 856-864.
17. Kuntz, I.D., Chen, K., Sharp, K.A., Kollman, P.A. The maximal affinity of ligands. *Proc. Natl. Acad. Sci. USA* **1999**, 96, 9997-10002.
18. Ferenczy, G.G., Keserű, G.M. Thermodynamics of fragment binding. *J. Chem. Inf. Model.* **2012**, 52, 1039-1045.
19. Hopkins, A.L., Groom, C.R., Alex, A. Ligand efficiency: a useful metric for lead selection. *Drug Discov. Today* **2004**, 9, 430-431.

20. Bohacek, R.S., McMartin, C., Guida, W.C. The art and practice of structure-based drug design: a molecular modeling perspective. *Med. Res. Rev.* **1996**, *16*, 3-50.
21. Blum, L.C., van Deursen, R., Reymond, J.L. Visualization and subsets of the chemical universe database GDB-13 for virtual screening. *J. Comput. Aided Mol. Des.* **2011**, *25*, 637-647.
22. Hartshorn, M.J., Murray, C.W., Cleasby, A., Frederickson, M., Tickle, I.J., Jhoti, H. Fragment-based lead discovery using X-ray crystallography. *J. Med. Chem.* **2005**, *48*, 403-413.
23. Zartler, E.R., Mo, H. Practical aspects of NMR-based fragment discovery. *Curr. Top. Med. Chem.* **2007**, *7*, 1592-1599.
24. Neumann, T., Junker, H.D., Schmidt, K., Sekul, R. SPR-based fragment screening: advantages and applications. *Curr. Top. Med. Chem.* **2007**, *7*, 1630-1642.
25. Piana, S., Lindorff-Larsen, K., Shaw, D.E. Atomic-level description of ubiquitin folding. *Proc. Natl. Acad. Sci. USA* **2013**, *110*, 5915-5920.
26. Jensen, M.Ø., Jogini, V., Borhani, D.W., Leffler, A.E., Dror, R.O., Shaw, D.E. Mechanism of voltage gating in potassium channels. *Science* **2012**, *336*, 229-233.
27. Kohlhoff, K.J., Shukla, D., Lawrenz, M. et al. Cloud-based simulations on Google Exacycle reveal ligand modulation of GPCR activation pathways. *Nat. Chem.* **2014**, *6*, 15-21.
28. Dror, R.O., Pan, A.C., Arlow, D.H. et al. Pathway and mechanism of drug binding to G protein-coupled receptors. *Proc. Natl. Acad. Sci. USA* **2011**, *108*, 13118-13123.
29. Ripphausen, P., Nisius, B., Peltason, L., Bajorath, J. Quo vadis, virtual screening? A comprehensive survey of prospective applications. *J. Med. Chem.* **2010**, *53*, 8461-8467.
30. Talele, T.T., Khedkar, S.A., Rigby, A.C. Successful applications of computer aided drug discovery: moving drugs from concept to the clinic. *Curr. Top. Med. Chem.* **2010**, *10*, 127-141.
31. Gleeson, M.P. Generation of a set of simple, interpretable ADMET rules of thumb. *J. Med. Chem.* **2008**, *51*, 817-834.
32. Wager, T.T., Hou, X., Verhoest, P.R., Villalobos, A. Moving beyond rules: the development of a central nervous system multiparameter optimization (CNS MPO) approach to enable alignment of druglike properties. *ACS Chem. Neurosci.* **2010**, *1*, 435-449.
33. Cumming, J.G., Davis, A.M., Muresan, S., Haeberlein, M., Chen, H. Chemical predictive modelling to improve compound quality. *Nat. Rev. Drug Discov.* **2013**, *12*, 948-962.
34. Gedeck, P., Lewis, R.A. Exploiting QSAR models in lead optimization. *Curr. Opin. Drug Discov. Devel.* **2008**, *11*, 569-575.
35. <https://www.ebi.ac.uk/chembl/db/>
36. Besnard, J., Ruda, G.F., Setola, V. et al. Automated design of ligands to polypharmacological profiles. *Nature* **2012**, *492*, 215-220.
37. <http://www.pdb.org/>
38. Liu, T., Tang, G.W., Capriotti, E. Comparative modeling: the state of the art and protein drug target structure prediction. *Comb. Chem. High Throughput Screen.* **2011**, *14*, 532-547.

39. Sousa, S.F., Ribeiro, A.J., Coimbra, J.T. et al. Protein-ligand docking in the new millennium – a retrospective of 10 years in the field. *Curr. Med. Chem.* **2013**, *20*, 2296-2314.
40. Durrant, J.D., McCammon, J.A. Molecular dynamics simulations and drug discovery. *BMC Biol.* **2011**, *9*, 71.
41. Katritch, V., Cherezov, V., Stevens, R.C. Diversity and modularity of G protein-coupled receptor structures. *Trends Pharmacol. Sci.* **2012**, *33*, 17-27.
42. Overington, J.P., Al-Lazikani, B., Hopkins, A.L. How many drug targets are there? *Nat. Rev. Drug Discov.* **2006**, *5*, 993-996.
43. Stevens, R.C., Cherezov, V., Katritch, V. et al. The GPCR Network: a large-scale collaboration to determine human GPCR structure and function. *Nat. Rev. Drug Discov.* **2013**, *12*, 25-34.
44. Salon, J.A., Lodowski, D.T., Palczewski, K. The significance of G protein-coupled receptor crystallography for drug discovery. *Pharmacol. Rev.* **2011**, *63*, 901-937.
45. Congreve, M., Carr, R., Murray, C., Jhoti, H. A 'rule of three' for fragment-based lead discovery? *Drug Discov. Today* **2003**, *8*, 876-877.
46. Jhoti, H., Williams, G., Rees, D.C., Murray, C.W. The 'rule of three' for fragment-based drug discovery: where are we now? *Nat. Rev. Drug Discov.* **2013**, *12*, 644-645.
47. Over, B., Wetzel, S., Grütter, C. Natural-product-derived fragments for fragment-based ligand discovery. *Nat. Chem.* **2013**, *5*, 21-28.
48. Ferenczy, G.G., Keserű, G.M. How are fragments optimized? A retrospective analysis of 145 fragment optimizations. *J. Med. Chem.* **2013**, *56*, 2478-2486.
49. Vulpetti, A., Dalvit, C. Design and generation of highly diverse fluorinated fragment libraries and their efficient screening with improved ¹⁹FNMR methodology. *ChemMedChem* **2013**, *8*, 2057-2069.
50. Lovering, F., Bikker, J., Humblet, C. Escape from flatland: increasing saturation as an approach to improve clinical success. *J. Med. Chem.* **2009**, *52*, 6752-6756.
51. Davis, B.J., Erlanson, D.A. Learning from our mistakes: the 'unknown knowns' in fragment screening. *Bioorg. Med. Chem. Lett.* **2013**, *23*, 2844-2852.
52. Rabal, O., Urbano-Cuadrado, M., Oyarzabal, J. Computational medicinal chemistry in fragment-based drug discovery: what, how and when. *Future Med. Chem.* **2011**, *3*, 95-134.
53. Chung, C.W., Dean, A.W., Woolven, J.M., Bamborough, P. Fragment-based discovery of bromodomain inhibitors part 1: inhibitor binding modes and implications for lead discovery. *J. Med. Chem.* **2012**, *55*, 576-586.
54. Sheng, C., Zhang, W. Fragment informatics and computational fragment-based drug design: an overview and update. *Med. Res. Rev.* **2013**, *33*, 554-598.
55. Lewell, X.Q., Judd, D.B., Watson, S.P., Hann, M.M. RECAP – retrosynthetic combinatorial analysis procedure: a powerful new technique for identifying privileged molecular fragments with useful applications in combinatorial chemistry. *J. Chem. Inf. Comput. Sci.* **1998**, *38*, 511-522.
56. Wang, J., Hou, T. Drug and drug candidate building block analysis. *J. Chem. Inf. Model.* **2010**, *50*, 55-67.
57. Lameijer, E.W., Kok, J.N., Bäck, T., Ijzerman, A.P. Mining a chemical database for fragment co-occurrence: discovery of 'chemical clichés'. *J. Chem. Inf. Model.* **2006**, *46*, 553-562.

58. Pitt, W.R., Parry, D.M., Perry, B.G., Groom, C.R. Heteroaromatic rings of the future. *J. Med. Chem.* **2009**, 52, 2952-2963.
59. Sándor, M., Kiss, R., Keserű, G.M. Virtual fragment docking by Glide: a validation study on 190 protein–fragment complexes. *J. Chem. Inf. Model.* **2010**, 50, 1165–1172.
60. Verdonk, M.L., Giangreco, I., Hall, R.J., Korb, O., Mortenson, P.N., Murray, C.W. Docking performance of fragments and druglike compounds. *J. Med. Chem.* **2011**, 54, 5422-5431.
61. Teotico, D.G., Babaoglu, K., Rocklin, G.J., Ferreira, R.S., Giannetti, A.M., Shoichet, B.K. Docking for fragment inhibitors of AmpC beta-lactamase. *Proc. Natl. Acad. Sci. USA* **2009**, 106, 7455-7460.
62. Marcou, G., Rognan, D. Optimizing fragment and scaffold docking by use of molecular interaction fingerprints. *J. Chem. Inf. Model.* **2007**, 47, 195-207.
63. Benson, M.L., Faver, J.C., Ucisik, M.N., Dashti, D.S., Zheng, Z., Merz, K.M. Prediction of trypsin/molecular fragment binding affinities by free energy decomposition and empirical scores. *J. Comput. Aided Mol. Des.* **2012**, 26, 647-659.
64. Kawatkar, S., Wang, H., Czerminski, R., Joseph-McCarthy, D. Virtual fragment screening: an exploration of various docking and scoring protocols for fragments using Glide. *J. Comput. Aided Mol. Des.* **2009**, 23, 527–539.
65. Kawatkar, S., Moustakas, D., Miller, M., Joseph-McCarthy, D. Virtual fragment screening: exploration of MM-PBSA re-scoring. *J. Comput. Aided Mol. Des.* **2012**, 26, 921-934.
66. Graves, A.P., Shivakumar, D.M., Boyce, S.E., Jacobson, M.P., Case, D.A., Shoichet, B.K. Rescoring docking hit lists for model cavity sites: predictions and experimental testing. *J. Mol. Biol.* **2008**, 377, 914-934.
67. Lyne, P.D., Lamb, M.L., Saeh, J.C. Accurate prediction of the relative potencies of members of a series of kinase inhibitors using molecular docking and MM-GBSA scoring. *J. Med. Chem.* **2006**, 49, 4805-4808.
68. Guimarães, C.R., Cardozo, M. MM-GB/SA rescoring of docking poses in structure-based lead optimization. *J. Chem. Inf. Model.* **2008**, 48, 958-970.
69. Mikulskis, P., Genheden, S., Rydberg, P., Sandberg, L., Olsen, L., Ryde, U. Binding affinities in the SAMPL3 trypsin and host-guest blind tests estimated with the MM/PBSA and LIE methods. *J. Comput. Aided Mol. Des.* **2012**, 26, 527-541.
70. Gleeson, M.P., Gleeson, D. QM/MM as a tool in fragment based drug discovery. A cross-docking, rescoring study of kinase inhibitors. *J. Chem. Inf. Model.* **2009**, 49, 1437-1448.
71. Mobley, D.L., Graves, A.P., Chodera, J.D., McReynolds, A.C., Shoichet, B.K., Dill, K.A. Predicting absolute ligand binding free energies to a simple model site. *J. Mol. Biol.* **2007**, 371, 1118-1134.
72. Haider, M.K., Bertrand, H.O., Hubbard, R.E. Predicting fragment binding poses using a combined MCSS MM-GBSA approach. *J. Chem. Inf. Model.* **2011**, 51, 1092-1105.
73. Clark, M., Meshkat, S., Talbot, G.T., Carnevali, P., Wiseman, J.S. Fragment-based computation of binding free energies by systematic sampling. *J. Chem. Inf. Model.* **2009**, 49, 1901-1913.

74. Clark, M., Guarnieri, F., Shkurko, I., Wiseman, J. Grand canonical Monte Carlo simulation of ligand-protein binding. *J. Chem. Inf. Model.* **2006**, 46, 231-242.
75. Clark, M., Meshkat, S., Wiseman, J.S. Grand canonical free-energy calculations of protein-ligand binding. *J. Chem. Inf. Model.* **2009**, 49, 934-943.
76. Kulp, J.L., Blumenthal, S.N., Wang, Q., Bryan, R.L., Guarnieri, F. A fragment-based approach to the SAMPL3 Challenge. *J. Comput. Aided Mol. Des.* **2012**, 26, 583-594.
77. Zhu, T., Lee, H., Lei, H. et al. Fragment-based drug discovery using a multidomain, parallel MD-MM/PBSA screening protocol. *J. Chem. Inf. Model.* **2013**, 53, 560-572.
78. Aqvist, J., Medina, C., Samuelsson, J.E. A new method for predicting binding affinity in computer-aided drug design. *Protein Eng.* **1994**, 7, 385-391.
79. van Gunsteren, W.F., Berendsen, H.J. Thermodynamic cycle integration by computer simulation as a tool for obtaining free energy differences in molecular chemistry. *J. Comput. Aided Mol. Des.* **1987**, 1, 171-176.
80. Kollman, P. Free energy calculations: Applications to chemical and biochemical phenomena. *Chem. Rev.* **1993**, 93, 2395-2417.
81. Wang, L., Deng, Y., Knight, J.L. et al. Modeling local structural rearrangements using FEP/REST: application to relative binding affinity predictions of CDK2 inhibitors. *J. Chem. Theory Comput.* **2013**, 9, 1282-1293.
82. Wang, L., Berne, B.J., Friesner, R.A. On achieving high accuracy and reliability in the calculation of relative protein-ligand binding affinities. *Proc. Natl. Acad. Sci. USA* **2012**, 109, 1937-1942.
83. Shivakumar, D., Harder, E., Damm, W., Friesner, R.A., Sherman, W. Improving the prediction of absolute solvation free energies using the next generation OPLS force field. *J. Chem. Theory Comput.* **2012**, 8, 2553-2558.
84. Liu, S., Wu, Y., Lin, T. et al. Lead optimization mapper: automating free energy calculations for lead optimization. *J. Comput. Aided Mol. Des.* **2013**, 27, 755-770.
85. Rathore, R.S., Sumakanth, M., Reddy, M.S. et al. Advances in binding free energies calculations: QM/MM-based free energy perturbation method for drug design. *Curr. Pharm. Des.* **2013**, 19, 4674-4686.
86. Howard, N., Abell, C., Blakemore, W. et al. Application of fragment screening and fragment linking to the discovery of novel thrombin inhibitors. *J. Med. Chem.* **2006**, 49, 1346-1355.
87. Zhao, L., Cao, D., Chen, T. et al. Fragment-based drug discovery of 2-thiazolidinones as inhibitors of the histone reader BRD4 bromodomain. *J. Med. Chem.* **2013**, 56, 3833-3851.
88. Rummey, C., Nordhoff, S., Thiemann, M., Metz, G. In silico fragment-based discovery of DPP-IV S1 pocket binders. *Bioorg. Med. Chem. Lett.* **2006**, 16, 1405-1409.
89. Chen, Y., Shoichet, B.K. Molecular docking and ligand specificity in fragment-based inhibitor discovery. *Nat. Chem. Biol.* **2009**, 5, 358-364.
90. Mpamhanga, C.P., Spinks, D., Tulloch, L.B. et al. One scaffold, three binding modes: novel and selective pteridine reductase 1 inhibitors derived from fragment hits discovered by virtual screening. *J. Med. Chem.* **2009**, 52, 4454-4465.

91. Ruda, G.F., Campbell, G., Alibu, V.P., Barrett, M.P., Brenk, R., Gilbert, I.H. Virtual fragment screening for novel inhibitors of 6-phosphogluconate dehydrogenase. *Bioorg. Med. Chem.* **2010**, 18, 5056-5062.
92. Brožič, P., Turk, S., Adeniji, A.O. et al. Selective inhibitors of aldo-keto reductases AKR1C1 and AKR1C3 discovered by virtual screening of a fragment library. *J. Med. Chem.* **2012**, 55, 7417-7424.
93. Giordanetto, F., Kull, B., Dellsén, A. et al. Discovery of novel class 1 phosphatidylinositide 3-kinases (PI3K) fragment inhibitors through structure-based virtual screening. *Bioorg. Med. Chem. Lett.* **2011**, 21, 829-835.
94. Oyarzabal, J., Zarich, N., Albarran, M.I. et al. Discovery of mitogen-activated protein kinase-interacting kinase 1 inhibitors by a comprehensive fragment-oriented virtual screening approach. *J. Med. Chem.* **2010**, 53, 6618-6628.
95. Blum, L.C., van Deursen, R., Bertrand, S. et al. Discovery of $\alpha 7$ -nicotinic receptor ligands by virtual screening of the chemical universe database GDB-13. *J. Chem. Inf. Model.* **2011**, 51, 3105-3112.
96. Newman, J., Fazio, V.J., Caradoc-Davies, T.T., Branson, K., Peat, T.S. Practical aspects of the SAMPL challenge: providing an extensive experimental data set for the modeling community. *J. Biomol. Screen.* **2009**, 14, 1245-1250.
97. Kumar, A., Zhang, K.Y. Computational fragment-based screening using RosettaLigand: the SAMPL3 challenge. *J. Comput. Aided Mol. Des.* **2012**, 26, 603-616.
98. Surpateanu, G., Iorga, B.I. Evaluation of docking performance in a blinded virtual screening of fragment-like trypsin inhibitors. *J. Comput. Aided Mol. Des.* **2012**, 26, 595-601.
99. de Graaf, C., Kooistra, A.J., Vischer, H.F. et al. Crystal structure-based virtual screening for fragment-like ligands of the human histamine H₁ receptor. *J. Med. Chem.* **2011**, 54, 8195-8206.
100. Sirci, F., Istyastono, E.P., Vischer, H.F. et al. Virtual fragment screening: discovery of histamine H₃ receptor ligands using ligand-based and protein-based molecular fingerprints. *J. Chem. Inf. Model.* **2012**, 52, 3308-3324.
101. Chen, D., Ranganathan, A., Ijzerman, A.P., Siegal, G., Carlsson, J. Complementarity between in silico and biophysical screening approaches in fragment-based lead discovery against the A_{2A} adenosine receptor. *J. Chem. Inf. Model.* **2013**, 53, 2701-2714.
102. Rouhana, J., Hoh, F., Estaran, S. et al. Fragment-based identification of a locus in the Sec7 domain of Arno for the design of protein-protein interaction inhibitors. *J. Med. Chem.* **2013**, 56, 8497-8511.
103. Murray, C.W., Verdonk, M.L., Rees, D.C. Experiences in fragment-based drug discovery. *Trends Pharmacol. Sci.* **2012**, 33, 224-232.
104. Keserű, G.M., Makara G.M. The influence of lead discovery strategies on the properties of drug candidates. *Nature Rev. Drug Disc.* **2009**, 8, 203-212.
105. Orita, M., Ohno, K., Warizaya, M., Amano, Y., Niimi, T. Lead generation and examples: opinion regarding how to follow up hits. *Methods Enzymol.* **2011**, 493, 383-419.
106. Tarcsay, A., Nyíri, K., Keserű, G.M. Impact of lipophilic efficiency on compound quality. *J. Med. Chem.* **2012**, 55, 1252-1260.

107. Freire, E. Do enthalpy and entropy distinguish first in class from best in class? *Drug Discov. Today* **2008**, 13, 869-874.
108. Loving, K., Alberts, I., Sherman, W. Computational approaches for fragment-based and de novo design. *Curr. Top. Med. Chem.* **2010**, 10, 14-32.
109. Edink, E., Rucktooa, P., Retra, K., et al. Fragment growing induces conformational changes in acetylcholine-binding protein: a structural and thermodynamic analysis. *J. Am. Chem. Soc.* **2011**, 133, 5363-5371.
110. Schubert, C.R., Stultz, C.M. The multi-copy simultaneous search methodology: a fundamental tool for structure-based drug design. *J. Comput. Aided. Mol. Des.* **2009**, 23, 475-489.
111. Li, H., Liu, A., Zhao, Z. Fragment-based drug design and drug repositioning using multiple ligand simultaneous docking (MLSD): identifying celecoxib and template compounds as novel inhibitors of signal transducer and activator of transcription 3 (STAT3). *J. Med. Chem.* **2011**, 54, 5592-5596.
112. Hoffer, L., Horvath, D. S4MPLE – sampler for multiple protein-ligand entities: simultaneous docking of several entities. *J. Chem. Inf. Model.* **2013**, 53, 88-102.
113. Ichihara, O., Barker, J., Law, R.J., Whittaker, M. Compound Design by Fragment-Linking. *Mol. Inf.* **2011**, 30, 298–306.
114. de Kloe, G.E., Bailey, D., Leurs, R., de Esch, I.J. Transforming fragments into candidates: small becomes big in medicinal chemistry. *Drug Discov. Today* **2009**, 14, 630-646.
115. Nishibata, Y., Itai, A. Automatic creation of drug candidate structures based on receptor structure. Starting point for artificial lead generation. *Tetrahedron* **1991**, 47, 8985–8990.
116. Durrant, J.D., Amaro, R.E., McCammon, J.A. AutoGrow: a novel algorithm for protein inhibitor design. *Chem. Biol. Drug Des.* **2009**, 73, 168-178.
117. Hartenfeller, M., Proschak, E., Schuller, A., Schneider, G. Concept of combinatorial de novo design of drug-like molecules by particle swarm optimization. *Chem. Biol. Drug Des.* **2008**, 72, 16–26.
118. Fechner, U., Schneider, G. Flux (1): A virtual synthesis scheme for fragment-based de novo design. *J. Chem. Inf. Model.* **2006**, 46, 699–707.
119. Fechner, U., Schneider, G. Flux (2): Comparison of molecular mutation and crossover operators for ligand-based de novo design. *J. Chem. Inf. Model.* **2007**, 47, 656–667.
120. Nicolaou, C.A., Apostolakis, J., Pattichis, C.S. De novo drug design using multiobjective evolutionary graphs. *J. Chem. Inf. Model.* **2009**, 49, 295–307.
121. Bhurruth-Alcor, Y., Rost, T., Jorgensen, M.R., et al. Synthesis of novel PPARalpha/gamma dual agonists as potential drugs for the treatment of the metabolic syndrome and diabetes type II designed using a new de novo design program PROTOBUILD. *Org. Biomol. Chem.* **2011**, 9, 1169–1188.
122. Ji, H., Stanton, B.Z., Igarashi, J. et al. Minimal pharmacophoric elements and fragment hopping, an approach directed at molecular diversity and isozyme selectivity. Design of selective neuronal nitric oxide synthase inhibitors. *J. Am. Chem. Soc.* **2008**, 130, 3900–3914.

123. Huang, Q., Li, L.L., Yang, S.Y. PhDD: A new pharmacophore-based de novo design method of drug-like molecules combined with assessment of synthetic accessibility. *J. Mol. Graph. Model.* **2010**, 28, 775–787.
124. Thompson, D.C., Denny, R.A., Nilakantan, R., Humblet, C., Joseph-McCarthy, D., Feyfant, E. CONFIRM: connecting fragments found in receptor molecules. *J. Comput. Aided. Mol. Des.* **2008**, 22, 761–772.
125. Degen, J., Rarey, M. FlexNovo: Structure-based searching in large fragment spaces. *ChemMedChem* **2006**, 1, 854–868.
126. Parn, J., Degen, J., Rarey, M. Exploring fragment spaces under multiple physicochemical constraints. *J. Comput. Aided. Mol. Des.* **2007**, 21, 327–340.
127. Kutchukian, P.S., Lou, D., Shakhnovich, E.I. FOG: Fragment Optimized Growth algorithm for the de novo generation of molecules occupying druglike chemical space. *J. Chem. Inf. Model.* **2009**, 49, 1630–1642.
128. Pierce, A.C., Rao, G., Bemis, G.W. BREED: Generating novel inhibitors through hybridization of known ligands. Application to CDK2, p38, and HIV protease. *J. Med. Chem.* **2004**, 47, 2768–2775.
129. Li, Y., Zhao, Y., Liu, Z., Wang, R. Automatic tailoring and transplanting: A practical method that makes virtual screening more useful. *J. Chem. Inf. Model.* **2011**, 51, 1474–1491.
130. Moriaud, F., Doppelt-Azeroual, O., Martin, L. et al. Computational fragment-based approach at PDB scale by protein local similarity. *J. Chem. Inf. Model.* **2009**, 49, 280–294.
131. Hiss, J.A., Hartenfeller, M., Schneider, G. Concepts and applications of ‘natural computing’ techniques in de novo drug and peptide design. *Curr. Pharm. Des.* **2010**, 16, 1656–1665.
132. Dey, F., Caflisch, A. Fragment-based de novo ligand design by multiobjective evolutionary optimization. *J. Chem. Inf. Model.* **2008**, 48, 679–690.
133. Yuan, Y., Pei, J., Lai, L. LigBuilder 2: A practical de novo drug design approach. *J. Chem. Inf. Model.* **2011**, 51, 1083–1091.
134. Vinkers, H.M., de Jonge, M.R., Daeyaert, F.F. et al. SYNOPSIS: SYNthesize and OPTimize System in Silico. *J. Med. Chem.* **2003**, 46, 2765–2773.
135. Boda, K., Seidel, T., Gasteiger, J. Structure and reaction based evaluation of synthetic accessibility. *J. Comput. Aided. Mol. Des.* **2007**, 21, 311–325.
136. Hartenfeller, M., Zettl, H., Walter, M. et al. DOGS: reaction-driven de novo design of bioactive compounds. *PLoS Comput. Biol.* **2012**, 8, e1002380.
137. Zaliani, A., Boda, K., Seidel, T. et al. Second-generation de novo design: A view from a medicinal chemist perspective. *J. Comput. Aided. Mol. Des.* **2009**, 23, 593–602.
138. Böhm, H.J. The computer program LUDI: a new method for the de novo design of enzyme inhibitors. *J. Comput. Aided. Mol. Des.* **1992**, 6, 61–78.
139. van der Horst, E., Marqués-Gallego, P., Mulder-Krieger, T. Multi-objective evolutionary design of adenosine receptor ligands. *J. Chem. Inf. Model.* **2012**, 52, 1713–1721.
140. Beccari, A.R., Cavazzoni, C., Beato, C., Costantino, G. LiGen: a high performance workflow for chemistry driven de novo design. *J. Chem. Inf. Model.* **2013**, 53, 1518–1527.

141. Tschinke, V., Cohen, N.C. The NEWLEAD program: A new method for the design of candidate structures from pharmacophoric hypotheses. *J. Med. Chem.* **1993**, 36, 3863–3870.
142. Proschak, E., Zettl, H., Tanrikulu, Y. et al. From molecular shape to potent bioactive agents I: Bioisosteric replacement of molecular fragments. *ChemMedChem* **2009**, 4, 41–44.
143. Proschak, E., Sander, K., Zettl, H., From molecular shape to potent bioactive agents II: Fragment-based de novo design. *ChemMedChem* **2009**, 4, 45–48.
144. EA-Inventor; Tripos International: St. Louis, MO. <http://www.tripos.com>
145. Lippert, T., Schulz-Gasch, T., Roche, O., Guba, W., Rarey, M. De novo design by pharmacophore-based searches in fragment spaces. *J. Comput. Aided. Mol. Des.* **2011**, 25, 931-945.
146. Liu, Q., Masek, B., Smith, K., Smith, J. Tagged fragment method for evolutionary structure-based de novo lead generation and optimization. *J. Med. Chem.* **2007**, 50, 5392–5402.
147. <http://www.certara.com/products/molmod/muse/>
148. Damewood, J.R., Lerman, C.L., Masek, B.B. NovoFLAP: A ligand-based de novo design approach for the generation of medicinally relevant ideas. *J. Chem. Inf. Model.* **2010**, 50, 1296–1303.
149. Henen, M.A., Coudevylle, N., Geist, L., Konrat, R. Toward rational fragment-based lead design without 3D structures. *J. Med. Chem.* **2012**, 55, 7909-7919.
150. Feher, M., Gao, Y., Baber, J.C., Shirley, W.A., Saunders, J. The use of ligand-based de novo design for scaffold hopping and sidechain optimization: two case studies. *Bioorg. Med. Chem.* **2008**, 16, 422-427.
151. Visegrády, A., Keserű, G.M. Fragment-based lead discovery on G-protein-coupled receptors. *Expert. Opin. Drug. Discov.* **2013**, 8, 811-820.
152. Stoddart, L.A., Vernall, A.J., Denman, J.L., Briddon, S.J., Kellam, B., Hill, S.J. Fragment screening at adenosine-A₃ receptors in living cells using a fluorescence-based binding assay. *Chem. Biol.* **2012**, 19, 1105-1115.
153. Albert, J.S., Blomberg, N., Breeze, A.L. et al. An integrated approach to fragment-based lead generation: philosophy, strategy and case studies from AstraZeneca's drug discovery programmes. *Curr. Top. Med. Chem.* **2007**, 7, 1600-1629.
154. Congreve, M., Andrews, S.P., Doré, A.S. et al. Discovery of 1,2,4-triazine derivatives as adenosine A_{2A} antagonists using structure based drug design. *J. Med. Chem.* **2012**, 55, 1898-1903.
155. Abad-Zapatero, C., Metz, J.T. Ligand efficiency indices as guideposts for drug discovery. *Drug Discov. Today* **2005**, 10, 464-469.
156. Reynolds, C.H., Bembenek, S.D., Tounge, B.A. The role of molecular size in ligand efficiency. *Bioorg. Med. Chem. Lett.* **2007**, 17, 4258-4261.
157. Orita, M., Ohno, K., Niimi, T. Two 'Golden Ratio' indices in fragment-based drug discovery. *Drug Discov. Today* **2009**, 14, 321-328.
158. Nissink, J.W. Simple size-independent measure of ligand efficiency. *J. Chem. Inf. Model.* **2009**, 49, 1617-1622.
159. Mortenson, P.N., Murray, C.W. Assessing the lipophilicity of fragments and early hits. *J. Comput. Aided Mol. Des.* **2011** 25, 663-667.

160. Hopkins, A.L., Keserű, G.M., Leeson, P.D., Rees, D.C., Reynolds, C.H. The role of ligand efficiency metrics in drug discovery. *Nat. Rev. Drug Discov.* **2014**, 13, 105-121.
161. <http://practicalfragments.blogspot.hu/2011/08/ligand-efficiency-metrics-poll-results.html>
162. Prime, version 3.0-3.2; Schrödinger, LLC: New York, NY.
163. <http://www.uniprot.org/>
164. Ballesteros, J. A., Weinstein, H. Integrated methods for the construction of three dimensional models and computational probing of structure-function relations in G protein-coupled receptors. *Methods Neurosci.* **1995**, 25, 366-428.
165. Lim, H. D., de Graaf, C., Jiang, W. et al. Molecular determinants of ligand binding to H₄R species variants. *Mol. Pharmacol.* **2010**, 77, 734-743.
166. MacroModel, version 9.9; Schrödinger, LLC: New York, NY.
167. Sherman, W., Day, T., Jacobson, M. P., Friesner, R. A., Farid, R. Novel procedure for modeling ligand/receptor induced fit effects. *J. Med. Chem.* **2006**, 49, 534-553.
168. Sherman, W., Beard, H. S., Farid, R. Use of an induced fit receptor structure in virtual screening. *Chem. Biol. Drug Des.* **2006**, 67, 83-84.
169. Schrödinger Suite 2011, Induced Fit Docking protocol, Glide version 5.7, Prime version 3.0, Schrödinger, LLC, New York, NY.
170. Schrödinger Suite 2010-2011-2013, Protein Preparation Wizard, Epik version 2.1-2.2-2.3, Impact version 5.6-5.7-5.8, Prime version 2.2-2.3-3.1; Schrödinger, LLC: New York, NY.
171. Sastry, G.M., Adzhigirey, M., Day, T., Annabhimoju, R., Sherman, W. Protein and ligand preparation: parameters, protocols, and influence on virtual screening enrichments. *J. Comput. Aided Mol. Des.* **2013**, 27, 221-234.
172. Kufareva, I., Rueda, M., Katritch, V., Stevens, R. C., Abagyan, R. GPCR Dock 2010 participants Status of GPCR modeling and docking as reflected by community-wide GPCR Dock 2010 assessment. *Structure* **2011**, 19, 1108-1126.
173. Jójárt, B., Martinek, T. A. Performance of the general Amber force field in modeling aqueous POPC membrane bilayers. *J. Comput. Chem.* **2007**, 28, 2051-2058.
174. Hornak, V., Abel, R., Okur, A., Strockbine, B., Roitberg, A., Simmerling, C. Comparison of multiple Amber force fields and development of improved protein backbone parameters. *Proteins* **2006**, 65, 712-725.
175. Wang, J., Wolf, R. M., Caldwell, J. W., Kollman, P. A., Case, D. A. Development and testing of a general Amber force field. *J. Comput. Chem.* **2004**, 25, 1157-1174.
176. Jorgensen, W. L., Chandrasekhar, J., Madura, J. D., Impey, R. W., Klein, M. L. Comparison of simple potential functions for simulating liquid water. *J. Chem. Phys.* **1983**, 79, 926-935.
177. Jójárt, B., Kiss, R., Viskolcz, B., Keserű, G. M. Theoretical investigation of the activation mechanism of the human histamine H₄ receptor – an explicit membrane molecular dynamics simulation study. *J. Chem. Inf. Model.* **2008**, 48, 1199-1210.
178. Bayly, C. I., Cieplak, P., Cornell, W. D., Kollman, P. A. A well behaved electrostatic potential based method using charge restraints for deriving atomic charges: the RESP model. *J. Phys. Chem.* **1993**, 102, 3787-3793.

179. Halgren, T. A. Merck molecular force field. I. Basis, form, scope, parameterization, and performance of MMFF94. *J. Comput. Chem.* **1996**, *17*, 490-519.
180. Molecular Operating Environment (MOE), 2010.09; Chemical Computing Group, Inc.: Montreal, Quebec, Canada, 2005.
181. Frisch, M. J., Trucks, G. W., Schlegel, H. B. et al. Gaussian 09 revision A1; Gaussian, Inc.: Wallingford CT, 2009.
182. Case, D. A., Cheatham, T. E., Darden, T. et al. The Amber biomolecular simulation programs. *J. Comput. Chem.* **2005**, *26*, 1668-1688.
183. Joung, S., Cheatham, T. E. Determination of alkali and halide monovalent ion parameters for use in explicitly solvated biomolecular simulations. *J. Phys. Chem. B* **2008**, *112*, 9020-9041.
184. Joung, I. S., Cheatham, T. E. Molecular dynamics simulations of the dynamic and energetic properties of alkali and halide ions using water-model-specific ion parameters. *J. Phys. Chem. B* **2009**, *113*, 13279-13290.
185. Phillips, J. C., Braun, R., Wang, W. et al. Scalable molecular dynamics with NAMD. *J. Comput. Chem.* **2005**, *26*, 1781-1802.
186. Martyna, G. J., Tobias, D. J., Klein, M. L. Constant pressure molecular dynamics algorithms. *J. Chem. Phys.* **1994**, *101*, 4177-4189.
187. Feller, S. E., Zhang, Y., Pastor, R. W., Brooks, B. R. Constant pressure molecular dynamics simulation: The Langevin piston method. *J. Chem. Phys.* **1995**, *103*, 4613-4621.
188. Darden, T., York, D., Pedersen, L. Particle mesh Ewald: An $N\log(N)$ method for Ewald sums in large systems. *J. Chem. Phys.* **1993**, *98*, 10089-10092.
189. Gatica, E. A., Cavasotto, C. N. Ligand and decoy sets for docking to G protein-coupled receptors. *J. Chem. Inf. Model.* **2012**, *52*, 1-6.
190. <http://integrity.thomson-pharma.com/integrity/xmlsl/>
191. <http://zinc.docking.org/>
192. Calculator, version 5.4.1.1-5.10.2, © 1998–2012 ChemAxon Ltd.
193. LigPrep, version 2.4-2.5-2.6; Schrödinger, LLC: New York, NY.
194. Epik, version 2.1-2.2-2.4; Schrödinger, LLC, New York, NY.
195. Shelley, J.C., Cholleti, A., Frye, L.L., Greenwood, J.R., Timlin, M.R., Uchiyama, M. Epik: a software program for pKa prediction and protonation state generation for drug-like molecules. *J. Comput. Aided Mol. Des.* **2007**, *21*, 681-691.
196. Greenwood, J.R., Calkins, D., Sullivan, A.P., Shelley, J.C. Towards the comprehensive, rapid, and accurate prediction of the favorable tautomeric states of drug-like molecules in aqueous solution. *J. Comput. Aided Mol. Des.* **2010**, *24*, 591-604.
197. Glide, version 5.6-5.7-5.8-5.9; Schrödinger, LLC: New York, NY.
198. Friesner, R. A., Banks, J. L., Murphy, R. B. et al. Glide: a new approach for rapid, accurate docking and scoring. 1. Method and assessment of docking accuracy. *J. Med. Chem.* **2004**, *47*, 1739-1749.
199. Halgren, T. A., Murphy, R. B., Friesner, R. A. et al. Glide: a new approach for rapid, accurate docking and scoring. 2. Enrichment factors in database screening. *J. Med. Chem.* **2004**, *47*, 1750-1759.

200. Friesner, R. A., Murphy, R. B., Repasky, M. P. et al. Extra precision Glide: docking and scoring incorporating a model of hydrophobic enclosure for protein-ligand complexes. *J. Med. Chem.* **2006**, 49, 6177-6196.
201. Lane, J.R., Chubukov, P., Liu, W. et al. Structure-based ligand discovery targeting orthosteric and allosteric pockets of dopamine receptors. *Mol. Pharmacol.* **2013**, 84, 794-807.
202. SiteMap, version 2.4-2.5; Schrödinger, LLC: New York, NY.
203. Roughley, S.D., Hubbard, R.E. How well can fragments explore accessed chemical space? A case study from heat shock protein 90. *J. Med. Chem.* **2011**, 54, 3989-4005.
204. SiteMap 2.4 User Manual, <http://www.schrodinger.com/supportdocs/18/20/>
205. Newman, A.H., Beuming, T., Banala, A.K. et al. Molecular determinants of selectivity and efficacy at the dopamine D₃ Receptor. *J. Med. Chem.* **2012**, 55, 6689-6699.
206. Reavill, C., Taylor, S.G., Wood, M.D. et al. Pharmacological actions of a novel, high-affinity, and selective human dopamine D₃ receptor antagonist, SB-277011-A. *J. Pharmacol. Exp. Ther.* **2000**, 294, 1154-1165.
207. Molecule File Converter, version 5.4.1.1, © 1999-2011 ChemAxon Ltd.
208. Galambos, J., Nógrádi, K., Ágai-Csongor, É. et al. PCT Int. Appl. WO2003/029233. *Chem. Abstr.* **2003**, 138, 287701.
209. Shimamura, T., Shiroishi, M., Weyand, S. et al. Structure of the human histamine H₁ receptor complex with doxepin. *Nature* **2011**, 475, 65- 70.
210. Wang, C., Jiang, Y., Ma, J. et al. Structural basis for molecular recognition at serotonin receptors. *Science* **2013**, 340, 610-619.
211. Wacker, D., Wang, C., Katritch, V. et al. Structural features for functional selectivity at serotonin receptors. *Science* **2013**, 340, 615-619.
212. Kalid, O., Toledo Warshaviak, D., Shechter, S., Sherman, W., Shacham, S. Consensus Induced Fit Docking (ciFD): methodology, validation, and application to the discovery of novel Crm1 inhibitors. *J. Comput. Aided Mol. Des.* **2012**, 26, 1217-1228.
213. Planesas, J. M., Pérez-Nueno, V. I., Borrell, J. I., Teixidó, J. Impact of the CXCR4 structure on docking-based virtual screening of HIV entry inhibitors. *J. Mol. Graphics Model.* **2012**, 38, 123-136.
214. Kiss, R., Noszá, B., Rácz, A., Falus, A., Eros, D., Keserú, G. M. Binding mode analysis and enrichment studies on homology models of the human histamine H₄ receptor. *Eur. J. Med. Chem.* **2008**, 43, 1059-1070.
215. Kiss, R., Kiss, B., Könczöl, A. et al. Discovery of novel human histamine H₄ receptor ligands by large-scale structure-based virtual screening. *J. Med. Chem.* **2008**, 51, 3145-3153.
216. Rueda, M., Bottegoni, G., Abagyan, R. Recipes for the selection of experimental protein conformations for virtual screening. *J. Chem. Inf. Model.* **2010**, 50, 186-193.
217. Korb, O., Olsson, T. S., Bowden, S. J. et al. Potential and limitations of ensemble docking. *J. Chem. Inf. Model.* **2012**, 52, 1262-1274.
218. Xu, M., Lill, M. A. Utilizing experimental data for reducing ensemble size in flexible-protein docking. *J. Chem. Inf. Model.* **2012**, 52, 187-198.

219. Raval, A., Piana, S., Eastwood, M. P., Dror, R. O., Shaw, D. E. Refinement of protein structure homology models via long, all-atom molecular dynamics simulations. *Proteins* **2012**, 80, 2071-2079.
220. Beuming, T., Sherman, W. Current assessment of docking into GPCR crystal structures and homology models: successes, challenges, and guidelines. *J. Chem. Inf. Model.* **2012**, 52, 3263-3277.
221. Wang, R., Wang, S., How does consensus scoring work for virtual library screening? An idealized computer experiment. *J. Chem. Inf. Comput. Sci.* **2001**, 41, 1422-1426.
222. Wielens, J., Headey, S.J., Rhodes, D.I. et al. Parallel screening of low molecular weight fragment libraries: do differences in methodology affect hit identification? *J. Biomol. Screen.* **2013**, 18, 147-159.
223. Cross, J.B., Thompson, D.C., Rai, B.K. et al. Comparison of several molecular docking programs: pose prediction and virtual screening accuracy. *J. Chem. Inf. Model.* **2009**, 49, 1455-1474.
224. Ekroos, M., Sjögren, T. Structural basis for ligand promiscuity in cytochrome P450 3A4. *Proc. Natl. Acad. Sci. USA* **2006**, 103, 13682-13687.
225. Atkins, W.M. Non-Michaelis-Menten kinetics in cytochrome P450-catalyzed reactions. *Annu. Rev. Pharmacol. Toxicol.* **2005**, 45, 291-310.
226. Houston, J.B., Galetin, A. Modelling atypical CYP3A4 kinetics: principles and pragmatism. *Arch. Biochem. Biophys.* **2005**, 433, 351-360.
227. Zhou, S.F., Zhou, Z.W., Yang, L.P., Cai, J.P. Substrates, inducers, inhibitors and structure-activity relationships of human cytochrome P450 2C9 and implications in drug development. *Curr. Med. Chem.* **2009**, 16, 3480-3675.
228. Tang, W., Stearns, R.A., Kwei, G.Y. et al. Interaction of diclofenac and quinidine in monkeys: stimulation of diclofenac metabolism. *J. Pharmacol. Exp. Ther.* **1999**, 291, 1068-1074.
229. Hutzler, J.M., Frye, R.F., Korzekwa, K.R., Branch, R.A., Huang, S.M., Tracy, T.S. Minimal in vivo activation of CYP2C9-mediated flurbiprofen metabolism by dapsone. *Eur. J. Pharm. Sci.* **2001**, 14, 47-52.
230. Egnell, A.C., Houston, B., Boyer, S. In vivo CYP3A4 heteroactivation is a possible mechanism for the drug interaction between felbamate and carbamazepine. *J. Pharmacol. Exp. Ther.* **2003**, 305, 1251-1262.
231. Egnell, A.C., Eriksson, C., Albertson, N., Houston, B., Boyer, S. Generation and evaluation of a CYP2C9 heteroactivation pharmacophore. *J. Pharmacol. Exp. Ther.* **2003**, 307, 878-887.
232. Egnell, A.C., Houston, J.B., Boyer, C.S. Predictive models of CYP3A4 heteroactivation: in vitro-in vivo scaling and pharmacophore modeling. *J. Pharmacol. Exp. Ther.* **2005**, 312, 926-937.
233. Locuson, C.W., Gannett, P.M., Ayscue, R., Tracy, T.S. Use of simple docking methods to screen a virtual library for heteroactivators of cytochrome P450 2C9. *J. Med. Chem.* **2007**, 50, 1158-1165.
234. Huth, J.R., Park, C., Petros, A.M. et al. Discovery and design of novel HSP90 inhibitors using multiple fragment-based design strategies. *Chem. Biol. Drug. Des.* **2007**, 70, 1-12.

235. Barker, J.J., Barker, O., Courtney, S.M. et al. Discovery of a novel Hsp90 inhibitor by fragment linking. *ChemMedChem* **2010**, 5, 1697-1700.
236. Murray, C.W., Carr, M.G., Callaghan, O. et al. Fragment based drug discovery applied to Hsp90. Discovery of two lead series with high ligand efficiency. *J. Med. Chem.* **2010**, 53, 5942-5955.
237. Szczepankiewicz, B.G., Liu, G., Hajduk, P.J. et al. Discovery of a potent, selective protein tyrosine phosphatase 1B inhibitor using a linked-fragment strategy. *J. Am. Chem. Soc.* **2003**, 125, 4087-4096.
238. Liu, G., Xin, Z., Liang, H. et al. Selective protein tyrosine phosphatase 1B inhibitors: targeting the second phosphotyrosine binding site with non-carboxylic acid-containing ligands. *J. Med. Chem.* **2003**, 46, 3437-3440.
239. Pei, Z., Li, X., Liu, G. et al. Discovery and SAR of novel, potent and selective protein tyrosine phosphatase 1B inhibitors. *Bioorg. Med. Chem. Lett.* **2003**, 13, 3129-3132.
240. Liu, G., Xin, Z., Pei, Z. et al. Fragment screening and assembly: a highly efficient approach to a selective and cell active protein tyrosine phosphatase 1B inhibitor. *J. Med. Chem.* **2003**, 46, 4232-4235.
241. Nair, P.C., Malde, A.K., Drinkwater, N., Mark, A.E. Missing fragments: detecting cooperative binding in fragment-based drug design. *ACS Med. Chem. Lett.* **2012**, 3, 322-326.
242. Ágai-Csongor, É., Domány, G., Nógrádi, K. et al. Discovery of cariprazine (RGH-188): a novel antipsychotic acting on dopamine D₃/D₂ receptors. *Bioorg. Med. Chem. Lett.* **2012**, 22, 3437-3440.
243. Chien, E.Y., Liu, W., Zhao, Q. et al. Structure of the human dopamine D₃ receptor in complex with a D₂/D₃ selective antagonist. *Science* **2010**, 330, 1091-1095.
244. Gorelik, B., Goldblum, A. High quality binding modes in docking ligands to proteins. *Proteins* **2008**, 71, 1373-1386.
245. Purisima, E.O., Hogues, H. Protein-ligand binding free energies from exhaustive docking. *J. Phys. Chem. B* **2012**, 116, 6872-6879.
246. Tarcsay, Á., Paragi, G., Vass, M., Jójárt, B., Bogár, F., Keserű, G.M. The impact of molecular dynamics sampling on the performance of virtual screening against GPCRs. *J. Chem. Inf. Model.* **2013**, 53, 2990-2999.
247. Vass, M., Schmidt, É., Horti, F., Keserű, G.M. Virtual fragment screening on GPCRs: a case study on dopamine D₃ and histamine H₄ receptors. *Eur. J. Med. Chem.* **2014**, 77, 38-46.
248. Vass, M., Tarcsay, Á., Keserű, G.M. Multiple ligand docking by Glide: implications for virtual second-site screening. *J. Comput. Aided Mol. Des.* **2012**, 26, 821-834.
249. Vass, M., Keserű, G.M. Fragments to link. A multiple docking strategy for second site binders. *MedChemComm* **2013**, 4, 510-514.
250. Vass, M., Ágai-Csongor, É., Horti, F., Keserű, G.M. Multiple fragment docking and linking in primary and secondary pockets of dopamine receptors. *ACS Med. Chem. Lett.* Submitted.

Appendix A

Sequence alignment of human H₄R and human H₁R.

```

H4      MADTNSTINLSLSTRVTLAFFMSLVAFAIMLGNALVILAFVVDKNNLRHRSYFFLNLAISDFFVGV
H1 (3RZE)      MPLVVVLSITICLVTVGLNLLVLVAVRSEKRLHTVGNLYIVSLSVADLIVGA

                |      TM1      |      ICL1      |      TM2
H4      ISIPLYIPHTLF~EWDGFKGKICVFWLTTDYLLCTASVYNIVLISYDRYLSVSNVAVSYRTQHTGVLK
H1 (3RZE)      VVMPMNILYLLMSKWSLGRPLCLFWLSMDYVASTASIFSVFILCIDRYRSVQQPLRYLKYRT~KTR

                |      ECL1      |      TM3      |      ICL2      |
H4      IVTLMVAVVWVLAFLVNGPMILVSESWKDEGSECEPGFFSEWYILAITSFLEFVIPVILVAYFNMMNI
H1 (3RZE)      ASATILGAWFLSFL~WVPIPLGWNH  RRED~KCETDFYDVTWPKVMTAII NFYLP TLLMLWFYAKI

                TM4      |      ECL2      |      TM5
H4      YWSLWKRDLHSRCQSHPGTLAVSSNICGHSFRGRLLSSRRSLSASTEVPA SFH SERQRRKSSLMFSS
H1 (3RZE)      YKAVRQHC

                |      ICL3
H4      RTKMNSNTIASKMGSFSQSDSVALHQREHVELLRARRLAKSLAILLGVFAVWCWAPYSLFTIVLSFY
H1 (3RZE)      LHMNRERKAAKQLGFIMAAFILCWIPYFIFFMVI AFC

                |      TM6      |
H4      SSATGPKSVWYRIAFWLQWFNSFVNPLLYPLCHKRFQKAFKIFCIIKKQPLPSQHSRSVSS
H1 (3RZE)      KNCC~NEHLHMFTIWLGYINSTLNPLIYPLCNENFKKTFKRILHI

                ECL3      |      TM7      |      H8      |

```

Sequence alignment of human 5HT₆R and human 5HT_{2B}R.

```

5HT6    MVPEPGPTANSTPAWGAGPPSAPGGSGWVAAALCVVIALTAAANSLI ALICTQPALRNTSNFFLV
5HT2B    EEQGNKHLHWAALLILMVIIPTIGGNTLVILAVSLEKKLQYATNYFLM

                |      TM1      |      ICL1      |
5HT6    SLFTSDLMVGLVVMPPAMLNALYG  RWVLARGLCLLWTAFDVMCCSASILNCLISLDRYLLILSP
5HT2B    SLAVADLLVGLFVMPIALLLTIMFEAMWPLPLVLCPAWFLFDLVLFSTASIWHLCAISVDRYIAIKKP

                TM2      |      ECL1      |      TM3      |
5HT6    LRYKLRMTPLRALALVLGAWSLAALASFLP LLLGWHELGHARPPVPGQCRLLA  SLPFVLVASGL
5HT2B    IQANQYNSRATAFIKITVWVLISIGIAIPVPIKGI  ET  NPNNITCVLTKERFGDFMFLGSLA

                ICL2      |      TM4      |      ECL2      |      TM5
5HT6    TFFLP SGAICFTYCRILLAARKQAVQVASLTTGMASQASET LQVPRTPRPGVESADSRRLATKHSR
5HT2B    AFFTFLAIMIVTYFLTIHALQKKA~~~~~~

                |      ICL3
5HT6    KALKASLTGILLGMFFVTWLPFFVANIVQAVCD~~~~~CISPGLFVDLTWLGVCNSTMNP I IYPLF
5HT2B    NEQRASKVLGIVFFFLFLMWCPPFITNITLVLCDS CNQTTLQMLLEIFVWVIGYVSSGVNPLVYTLF

                TM6      |      ECL3      |      TM7      |
5HT6    MRDFKRALGRFLPCPRCP RERQASLASPSLRTSHSGPRPGLSLQQVLP LPLPPDS DSDSDAGSGGS
5HT2B    NKTFRDAFGRYITCN YR

                H8      |
5HT6    SGLRLTAQLLLPGEATQDPPLP TRAAAVNF
5HT2B

```

Sequence alignment of human D₂R and human D₃R (PDB ID: 3PBL).

```

                                     |          TM1
hD2R MDPLNLSWYDDDLERQNSRPFNGSDGKADRPHYNYATLLTLLIAVIVF
3PBL                                     YALSYCALILAIVF

          |      ICL1      |          TM2      |
hD2R  GNVLVCMVAVSREKALQTTTNYLIVSLAVADLLVATLVMPWVVYLEVV~GE
3PBL  GNGLVCMAVLKERALQTTTNYLVVSLAVADLLVATLVMPWVVYLEVTGGV

          ECL1      |          TM3      |          ICL2
hD2R  WKFSRIHCDIFVTLDVMMCTASILNLCAISIDRYTAVAMPMLYNTRYSG~
3PBL  WNFSRICCDVFTLVMMCTASIWNLCAISIDRYTAVMPVHYQHGTGQS

          |          TM4      |          ECL2      |
hD2R  SKRRVTVMISIVWVLSFTISCPPLFGLNNA~DQNECIIANPAFVVYSSIV
3PBL  SCRRVALMITAVVWLAFVSCPLLFGFNTTGDPTVCSISNPDFVIYSSV

          TM5      |          ICL3
hD2R  SFYVPFIVTLLVYIKIYIVLRRRRKRVNTKRSSRAFRAHLRAPLKGNCTH
3PBL  SFYLPFGVTVLVYARIYVVLKQRRK~

hD2R  PEDMKLCTVIMKSNNGSFPVNRRRVEARRAQELEMEMLSSTSPPERTRYG
3PBL  ~~~~~

hD2R  PIPPSHHQLTLPDPSHHGLHSTPDSPAKPEKNGHAKDHPKIAKIFEIQTM
3PBL  ~~~~~

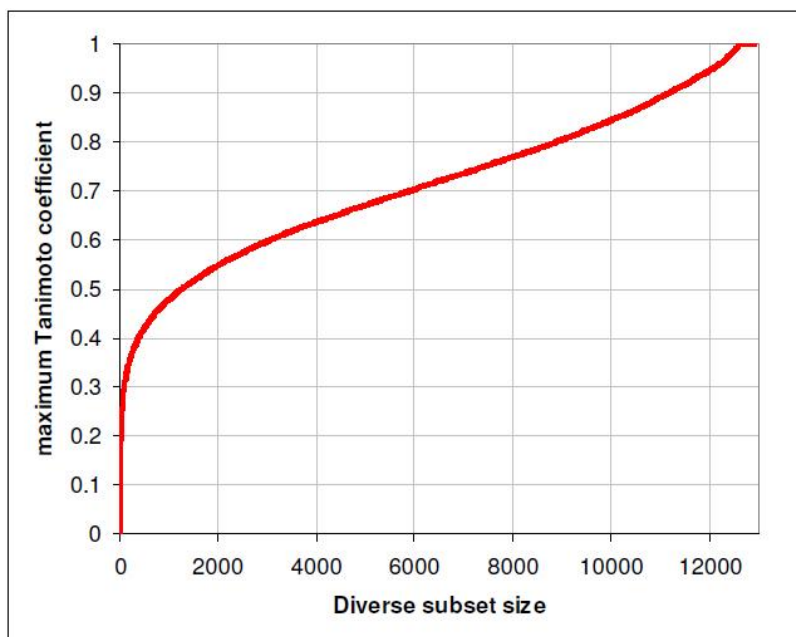
          |          TM6      |
hD2R  PNGKTRTSLKTMSRRKLSQQKEKKATQMLAIVLGVFII CWLPFFITHILN
3PBL  ~~~~~GVPLREKKATQMVAVILGAFIVCWLPFFLTHVLN

          ECL3      |          TM7      |          H8      |
hD2R  IHCD~CNIPPVLYSAFTWLGYN SAVNPIIYTTFNIEFRKAFKILHC
3PBL  THCQTCHVSP ELYSATTWLGYN SALNPVIYTTFNIEFRKAFKILSC

```

Appendix B

Diversity of the Gedeon Richter fragment collection assessed by the maximum Tanimoto coefficient between all compounds of a diverse subset of a given size. Diversity sorting was performed with the stepwise elimination algorithm using the ChemAxon linear hashed fingerprint of length 1024 bits, linear paths of 5 bonds and 2 bits per path.



Appendix C

PDB ID codes and chain identifiers of the structures used in small molecule secondary site modeling.

Structures containing 2 similar ligands:

1dog/A, 1e7c/A, 1eb9/AB, 1egy/A, 1eup/A, 1fm4/A, 1gnw/AB, 1hkk/A, 1k0y/ABCD, 1l5q/AB, 1oni/ABC, 1pzo/A, 1qiw/A, 1t93/A, 1tw4/A, 1txc/AB, 1v08/AB, 1z62/A+mate, 1znd/A, 2ayw/A, 2b99/ABCDE, 2bjv/A, 2cbo/A, 2cbt/AB, 2d0e/A, 2d41/A, 2e93/AB, 2e9a/AB, 2flh/D, 2ft9/A, 2g8r/A, 2hfp/AB, 2iei/AB, 2nss/A, 2nvd/A, 2oz5/A, 2p70/A, 2uxi/AB, 2wbb/ABCD, 2wbd/ABCD, 2whf/A, 2whh/A, 2wrm/A, 2x0v/B, 2xuc/A, 2xys/ABCDE, 2xzi/A, 2y5k/ABCD, 2y5l/ABCD, 2ybt/A, 2ybu/ABCD, 2z3u/A, 2z4y/AB, 2zeb/ABCD, 2zf4/AB, 3a73/A, 3ads/AB, 3adv/AB, 3ao1/AB, 3arr/A, 3arv/A, 3as1/A, 3arz/A, 3b6c/AB, 3bc4/A+mate, 3bxs/AB, 3cz0/AB, 3cz1/AB, 3dzl/AB, 3e7s/AB, 3etd/ABCDEF, 3etg/ABCDEF, 3f3t/A, 3f3u/A, 3g35/B, 3g35/B, 3g6m/A, 3gqt/ABCD, 3h78/AB, 3hlw/A, 3htf/A, 3ilt/BE, 3km4/A, 3ko0/AB, 3krq/A, 3lc3/AB, 3n0h/A, 3nsr/BD, 3okh/AB, 3os9/ABCD, 3p9t/AB, 3pxf/A, 3rpn/AD, 3rv5/A, 3sfc/A

Structures containing 2 different ligands:

1me7/A+mate, 1s9q/AB+2mates, 2aov/A, 2qfo/A, 2vq5/AB, 2wk2/A, 2xdu/A, 2y1w/ABCD, 2yei/A, 2yej/A, 3hz1/A, 3jun/AB, 3ndv/ABCD, 3o2k/A, 3p2h/A

Structures containing 3 ligands:

1dtl/A, 1e7c/A, 1lin/A, 1n8v/A, 2a3b/A, 2d5z/ABCD, 2hdu/B, 2x45/A, 3b99/A, 3dhh/ABCE, 3ej0/A+3mates, 3g5n/D, 3p2r/AB

Structures containing 4 ligands:

1wrk/AB, 2a3a/A, 2e98/AB, 2fsz/AB+2mates, 2qim/A, 3e85/A

Structures containing 5 ligands: 3elz/A

Structures containing 6 ligands: 3lsl/AD

The two structures added in the CYP case study: 2nnh/A, 2v0m/A

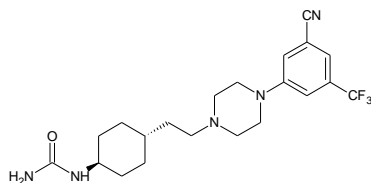
Appendix D

PDB ID codes and SMILES representation of the docked ligands for the structures used in fragment secondary site modeling.

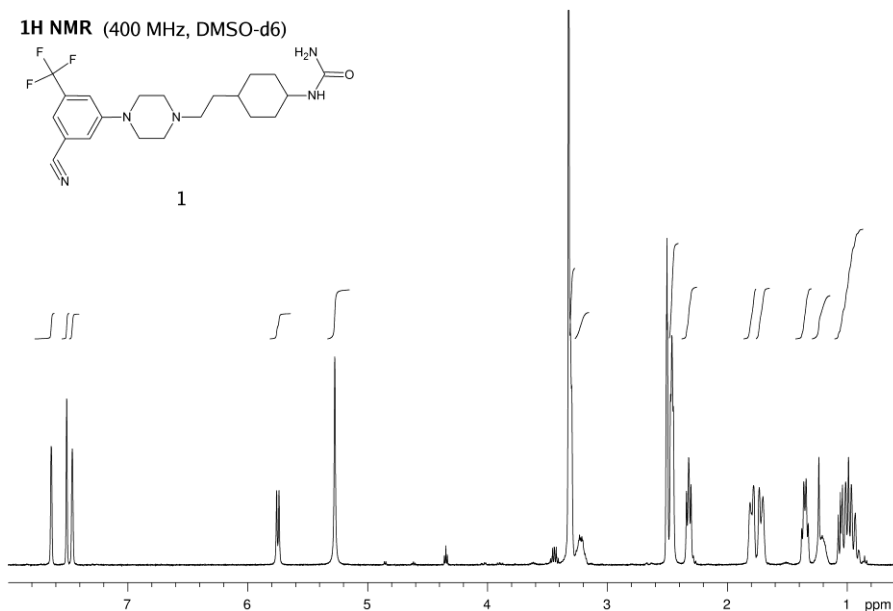
PDB ID	1 st ligand SMILES	2 nd ligand SMILES
1nny	<chem>OC(=O)C(O)N(c1cccc1C(O)=O)c1cccc2cccc12</chem>	<chem>COc1cc2cccc2cc1C(O)=O</chem>
1pho	<chem>OC(=O)C(O)N(c1cccc1)c1cccc1C(O)=O</chem>	<chem>COC(=O)c1cccc1O</chem>
1pyn	<chem>OC(=O)C(O)c1cccc1C(O)=O</chem>	<chem>COC(=O)c1cccc1O</chem>
1q1m	<chem>OC(=O)c1cc(om1)c1cccc1F</chem>	<chem>COC(=O)c1cccc1O</chem>
2ijk	<chem>CCNC(=O)NS(=O)(=O)c1cccc(C)c1</chem>	<chem>CCNC(=O)NS(=O)(=O)c1cccc(C)c1</chem>
2jt6	<chem>CC(=O)NO</chem>	<chem>Oc1ccc(cc1)c1ccc(cc1)C#N</chem>
2ohp	<chem>Nc1cccn1</chem>	<chem>c1cc2cccc2[nH]1</chem>
2ohq	<chem>Nc1cccn1</chem>	<chem>COc1cccc(ct)c1ccccc1</chem>
2vts	<chem>CCN(C(O)=NS(=O)(=O)c1ccc(N)cc1</chem>	<chem>CCNC(O)=NS(=O)(=O)c1ccc(N)cc1</chem>
2vti	<chem>c1n[nH]c2cccc12</chem>	<chem>NS(=O)(=O)c1cccc1</chem>
3a7x	<chem>NC(=N)c1ccccc1</chem>	<chem>OCC(O)=O</chem>
3daj	<chem>CNc1nnc2[nH]cnc12</chem>	<chem>CCCCNC(=O)c1cccc(NC(C)=O)c1</chem>
3fci	<chem>O=C1NC=CC(=O)N1</chem>	<chem>oC1(=O)c1cccc1</chem>
3ftx	<chem>CC(C)C[C@H](NC(=O)[C@@H](O)[C@H](N)Cc1cccc1)C(O)=O</chem>	<chem>Oc1ccc(CCC2cc(O)cc(O)c2)cc1</chem>
3fue	<chem>CC(C)C[C@H](NC(=O)[C@@H](O)[C@H](N)Cc1cccc1)C(O)=O</chem>	<chem>Clc1ccc2[nH]ccc2c1</chem>
3fuf	<chem>CC(C)C[C@H](NC(=O)[C@@H](O)[C@H](N)Cc1cccc1)C(O)=O</chem>	<chem>Fc1ccc2[nH]ccc2c1</chem>
3fuh	<chem>CC(C)C[C@H](NC(=O)[C@@H](O)[C@H](N)Cc1cccc1)C(O)=O</chem>	<chem>Oc1ccc2[nH]ccc2c1</chem>
3img	<chem>COc1ccc2[nH]ccc2c1</chem>	<chem>OC(=O)c1cc2cccc2o1</chem>
3le8	<chem>COc1ccc2n1(CC(O)=O)ccc2c1</chem>	<chem>OC(=O)c1cc2cccc2o1</chem>
3lka	<chem>CC(=O)NO</chem>	<chem>COc1ccc(cc1)S(N)(=O)=O</chem>
3qc4	<chem>O=C1Nc2cccc2N1</chem>	<chem>CNC(=O)C1=CC=CN(Cc2ccc(F)c(F)c2)C1=O</chem>
3ry2	<chem>C[C@H]1CNC(=O)N1</chem>	<chem>CCCCC(O)=O</chem>
4a7i	<chem>NC(=O)c1ccc(Cl)s1</chem>	<chem>CC(C)N1CCC(CC1)NS(C)=O</chem>
4ajh	<chem>Cc1nc2ccc(NC(=O)CCNC(N)=O)cc2s1</chem>	<chem>OC(=O)C(O)c1ccc(Br)cc1C(O)=O</chem>
4ajj	<chem>Cc1nc2ccc(NC(=O)CCNC(N)=O)cc2s1</chem>	<chem>COc1ccc(CC(C(O)=O)C(O)=O)cc1OC</chem>
4dm3	<chem>Oc1cccc(O)c1</chem>	<chem>c1c[nH]en1</chem>
2c8w	<chem>COc1ccc(cc1)S(=O)(=O)NC[C@@H](O)[C@@H](N)Cc1cccc1</chem>	<chem>Clc1ccc(cc1)n1cnm1</chem>
2qfo	<chem>Cc1cc(nc(N)n1)C(F)F</chem>	<chem>O=C1OCC1=C/Nc1ccccc1</chem>
3hz1	<chem>CN(C)c1nnc2nc[nH]c12</chem>	<chem>COC(=O)c1c(C)[nH]nc1c1ccco1</chem>
2xdu	<chem>Nc1nccn1</chem>	<chem>Cc1nnc(Cl)c2ccccc12</chem>
2yei	<chem>COC(=O)Cc1cc(O)cc(O)c1</chem>	<chem>COC(=O)c1c(C)[nH]nc1c1cco1</chem>
2yje	<chem>CSc1nc(C)nc(N)n1</chem>	<chem>COC(=O)c1c(C)[nH]nc1c1cco1</chem>

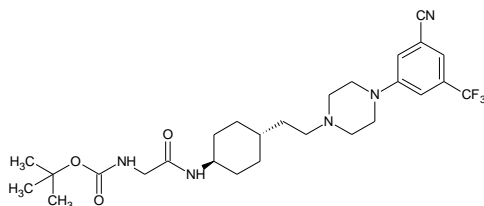
Appendix E

Synthetic methods and analysis details.

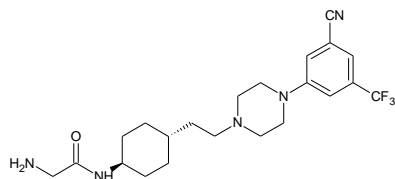


trans-1-[4-(2-{4-[3-cyano-5-(trifluoromethyl)phenyl]piperazin-1-yl}ethyl)cyclohexyl]urea (**19**): 0.46 g (1.0 mmol) *trans*-4-{2-[4-(3-cyano-5-trifluoromethylphenyl)-piperazin-1-yl]-ethyl}-cyclohexyl-amine dihydrochloride (Intermediate 1, see synthesis in [208]) was suspended in dry dichloromethane (30 ml), triethylamine (0.6 ml, 3.2 mmol) was added followed by triphosgene (0.13 g (0.44 mmol)). After 15 minutes stirring at room temperature ammonia (20 %) in ethanol solution (8 ml) was added and the stirring was continued for 24 hours. The mixture was evaporated in *vacuo*. The residue was suspended in water (15 ml) stirred for one hour, filtered and dried. Purification by column chromatography (silica gel, dichloromethane: methanol 9:1) afforded the title compound (0.14 g, 33 %). M.p.: 202-4 °C. LC-MS purity: 100.00%. LC-MS base peak *m/z*: 424.2.

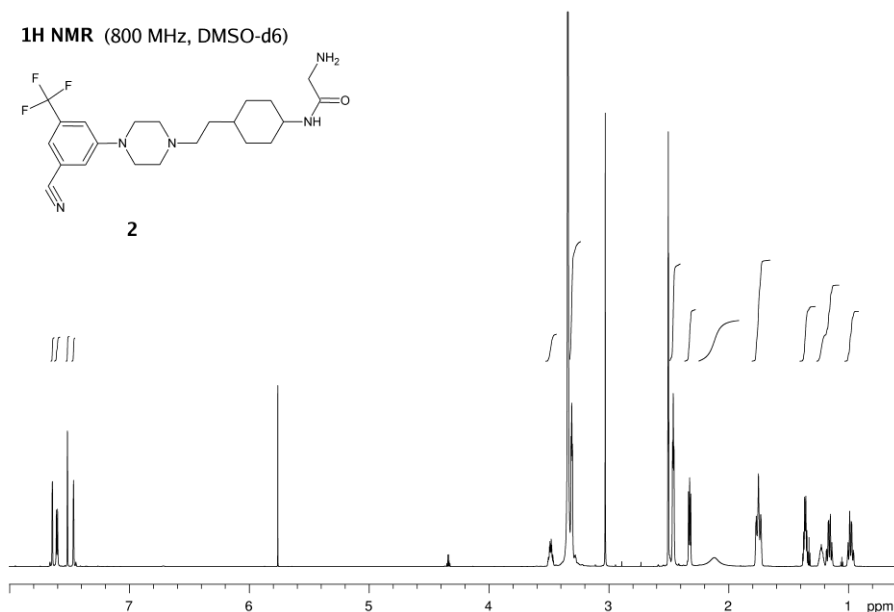


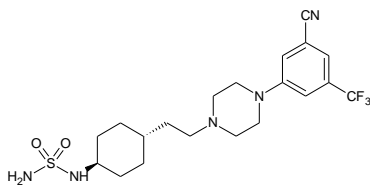


trans-tert-butyl-N-({[4-(2-{4-[3-cyano-5-(trifluoromethyl)phenyl]piperazin-1-yl}ethyl)cyclohexyl]carbonyl}methyl)carbamate (Intermediate 2): Boc-glycine (0.2 g, 1.14 mmol) was dissolved in dichloromethane (20 ml) and N-(3-dimethylaminopropyl)-N'-ethylcarbodiimide hydrochloride (0.22 g, 1.14 mmol) was added followed by 1-hydroxy-benzotriazole hydrate (0.18 g, 1.14 mmol) and stirred for 20 minutes. Triethylamine (0.42 ml, 3 mmol) followed by Intermediate 1 (0.45 g, 1 mmol) was added and the mixture was stirred for 10 hours at room temperature then washed with 10% Na₂CO₃ solution and water (10-10 ml), dried (Na₂SO₄) and evaporated in *vacuo*. Purification by column chromatography (silica gel, dichloromethane: methanol 15:1) afforded the title compound (0.34 g, 63 %).

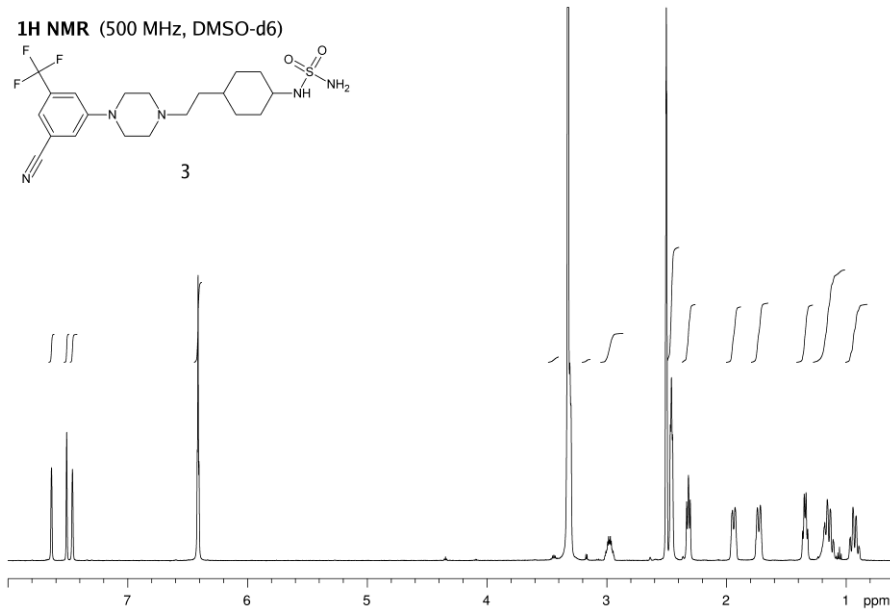


trans-2-amino-N-[4-(2-{4-[3-cyano-5-(trifluoromethyl)phenyl]piperazin-1-yl}ethyl)cyclohexyl]acetamide (**20**): Intermediate 2 (0.34 g, 0.63 mmol) was dissolved in ethylacetate (5 ml) cooled to 5°C and ethylacetate saturated with gaseous hydrogenchloride (8 ml) was dropped in and the suspension stirred for 3 hours at room temperature, the precipitate filtered and washed with diethylether (10 ml). The crude product was purified by column chromatography (silica gel, dichloromethane: ammoniumhydroxide solution: methanol 9:1:0.1) affording the title compound (0.15 g, 54 %). M.p.:134-6 °C. LC-MS purity: 93.45%. LC-MS base peak m/z: 438.2.





trans-N-[4-(2-{4-[3-cyano-5-(trifluoromethyl)phenyl]piperazin-1-yl}ethyl)cyclohexyl]aminosulfonamide (**21**): Intermediate 1 (0.44 g, 1 mmol) was suspended in acetonitrile (35 ml), triethylamine (0.7 ml, 5 mmol) was added followed by sulfamoylchloride (0.23 g, 2 mmol). The reaction mixture was refluxed for 8 hours, cooled to room temperature and filtered. The filtrate was evaporated in *vacuo*, dissolved in ethylacetate (30 ml) and washed with saturated Na₂CO₃ solution (10 ml). The organic layer was dried (Na₂SO₄) and evaporated in *vacuo*. The crude product was purified by column chromatography (silica gel, dichloromethane: methanol: ammoniumhydroxide solution 9:1:0.1) affording the title compound (66 mg, 14 %). M.p.: 162-4 °C. LC-MS purity: 96.76%. LC-MS base peak m/z: 460.2.



Appendix F

EF and AUC values of the different receptor models in retrospective small molecule virtual screening used to construct Figure 22.

CXCR ₄	EF1%	EF2%	EF5%	AUC	AvgGlideScore
X-ray	0.00	3.33	2.00	0.602	-3.77
Homology model	0.00	0.00	1.33	0.586	-7.29
MD	6.67	5.00	3.33	0.604	-5.67

D ₃	EF1%	EF2%	EF5%	AUC	AvgGlideScore
X-ray	0.31	0.79	1.26	0.597	-6.11
Homology model	0.63	0.95	1.26	0.526	-6.39
MD	3.46	2.53	2.46	0.613	-6.56

H ₄	EF1%	EF2%	EF5%	AUC	AvgGlideScore
Homology model	13.33	6.67	2.67	0.685	-6.55
MD	26.67	13.33	6.67	0.835	-5.33

5HT ₆	EF1%	EF2%	EF5%	AUC	AvgGlideScore
Homology model	0.00	0.00	1.11	0.719	-4.55
MD	14.10	8.46	5.56	0.757	-5.99

Appendix G

Correlation matrix of SiteMap descriptors and enrichment factors for the MD frames in retrospective small molecule virtual screening.

H₄	Mean	Std.Dev.	EF1%	EF2%	EF5%
SiteScore	1.06	0.02	0.15	0.11	0.05
size	278.45	64.81	-0.42	-0.37	-0.42
Dscore	1.09	0.03	0.28	0.23	0.24
volume	889.62	167.37	-0.22	-0.24	-0.26
exposure	0.56	0.05	0.53	0.48	0.59
enclosure	0.77	0.03	-0.11	-0.18	-0.30
contact	0.96	0.05	-0.31	-0.35	-0.49
phobic	0.85	0.22	0.08	0.12	0.05
philic	0.96	0.08	-0.39	-0.39	-0.48
balance	0.91	0.31	0.16	0.20	0.17
don/acc	1.31	0.31	0.22	0.20	0.28

D₃	Mean	Std.Dev.	EF1%	EF2%	EF5%
SiteScore	1.10	0.03	0.00	-0.04	-0.06
size	164.53	25.41	-0.10	-0.06	-0.04
Dscore	1.14	0.03	-0.05	-0.05	-0.11
volume	521.51	63.80	0.10	0.09	-0.02
exposure	0.51	0.05	0.07	0.11	0.02
enclosure	0.80	0.03	0.08	0.01	0.04
contact	1.01	0.05	-0.05	-0.09	-0.01
phobic	1.22	0.20	-0.13	-0.16	-0.17
philic	0.87	0.09	0.12	0.07	0.16
balance	1.41	0.32	-0.16	-0.16	-0.21
don/acc	1.56	0.41	-0.26	-0.20	-0.25

CXCR ₄	Mean	Std.Dev.	EF1%	EF2%	EF5%
SiteScore	1.09	0.02	0.06	0.01	0.02
size	146.60	34.00	-0.04	0.06	-0.11
Dscore	1.14	0.03	0.09	0.08	0.05
volume	696.69	125.21	0.08	0.17	-0.06
exposure	0.67	0.04	0.22	0.15	0.10
enclosure	0.77	0.03	-0.08	-0.16	-0.08
contact	0.85	0.06	-0.25	-0.22	-0.16
phobic	0.84	0.19	-0.12	-0.10	0.07
philic	0.80	0.08	-0.06	-0.17	-0.05
balance	1.07	0.31	-0.07	0.00	0.07
don/acc	1.52	0.37	0.22	0.25	-0.17

5HT ₆	Mean	Std.Dev.	EF1%	EF2%	EF5%
SiteScore	1,09	0,02	0,11	0,02	0,01
size	206,26	31,09	0,12	0,05	-0,03
Dscore	1,14	0,02	0,14	0,09	0,03
volume	715,19	72,17	0,06	0,12	-0,05
exposure	0,50	0,07	-0,01	0,09	0,04
enclosure	0,78	0,03	0,02	-0,09	-0,03
contact	0,97	0,06	0,07	-0,03	-0,01
phobic	1,18	0,19	0,14	0,06	0,01
philic	0,84	0,08	-0,11	-0,14	-0,05
balance	1,43	0,33	0,14	0,09	0,00
don/acc	1,38	0,24	0,06	0,12	0,09

Definitions of SiteMap descriptors.

SiteScore	This score is constructed and calibrated so that the average SiteScore for 157 investigated submicromolar sites is 1.0. Thus, a score of greater than 1 suggests a site of particular promise. A SiteScore of 0.80 has been found to accurately distinguish between drug-binding and non-drug-binding sites.
size	The number of site points that make up the site (a measure of the size of the site).
Dscore	Dscore uses the same properties as SiteScore but different coefficients.
volume	Volume of the binding site.
exposure	The value of the property is the ratio of the number of extension points to the number of original plus extension points. A shallow, open site would allow many more site points to be added, giving a high exposure score. The lower the score, the better; the average for the tight-binding sites investigated is 0.49.
enclosure	This property measures of how open the site is to solvent. Higher scores are better, with the average enclosure score for a tight-binding site being 0.78.
contact	The contact property measures how strongly the average site point interacts with the surrounding receptor via van der Waals nonbonded interactions, when the site point is given nominal van der Waals parameters. The contact core has been calibrated so that the average score for a tight-binding site is 1.0.
phobic	Hydrophobic—regions that are favorable for occupancy by hydrophobic ligand groups
philic	Hydrophilic—regions that are favorable for occupancy by hydrophilic ligand groups
balance	The properties, labeled phob and phil, measure the relative hydrophobic and hydrophilic character of the site. The balance property expresses the ratio of the two.
don/acc	This property, labeled don/acc, indicates the degree to which a well-structured ligand might be expected to donate, rather than accept, hydrogen bonds, as inferred from the sizes and intensities of donor and acceptor SiteMap regions.

Reference: SiteMap 2.6 User Manual, Schrödinger, LLC, New York, 2012.

Appendix H

Number of structures with at least two successful consecutive docking steps for all docking protocols, scoring functions and structure filters used to construct Figure 32. GS=GlideScore, Em=Emodel, GE=Glide Energy.

	all			drug-like			drug-like & closed		
	GS	Em	GE	GS	Em	GE	GS	Em	GE
	SP								
all structures	131	131	131	110	110	110	68	68	68
top 30 poses	72	72	72	65	65	65	46	46	46
top 3 poses	49	52	46	43	47	41	32	34	30
top pose	36	41	39	32	36	34	22	25	25
	XP								
all structures	131	131	131	110	110	110	68	68	68
top 30 poses	48	48	48	44	44	44	32	32	32
top 3 poses	40	41	39	36	37	35	27	27	26
top pose	33	33	32	30	29	28	23	20	19
	SP hard								
all structures	131	131	131	110	110	110	68	68	68
top 30 poses	75	75	75	67	67	67	48	48	48
top 3 poses	52	51	51	46	45	44	35	34	33
top pose	43	44	38	37	39	33	27	29	25

Appendix I

Details of the PDB structures compiled for multiple fragment docking and numeric docking results used to construct Figure 35.

PDB ID	resolution (Å)	N lig.	Target	Method	1 st RMSD	1 st rank	2 nd RMSD	2 nd rank
1mny	2.40	1	protein tyrosine phosphatase 1B	linking	0,66	1	0,49	1
1ph0	2.20	1	protein tyrosine phosphatase 1B	linking	1,97	1	0,25	1
1pyn	2.20	1	protein tyrosine phosphatase 1B	linking	1,15	1	0,26	1
1q1m	2.60	1	protein tyrosine phosphatase 1B	linking	0,24	1	0,23	1
2ijk	2.00	1	fructose-1,6-bisphosphatase 1	tethering	0,29	1	0,26	1
2j16	NMR	1	matrix metalloproteinase 3	linking	1,26	1	0,98	6
2ohp	2.25	1	beta-secretase 1	growing through linker	0,48	1	1,10	2
2ohq	2.10	1	beta-secretase 1	growing through linker	0,25	1	1,22	5
2vt5	2.20	1	fructose-1,6-bisphosphatase 1	tethering	0,83	1	0,23	1
2vfi	2.00	1	cyclin dependent kinase 2	growing through linker	0,08	1	0,58	1
3a7x	1.75	1	cationic trypsin	tethering	0,30	1	0,32	12
3daj	2.00	1	aurora A kinase	tethering	0,18	1	1,88	1
3fci	1.27	1	uracil DNA glycosylase	tethering	0,39	1	1,51	1
3ftx	1.96	2	leukotriene A4 hydrolase	ternary complex	0,23	1	0,24	1
3fue	2.38	2	leukotriene A4 hydrolase	ternary complex	1,05	1	0,37	1
3tuf	2.60	2	leukotriene A4 hydrolase	ternary complex	0,41	1	0,63	4
3tuh	1.80	2	leukotriene A4 hydrolase	ternary complex	0,75	1	0,40	3
3img	1.80	2	MTB pantothenate synthetase	linking	0,21	1	0,51	20
3le8	1.70	1	MTB pantothenate synthetase	linking	0,32	1	1,98	1
3lka	1.80	2	matrix metalloproteinase 12	linking	0,32	8	0,43	1
3qc4	1.80	1	3-phosphoinositide dependent kinase 1	tethering	0,20	1	1,05	1
3ry2	0.95	1	streptavidin	deconstruction	0,27	1	0,69	1
4a71	2.40	1	factor Xa	deconstruction	1,20	1	0,33	1
4ajh	1.93	2	lactate dehydrogenase A	linking	0,32	1	0,50	1
4ajj	1.75	2	lactate dehydrogenase A	linking	0,50	1	0,20	1
4dm3	2.40	2	phenylethanolamine N-methyltransferase	ternary complex	0,37	5	0,61	1
Structures with waters included in docking:								
2c8w	1.96	1	thrombin	linking	0,17	1	0,46	1
2qfo	1.68	2	heat shock protein 90-α	linking	0,34	1	0,20	1
3hz1	2.30	2	heat shock protein 90-α	linking	0,51	1	0,41	1
2xdx	1.74	2	heat shock protein 90-α	ternary complex	0,26	1	0,15	1
2yej	2.20	2	heat shock protein 90-α	ternary complex	0,37	1	0,94	1
2yej	2.20	2	heat shock protein 90-α	ternary complex	1,04	1	0,19	1

Appendix J

Numeric cross-docking results used to construct Figure 38 (cells contain 1st RMSD, 1st rank, 2nd RMSD and 2nd rank from left to right and top to bottom).

Lig	3img	3le8	4ajj	4jh	2jjk	2v15	2ohp	2ohq
Prot	0.21 1 1.00 1	0.51 20 1.39 14	0.32 1 0.37 1	0.50 1 0.41 1	0.29 1 0.26 1	0.90 1 0.83 1	0.48 1 1.10 2	0.37 1 0.68 1
3img	0.31 1 0.32 1	1.95 3 1.98 1	0.73 1 0.50 1	0.59 1 0.20 1	1.78 1 0.23 1	0.49 1 1.48 1	0.25 1 1.22 5	
3le8								

Lig	1nny	1ph0	1pyn	1q1m	3ftx	3fue	3fuf	3fuh
Prot	0.66 1 1.99 1	0.49 1 1.27 17	1.49 1 1.21 1	1.21 1	0.23 1 0.24 1	0.36 1 -	0.37 1 0.81 1	0.19 5
1nny	0.77 1 1.97 1	1.57 1 0.25 1	1.32 1 1.48 1	0.36 1	0.23 1 1.05 1	1.05 1 0.37 1	0.24 1 0.24 1	0.33 1
1ph0	0.73 1 0.35 1	1.30 1 1.98 1	1.15 1 1.49 2	0.35 1	0.39 1 0.97 3	0.41 1 0.49 1	0.39 1 0.63 4	0.49 16
1pyn	1.30 1 1.98 1	- - 0.39 9	0.54 1 0.24 1	0.23 1	1.66 1 0.36 1	0.63 4 0.53 7	0.26 1 0.55 1	0.75 1
1q1m	- - - -	- - - -	0.30 1 0.23 1		0.62 1 0.96 6	1.45 12 0.40 3		

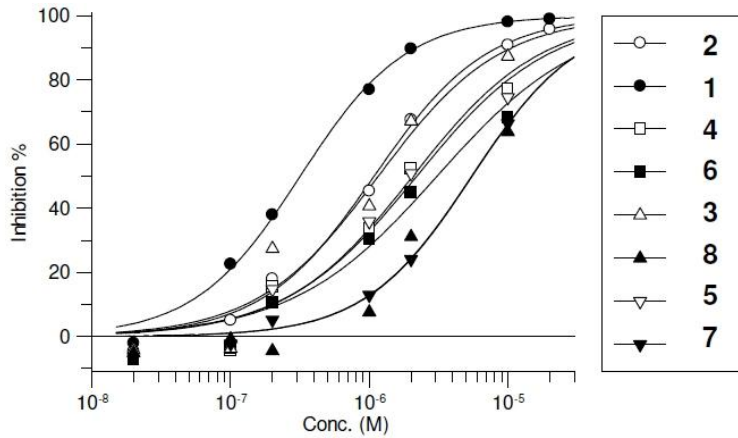
Lig	3img	3le8	4ajj	4jh	2jjk	2v15	2ohp	2ohq
Prot	0.21 1 1.00 1	0.51 20 1.39 14	0.32 1 0.37 1	0.50 1 0.41 1	0.29 1 0.26 1	0.90 1 0.83 1	0.48 1 1.10 2	0.37 1 0.68 1
3img	0.31 1 0.32 1	1.95 3 1.98 1	0.73 1 0.50 1	0.59 1 0.20 1	1.78 1 0.23 1	0.49 1 1.48 1	0.25 1 1.22 5	
3le8								

Lig	2qfo	3hz1	2xdu	2yei	2yej
Prot	0.34 1 0.20 1	0.93 12 - -	0.55 1 - -	1.37 3 - -	0.76 3 - -
2qfo	- - 0.51 1	0.41 1 0.91 1	0.79 1 1.20 1	1.20 1 1.23 1	- - - -
3hz1	- - 0.51 1	0.41 1 0.91 1	0.79 1 1.20 1	1.20 1 1.23 1	- - - -
2xdu	0.72 1 0.79 7	0.54 1 0.64 1	0.26 1 0.15 1	0.56 1 - -	0.81 1 0.96 9
2yei	0.50 1 1.86 5	0.47 1 0.82 1	0.18 1 0.47 3	0.37 1 0.94 1	0.44 1 0.25 1
2yej	0.75 1 0.54 13	0.44 1 0.60 3	0.50 1 0.38 4	0.38 1 1.93 20	1.04 1 0.19 1

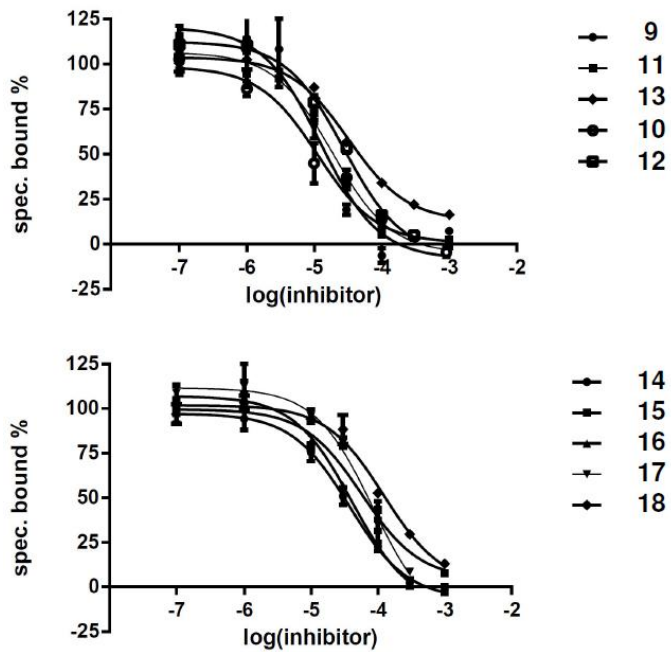
Lig	1nny	1ph0	1pyn	1q1m	3ftx	3fue	3fuf	3fuh
Prot	0.66 1 1.99 1	0.49 1 1.27 17	1.49 1 1.21 1	1.21 1	0.23 1 0.24 1	0.36 1 -	0.37 1 0.81 1	0.19 5
1nny	0.77 1 1.97 1	1.57 1 0.25 1	1.32 1 1.48 1	0.36 1	0.23 1 1.05 1	1.05 1 0.37 1	0.24 1 0.24 1	0.33 1
1ph0	0.73 1 0.35 1	1.30 1 1.98 1	1.15 1 1.49 2	0.35 1	0.39 1 0.97 3	0.41 1 0.49 1	0.39 1 0.63 4	0.49 16
1pyn	1.30 1 1.98 1	- - 0.39 9	0.54 1 0.24 1	0.23 1	1.66 1 0.36 1	0.63 4 0.53 7	0.26 1 0.55 1	0.75 1
1q1m	- - - -	- - - -	0.30 1 0.23 1		0.62 1 0.96 6	1.45 12 0.40 3		

Appendix K

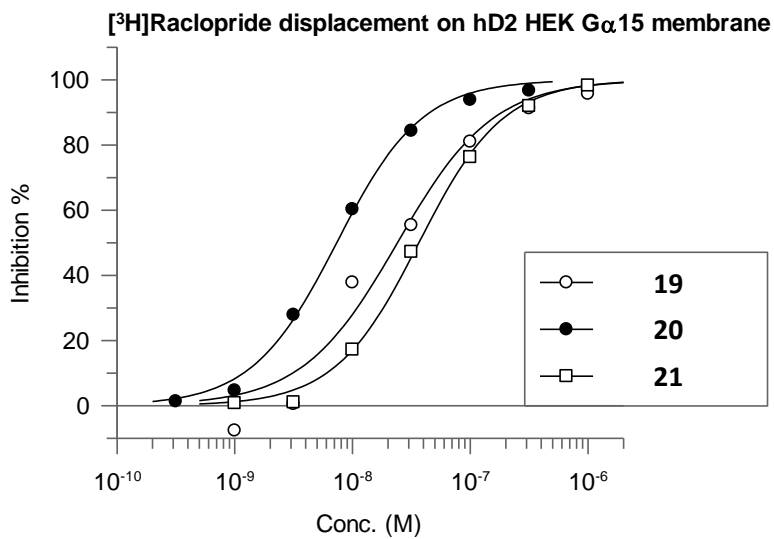
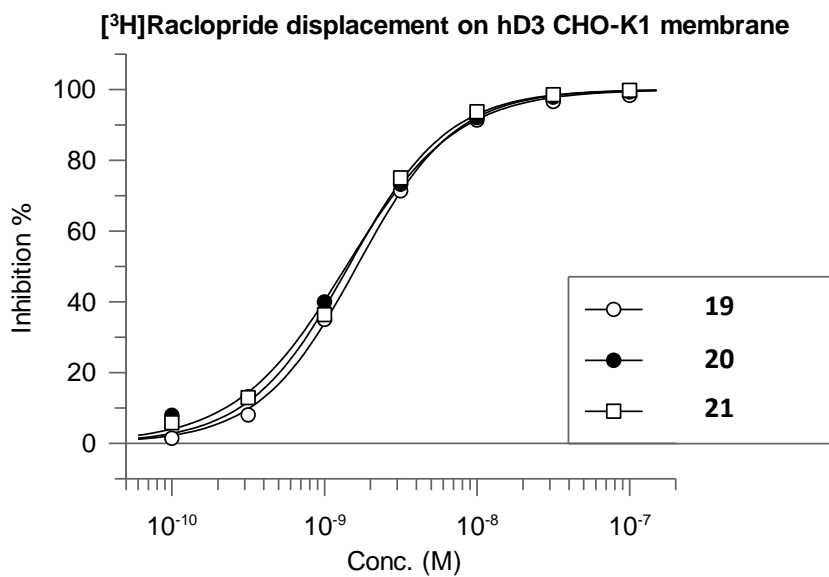
Dose-response curves of D₃ fragment hits **1-8** in [³H]raclopride displacement assay.



Dose-response curves of H₄ fragment hits **9-18** in histamine displacement assay.



Dose-response curves of linked compounds **19-21** in D₃ and D₂ [³H]raclopride displacement assays.



NYILATKOZAT

Alulírott kijelentem, hogy ezt a doktori értekezést magam készítettem és abban csak a megadott forrásokat használtam fel. Minden olyan részt, amelyet szó szerint, vagy azonos tartalomban, de átfogalmazva más forrásból átvettem, egyértelműen, a forrás megadásával megjelöltem.

Budapest, 2014. május 29.
